WIRELESS SENSING AND DECENTRALIZED CONTROL FOR CIVIL STRUCTURES: THEORY AND IMPLEMENTATION

A DISSERTATION SUBMITTED TO
THE DEPARTMENT OF CIVIL AND ENVIRONMENTAL ENGINEERING
AND THE COMMITTEE ON GRADUATE STUDIES
OF STANFORD UNIVERSITY
IN PARTIAL FULFILLMENT OF THE REQUIREMENTS
FOR THE DEGREE OF
DOCTOR OF PHILOSOPHY

Yang Wang

September 2007

I certify that I have read this dissertation and that, in my opinion, it is fully adequate in scope and quality as a dissertation for the degree of Doctor of Philosophy.

Kincho H. Law
(Principal Advisor)

I certify that I have read this dissertation and that, in my opinion, it is fully adequate in scope and quality as a dissertation for the degree of Doctor of Philosophy.

Jerome P. Lynch
(Co-advisor)

I certify that I have read this dissertation and that, in my opinion, it is fully adequate in scope and quality as a dissertation for the degree of Doctor of Philosophy.

Anne S. Kiremidjian

I certify that I have read this dissertation and that, in my opinion, it is fully adequate in scope and quality as a dissertation for the degree of Doctor of Philosophy.

Jack W. Baker

Approved for the University Committee on Graduate Studies:

Abstract

Structural health monitoring and control have attracted much research interest over the last few decades. With recent advances in wireless communication technology, wireless networks can potentially offer a low-cost alternative to traditional cable-based sensing and control systems. Another advantage of a wireless system is the ease of relocating sensors and controllers, thus providing a flexible and reconfigurable system architecture. In the first stage of this research, a prototype wireless structural sensing system is developed. This integrated hardware and software system is designed and implemented using low-cost off-the-shelf electronic components. Hardware drivers, data streaming protocols, and various computational algorithms (such as the Fast Fourier Transform and auto-regressive analysis) have been successfully embedded in the wireless sensor nodes. Operating deflection shape analysis of bridges spanning hundreds of feet has been successfully carried out using the high-quality sensor data collected by the wireless system.

The functionality of the wireless structural sensing system is extended to support feedback structural control. Hardware and software interfaces are designed so that the wireless sensing units are capable of processing real-time sensor data, making control decisions, and commanding structural actuators. The wireless structural feedback control system has been successfully validated using a half-scale three-story laboratory structure instrumented with magnetorheological dampers. Provided the range and bandwidth

constraints of wireless communication technologies, centralized control architectures are difficult to implement in a wireless control system. As a result, also validated during the experimentation is the potential of applying decentralized control architectures, in which an actuator only requires data from neighboring sensors for control decisions. Numerical simulations have been conducted to further evaluate the feasibility of applying decentralized wireless control for large-scale building structures.

Acknowledgments

The completion of this thesis would have been impossible without the great support from my family in China. Their unconditional love and encouragement from the distance have sustained me and enabled my every accomplishment over the years.

I would like to express my profound gratitude to my advisor, Prof. Kincho H. Law, and my co-advisor, Prof. Jerome P. Lynch, for their continuous commitment, guidance, and support. It has been a great privilege for me to share their passion and insights in research. I would like to extend my gratitude to my dissertation committee, Prof. Anne S. Kiremidjian and Prof. Jack W. Baker, for their advice, criticism, and recommendations. I also want to thank Prof. John M. Pauly for chairing my oral defense on such short notice.

Many other people contributed to the development of this research. Prof. Chin-Hsiung Loh, Mr. Kung-Chun Lu, and Dr. Pei-Yang Lin at National Taiwan University provided generous support for conducting the shake table experiments at NCREE, Taiwan. I would like to express my gratitude to Professors Chung-Bang Yun and Jin-Hak Yi from the Korea Advanced Institute of Science and Technology (KAIST), who kindly provided access for the Geumdang Bridge tests. I would also like to express my gratitude to Prof. Ahmed Elgamal and Dr. Michael Fraser of the University of California, San Diego, for their generous assistance throughout the field validation tests at Voigt Bridge. I want to thank Dr. Charles Farrar at Los Alamos National Laboratory and Prof. Hoon Sohn at the

Korea Advanced Institute of Science and Technology, for their advice and encouragement through the last few years, and for generously providing the DIAMOND modal analysis software package.

During this study, I have received valuable instruction and advice on electronic design from Prof. Ed Carryer in the Mechanical Engineering Department at Stanford University. I learned about modern system control and received insightful opinions on optimal structural control from Prof. Sanjay Lall in the Department of Aeronautics and Astronautics at Stanford University. Members in Prof. Jerome Lynch's group at the University of Michigan, including R. Andrew Swartz, Kenneth J. Loh, Tsung-Chin Hou, and Andrew Zimmerman, have greatly contributed to the validation tests and further development of the wireless sensing and control system presented in this thesis. I appreciate the generous assistance from the individuals acknowledged above.

I am grateful to the members of the EIG (Engineering Informatics Group) at Stanford University, including Amy Askin, Chin Pang Cheng, Jim Cheng, Chuck Han, Charles Heenan, Shawn Kerrigan, Gloria Lau, Bill Labiosa, David Liu, Hyun Woo Park, Arvind Sundararajan, Pooja Trivedi, Jiayi Pan, Xiaoshan Pan, Jun Peng, Haoyi Wang, Jie Wang, and Li Zhang, for helping me with various aspects of my research and life. The remarkable diversity of the research in the EIG motivated and assisted me in the highly interdisciplinary research involved in this thesis.

I am grateful to my friends in the John A. Blume Earthquake Engineering Center, and to many other friends at Stanford University. I would like to especially thank Krishnan Nair, Renee Lee, and Ajay Rajasekharan, who have truly been my extended family at Stanford. My fondest memories of Stanford would have been different without them.

This research was supported in part by a Stanford Graduate Fellowship sponsored by the Office of Technology Licensing at Stanford University. I would like to thank Ms. Patricia Cook for her efficient management of my fellowship program. This research is also supported in part by NSF Grant Number CMS-9988909.

Table of Contents

List of Tables

List of Figures

Chapter 1

Introduction

1.1 Background

Ensuring the safety of civil structures, including buildings, bridges, dams, tunnels, and others, is of utmost importance to society. In recent years, structural health monitoring (SHM) and control technologies have attracted much interest because of their great potential to monitor and maintain the safety of civil structures. Structural health monitoring involves recording structural behavior with various types of sensing devices, and evaluating structural safety condition using certain damage diagnosis or prognosis approaches (Chang*, et al.* 2003, Farrar*, et al.* 2003, Sohn*, et al.* 2003). On the other hand, structural control utilizes passive and active devices to apply forces to the structure or to introduce appropriate changes in the mass, damping, and stiffness properties of the structure, so that excessive structural responses can be mitigated during earthquakes or strong winds (Yao 1972, Soong 1990, Housner*, et al.* 1997, Spencer and Nagarajaiah 2003). Concurrent developments in many engineering fields, notably electrical engineering, mechanical engineering, material science, and computer science are offering many exciting opportunities for structural health monitoring and control applications.

Structural monitoring or control requires the installation of sensors and/or controllers to measure the response of a structure. In order to transfer real-time information in a structural monitoring or control system, coaxial cables are normally deployed as the primary communication link. While wired communication represents a reliable dedicated communication link, cable installation can be time consuming and costs can exceed a few thousand dollars per sensing channel (Çelebi 2002). Large-scale structures, such as long-span cable-stayed bridges, could easily require hundreds, if not thousands of sensors; such dense sensor networks would require miles of cables. To eradicate the high cost incurred in the use of cables, wireless systems could serve as a viable alternative. Wireless communication standards, such as Bluetooth (IEEE 802.15.1), Zigbee (IEEE 802.15.4), and Wi-Fi (IEEE 802.11b), are now mature and reliable technologies widely adopted in many industrial applications (Cooklev 2004). This thesis explores the viability of developing a wireless sensing and control system for applications to civil structures. This section provides a brief review of the application of wireless communication in structural health monitoring, and the current state-of-practice in structural control.

1.1.1 Wireless Structural Monitoring

As civil structures are continuously subject to loads and other environmental effects, the condition of the structure may deteriorate over time. For example, more than half of the bridges in the United States were built before the 1940's, and nearly 42% of them were reported to be structurally deficient and below established safety standards (Stallings, *et al.* 2000). To protect the public from unsafe bridge structures, current U.S. federal requirements necessitate local transportation authorities to visually inspect the entire inventory of well over 580,000 highway bridges biannually (Chase 2001). An inherent drawback of visual inspections is that they only consider damage that is visible on the surface of the structure; damage located below the surface often remains elusive to inspectors. Furthermore, bridge inspections can be subjective. For example, a recent

study by the U.S. Federal Highway Administration (FHWA) quantified the reliability of visual inspections; their findings include wide variability in condition ratings assigned by trained inspectors to an intentionally damaged bridge (Moore, *et al.* 2001). With visual inspections both costly and labor intensive, low-cost sensing systems that can quantitatively assess the integrity and remaining life of a structure are needed (Liu, *et al.* 2006).

As a complimentary approach and promising alternative to visual structural inspections, structural health monitoring (SHM) systems have been proposed to predict, identify, and locate the onset of structural damage (Doebling, *et al.* 1998, Chang, *et al.* 2003). A four-step paradigm for structural health monitoring has been identified (Sohn, *et al.* 2003): (1) operational evaluation, (2) data acquisition, fusion, and cleansing, (3) feature extraction and information condensation, and (4) statistical model development for feature discrimination (Figure 1.1). In SHM systems, smart sensor technologies are employed to assist in identifying subtle structural abnormality based on measured structural response parameters (Farrar, *et al.* 2003). Various types of structural sensors, including accelerometers, displacement transducers, strain gages, and thermometers, can be deployed to provide valuable real-time information about the behavior of a structure or its environmental conditions.

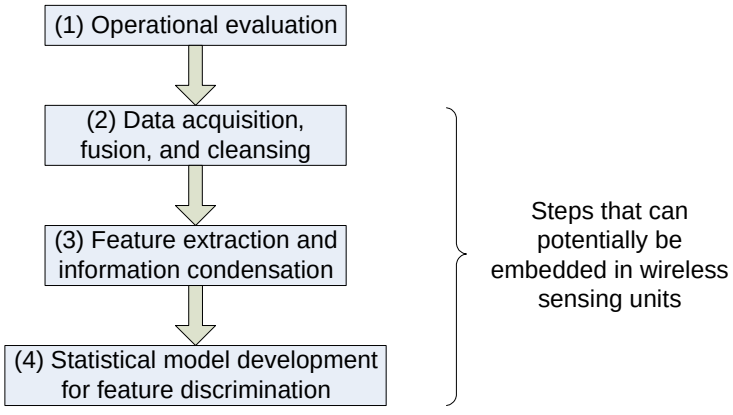

Figure 1.1 A four-step paradigm for structural health monitoring (Sohn, *et al.* 2003)

A necessary element of a SHM system is the data acquisition (DAQ) system used to collect sensor measurements and to store the data in a centralized location. Current commercial DAQ systems designed for permanent installation or for short-term vibration tests employ cables to transmit sensor data to the central data repository. By running cables between sensors and the data server, traditional DAQ systems suffer from high installation costs in terms of both time and money. Installing extensive lengths of cables can consume over 75% of the total SHM system installation time (Straser and Kiremidjian 1998). In the U.S., the cost of installing a typical structural monitoring system in buildings can exceed a few thousand dollars per sensing channel (Çelebi 2002). As structural size grows and the number of sensing nodes in the system rises, the installation cost and time for wired systems increase significantly. For example, over 1000 sensors have been instrumented in the three major bridges in Hong Kong (Tsing Ma Bridge, Kap Shui Mun Bridge, and Ting Kau Bridge). The wired structural sensing system consumed 36 km of copper cable and 14 km of fiber optic cable; furthermore, the installation took over one year (Solomon, *et al.* 2000).

Recent developments in the fields of microelectromechanical systems (MEMS) and wireless communications have introduced new opportunities to reduce the installation costs of DAQ systems (Akyildiz, *et al.* 2002, Warneke and Pister 2002). MEMS technology has led to the development of sensors that are low-cost, low-power, compact, and easy to install. Wireless technology allows for transmitting sensor measurements without the need for cables. The use of wireless communications as a means for eradicating cables within a structural monitoring system has been demonstrated by Straser and Kiremidjian (1998). Their work illustrated both the feasibility and the cost-effectiveness of wireless SHM systems. With respect to the architectural design of wireless SHM systems, Kottapalli, *et al.* (2003) proposed a two-tiered wireless sensor network topology that especially addresses the power consumption, data rate, and communication range limitations of current wireless monitoring systems. Lynch *et al.* (2004a) explored further the concept of embedding damage identification algorithms directly into wireless sensing units and harnessing the computational resources of these

devices to execute data interrogation algorithms. The embedment of engineering algorithms within the wireless sensing units serves as a means of reducing power-consuming wireless communications, and greatly improves the scalability of the system. As shown in Figure 1.1, not only can the data acquisition step in a SHM system, but also the feature extraction and discrimination steps can potentially be embedded in a distributed network of wireless sensing nodes. Many other research efforts in developing wireless sensing platforms for structural health monitoring have been reported in the literature (Hill 2003, Arms, *et al.* 2004, Glaser 2004, Mastroleon, *et al.* 2004, Ou, *et al.* 2004, Shinozuka, *et al.* 2004, Spencer, *et al.* 2004, Kling, *et al.* 2005, Wang, *et al.* 2005, Kim, *et al.* 2007). A comprehensive review of wireless sensors and their adoption in structural health monitoring has been provided by Lynch and Loh (2006).

Compared to traditional wire-based systems, wireless structural monitoring systems have a unique set of technical challenges. First, wireless sensing units will most likely employ batteries, which represent a limited supply of energy. It is probable that batteries will be used in the short-term because current power harvesting techniques cannot yet provide a reliable, convenient, and low-cost solution for powering typical wireless structural sensors (Churchill, *et al.* 2003, Roundy 2003, Sodano, *et al.* 2004). In terms of power consumption, the wireless transceiver often consumes the greatest amount of energy than any of the other hardware component in a wireless sensing unit (Lynch, *et al.* 2004a). As a result, local data processing that balances data transmission and energy consumption is desirable. Second, the transmission of data in a wireless network is inherently less reliable than in cable-based networks; reliability decreases as the communication range becomes farther. Third, the limited amount of wireless bandwidth usually impedes high-speed real-time data collection from multiple sensors. Fourth, time delays encountered during data transmission between different wireless sensing units due to sensor blockage or clock imprecision need to be thoroughly considered (Lei, *et al.* 2005). These technical challenges in wireless structural health monitoring will continue to be forefront issues addressed by researchers in the near future.

1.1.2 Structural Control

During the past three decades, significant development has been achieved in the field of structural control to mitigate excessive structural responses during earthquakes or strong winds (Soong and Spencer 2002, Chu, *et al.* 2005). Structural control systems can be categorized into three major types: (a) passive control (e.g. base isolation), (b) active control (e.g. active mass dampers), and (c) semi-active control (e.g. semi-active variable dampers). Passive control systems entail the use of passive energy dissipation devices to control the response of a structure without the use of sensors, controllers, and actuators. Active control systems use large-capacity actuators for direct application of control forces. In a semi-active control system, control devices are used for indirect application of control forces. Semi-active control is currently preferred over active control because it can achieve at least an equivalent level of performance but it consumes orders of magnitude less power and provides higher levels of reliability. Examples of semi-active actuators include active variable stiffness (AVS) devices, semi-active hydraulic dampers (SHD), electrorheological (ER) dampers, and magnetorheological (MR) dampers (Housner, *et al.* 1997). Additional advantages associated with semi-active control include adaptability to real-time excitation, inherent bounded input / bounded output (BIBO) stability, and invulnerability to power failure. The shift from active to semi-active control devices, which are smaller, less costly and more energy-efficient, will lead to the potential deployment of larger quantities of devices in a structure.

Due to the rapid development in structural control research, many full-scale control systems have been installed in actual structures. It has been reported that from 1989 to 2003, 49 structural control systems were installed in buildings and towers, out of which 43 were in Japan (Chu, *et al.* 2005). For example, a full-scale control system using semi-active hydraulic dampers (SHD) was installed in the Kajima Shizuoka Building in Shizuoka, Japan (Kurata, *et al.* 1999). A total of eight SHD dampers were adopted to control a 5-story building. Each damper comprises of a control valve, a check valve and an accumulator. Using 70W of power, the SHD damper provides an adjustable force of

up to 1000kN. Recently, tens or hundreds of SHD devices have been installed in some tall skyscrapers in Japan (Spencer and Nagarajaiah 2003). In another example, 312 magnetorheological (MR) dampers (RD-1005) from Lord Corporation, have been installed in the cable-stayed Dongting Lake Bridge for mitigating rain-wind-induced vibration of 156 cables (Ko, *et al.* 2002). To control the cable vibration, two MR dampers are diagonally installed within a plane normal to the cable. The damper cylinder houses a piston, a magnetic circuit, an accumulator, and 50 ml of MR fluid. Each MR damper can generate a controllable force ranging from 50 N to 2500 N.

When the scale of the structure is large, centralized control systems have high instrumentation cost, are difficult to reconfigure, and potentially suffer from single-point failure at the controller. Decentralized control strategies may potentially resolve some of these difficult issues (Sandell, *et al.* 1978, Siljak 1991). Studies have been reported for decentralized control in structural engineering. Examples include control of cable-stayed bridges (Volz, *et al.* 1994, Cao, *et al.* 2000, Luo, *et al.* 2002) and control of building structures (Zhang and Iwan 2002a, Zhang and Iwan 2002b). Typically, the interactions between dynamically coupled subsystems are treated as unknown disturbances and individual controller is each designed as a single-input, single-output (SISO) subsystem. Since these decentralized control algorithms treat the interconnections between subsystems as unknown disturbances, the objective of each decentralized controller is to improve local control performance, which generally does not result in globally optimal control. If the controller of a subsystem fails to operate properly during a dynamic excitation, this subsystem may experience disadvantageous situations because its neighboring subsystems focus on their own control performance, without paying attention to the malfunctioning subsystem. The system architecture of this type of control strategy is illustrated in Figure 1.2(a), i.e. the controller of each subsystem requires local sensor data only, and the objective of each controller focuses on controlling the local subsystem.

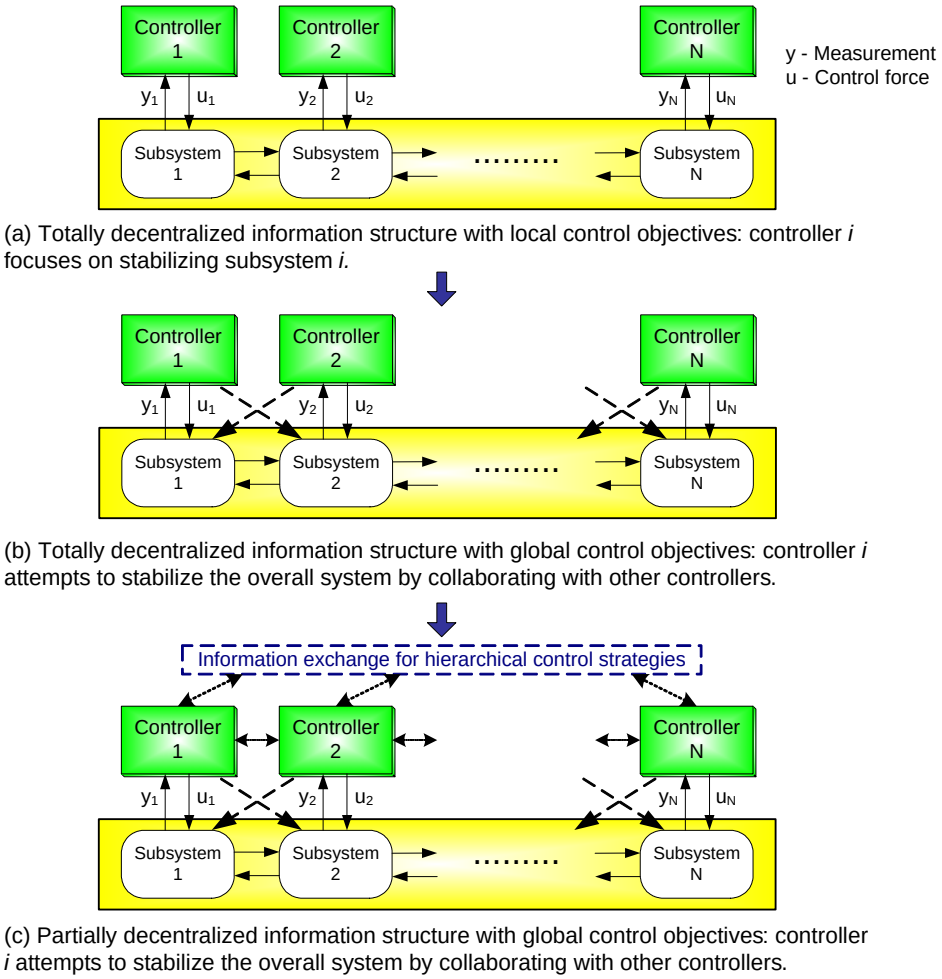

(a) Totally decentralized information structure with local control objectives: controller *i* focuses on stabilizing subsystem *i*.

(b) Totally decentralized information structure with global control objectives: controller *i* attempts to stabilize the overall system by collaborating with other controllers.

(c) Partially decentralized information structure with global control objectives: controller *i* attempts to stabilize the overall system by collaborating with other controllers.

Figure 1.2 Different combinations of decentralized information structures and control objectives

Another approach for decentralized structural control is to estimate global (or subsystem) state information (Dyke, *et al.* 1996, Mutambara 1998, Yook, *et al.* 2002, Lynch and Tilbury 2005). For example, distributed Kalman filters can be designed for each decentralized subsystem to estimate the global structural state using local sensor data. With the global state information available, the controller is designed to optimize the overall system performance. The difficulty of this control strategy lies in the estimation accuracy which is impaired by the unavailability of global sensor data. While estimation can be improved by sharing (estimated or measured) information or control decisions,

many issues are to be addressed to fully realize the practical implementations of these theoretical studies. For example, appropriate selections of what information subsystems share with each other must be made. Furthermore, inter-subsystem information sharing requiring additional communication among subsystems may result in significant time delay in the feedback loop. In summary, a decentralized control strategy using distributed Kalman filters can be implemented according to the system architecture shown in Figure 1.2(b), given that communication between distributed Kalman estimators is not allowed. Alternatively, it can be implemented according to the system architecture shown in Figure 1.2(c) by allowing some communication between subsystems. For the architectures shown in Figure 1.2(b) and Figure 1.2(c), different subsystems controllers collaborate with each other to achieve a control strategy that is globally optimal.

A structural control system that is linear time invariant (LTI) can be schematically illustrated in Figure 1.3 (Doyle 1983). The structure and the controller are represented as two inter-connected systems. Inputs to the structural system include the disturbances and the control forces. Both dynamic excitation (such as excitations from earthquakes or strong winds) and sensor noises can be modeled as disturbances. Outputs from the structural system include the structural response and sensor measurements. For the controller, the input is the sensor measurements while the output is the control forces. The objective governing the design of the control system is to find a controller that generates control forces according to the sensor measurements, so that structural response can be mitigated. For such a control system, sensors need to be deployed in the structure to collect structural response data during dynamic loading. Response data is then fed into controllers to determine required actuation forces and to apply control commands to the system actuators. Commanded by control signals, actuators apply control forces intended to mitigate the undesirable structural responses. In traditional control systems, coaxial wires are used to provide communication links between sensors, actuators and controllers. With the rapid emergence of wireless communication and embedded computing technologies, a natural extension of the wireless sensing technology is to explore its applicability in semi-active or active control systems to eliminate the cables

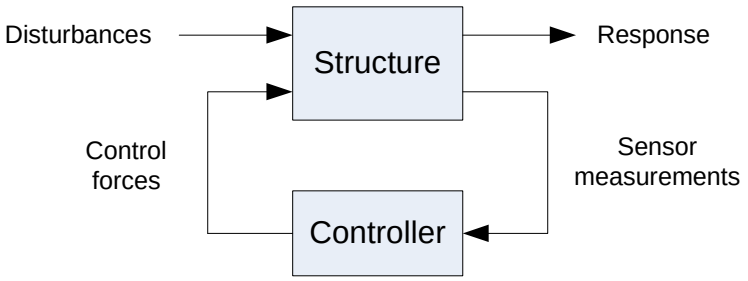

Figure 1.3 Schematic of a structural control system

associated with traditional control systems. If successful, wireless communication may result in substantial reduction in the cost and installation time of future control systems.

The development of autonomous, self-sensing and self-actuating devices for structural monitoring and control applications poses as an intriguing, interdisciplinary research challenge in structural and electrical engineering. Researchers have begun to incorporate actuation interface in wireless sensors for damage detection applications (Lynch, *et al.* 2004b, Grisso, *et al.* 2005, Liu, *et al.* 2005). For example, actuation interfaces can be used to induce stress waves in structural components by "active" sensors (e.g. PZT pads). Corresponding strain responses to propagating stress waves are examined to infer the health of the component. An integrated actuation interface can also be used to potentially operate actuators for structural control. Casciati and Rossi (2003) illustrated the use of wireless communication links within a fuzzy logic control system. In their experimental work, one fuzzy module collects data from accelerometers mounted on the floors of a 3-story test structure and the shake table. The fuzzy module sends the acceleration data to a second fuzzy module through a wireless communication link. The second module then makes control decisions for an active mass damper installed on the top of the test structure. In another research project, Seth, *et al.* (2005) assessed the feasibility of using wireless communications to eliminate the need for cables in a real-time structural control system. Performance of the decentralized control system was evaluated in a simulation environment using a numerical model of a semi-actively controlled building. Outside of

structural engineering, a few examples of wireless feedback control systems have been reported. Eker *et al.* (2001) has investigated the feasibility of using Bluetooth wireless communication for closed-loop control of an inverted pendulum system. Ploplys, *et al.* (2004) examined the control of an inverted pendulum with the feedback loop completed by a 802.11b wireless network.

1.2 Research Objectives

The objective of this research is to design, implement, and validate a decentralized wireless structural sensing and control system. The first stage of this research involves the development of a wireless structural sensing system (Wang, *et al.* 2005). The system includes one wireless server and multiple wireless sensing units. Each unit consists of a sensing interface to which analog sensors can be attached, an embedded microcontroller for data processing, and a spread spectrum wireless radio for communication. For field applications where signals collected from ambient vibrations are dominated by high noise floors, signal conditioning hardware is designed to amplify and filter the analog sensor signal. Hardware drivers, data streaming protocols, and various computational algorithms (such as the Fast Fourier Transform and auto-regressive time series models) are embedded in the wireless sensor nodes. Sophisticated engineering analyses, such as operating deflection shape analysis, can be conducted using the high-quality sensor data collected by this wireless structural sensing system. The development and validation of this wireless structural sensing system are described in this thesis.

The functionality of the prototype wireless structural sensing system is extended to support wireless feedback structural control (Wang, *et al.* 2006a). When replacing wired communication channels with wireless ones for feedback structural control, issues such as coordination of sensing and control units, communication range, time delay and potential data loss need to be thoroughly examined. Time delay due to wireless

communication will cause degradation of the real-time performance of a control system (Lynch and Tilbury 2005). The time delay problem is common for any distributed network control systems, regardless of their use of wired or wireless communication (Lian, *et al.* 2002). To resolve the difficulties associated with limited communication ranges and long communication latencies, decentralized control strategies may be adopted. In decentralized control, the control problem is divided into a collective set of smaller, distributed control sub-systems. Controllers assigned to a subsystem only require local and neighboring sensor data to make control decisions. In a wireless network, this leads to reduced use of the communication channel and results in higher control sampling rates. Shorter communication ranges may also result in more reliable wireless data transmission. The control decisions can be executed in parallel using multiple wireless sensors in decentralized control architectures. However, decentralized control may only achieve sub-optimal global control performance when compared to centralized control solutions, because each subsystem only has local and neighboring sensor information from which control decisions are made. This thesis intends to explore the feasibility of applying decentralized wireless control to civil structures.

In order to build a wireless feedback control system, numerous hardware and software interfaces must be designed so that wireless sensing units are capable of processing real-time sensor data, making control decisions, and commanding structural actuators. The wireless structural feedback control system is validated using a 3-story laboratory structure instrumented with magnetorheological dampers (Wang, *et al.* 2007a). Also to be validated in the experiments is the potential of applying decentralized optimal structural control strategies, in which an actuator only requires data from neighboring sensors to make control decisions. In this study, a decentralized structural control algorithm based on linear quadratic regulator (LQR) control design has been developed. The information structure in the wireless structural control system can be translated into shape constraints on the LQR gain matrix according to the architectures illustrated in Figure 1.2(b) or Figure 1.2(c). These constraints reflect the communication requirements among neighboring sensors (or subsystems). This thesis describes the design and

validation of the wireless structural control system, as well as the decentralized structural control algorithms developed along the LQR control design principles. Theoretical and practical issues involved in decentralized control with communication time delays are also examined.

1.3 Thesis Outline

This thesis first introduces the hardware and software building blocks of a distributed wireless structural sensing and control network (i.e. the wireless sensing and actuation units). A wireless structural sensing system is first constructed using the wireless sensing units, and validated through both laboratory and field tests. Next, the wireless sensing units are used to construct a wireless structural control network that is validated through laboratory experiments. A decentralized structural control algorithm that considers the effects of feedback time delay is developed and incorporated in the wireless structural control system. In addition to experimental validation, numerical simulations are conducted to examine the effects of control decentralization and wireless communication delays.

The thesis is organized as follows:

- Chapter 2 introduces the hardware and software design of the wireless sensing and actuation units. Hardware modules that provide functionalities for communication, sensing, computing, and actuation will be described. This chapter also introduces the three-layer embedded software architecture that includes the microcontroller peripherals, system management modules, and application software routines.

- Chapter 3 describes the design of a wireless structural sensing system and the validation tests conducted on this system. The communication protocol between

the wireless sensing units and the wireless server is designed to ensure robust system performance (i.e. no data loss). The results from a laboratory test using a 3-story steel structure and two field tests upon actual bridges are presented. Data collected by the wireless sensing system is compared with data collected by baseline wired systems. Validation of the embedded computing capability of the wireless sensing units is also conducted. For the two bridge structures spanning hundreds of feet, the wireless acceleration data sets are used to conduct operating deflection shape analysis.

- Chapter 4 describes the design of a wireless structural control system, the development of decentralized structural control algorithms, and the experimental and simulation results for decentralized wireless structural control. First, the architecture and implementation of the decentralized wireless structural control system is introduced. Then a heuristic decentralized structural control algorithm is proposed and validated by numerical simulations. Laboratory validation experiments of the wireless structural control system using a 3-story steel frame instrumented with three magnetorheological (MR) dampers are then presented. Finally, the performance of the decentralized feedback control strategies for large-scale structures is investigated through numerical simulations with a 5-story and a 20-story building structure.

- Chapter 5 serves as a summary to the thesis and discusses possible future research directions.

Chapter 2

Hardware and Software Design of the Wireless Sensing and Actuation Unit

Wireless sensing and actuation units represent fundamental building blocks of a wireless structural sensing and control system. For the prototype system, each wireless unit is designed to be able to collect sensor data, communicate with other units, perform engineering analyses, and issue commands to structural actuators. Through the wireless communication channel, these individual units form an integrated sensing and/or control network. This chapter describes in detail the hardware and software design of the prototype wireless sensing and actuation unit for civil structural applications. Section 2.1 describes the hardware modules that provide communication, sensing, computing, and actuation functionalities. Section 2.2 introduces the embedded software for the microcontroller of the proposed wireless unit. The embedded software is organized in a three-layer architecture which implements functions to support the microcontroller peripherals, system management modules, and application software routines.

2.1 Hardware Design of the Wireless Sensing and Actuation Unit

The prototype wireless unit is designed in such a way that the unit can serve as either a sensing unit (i.e., a unit that collects data from sensors and wirelessly transmits the data), an actuation unit (i.e., a unit that calculates control forces and issue commands to the actuators), or a unit for both sensing and actuation. This flexibility is supported by an integrated hardware design of the wireless sensing and actuation unit. Figure 2.1 shows the overall hardware design of the prototype wireless sensing unit and two optional off-board auxiliary modules for conditioning analog sensor signals and generating actuation signals. The functional diagram of the proposed wireless sensing unit is shown in the top part of the figure. The wireless sensing unit consists of three functional modules: sensor signal digitization, computational core, and wireless communication. The auxiliary sensor signal conditioning module (shown in the bottom part of the figure) assists in amplifying, filtering, and offsetting analog sensor signals prior to digitization. The auxiliary actuation signal generation module also offers an interface through which the wireless unit sends analog control commands to structural actuators.

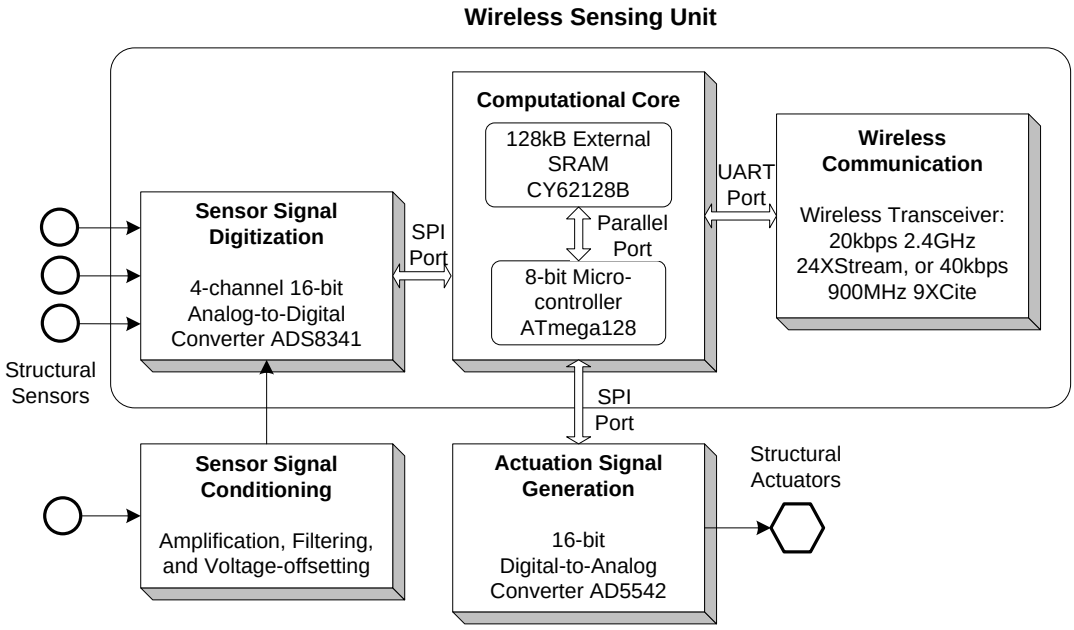

Figure 2.1. Functional diagram detailing the hardware design of the wireless sensing and actuation unit

The prototype wireless sensing and actuation unit is judiciously designed for applications in civil structures. Some of the main design objectives of this prototype wireless sensing and actuation unit are: (1) low-power consumption while achieving long communication ranges with robust communication protocols for reliable data acquisition, (2) accurate time-synchronized wireless data collection from a heterogeneous array of analog sensors at a reasonable sampling rate suitable for civil structural applications, (3) high-precision analog-to-digital conversion, (4) considerable local data processing capability at the wireless sensing units to reduce energy consumption and to enhance system scalability, (5) accommodation of peer-to-peer communication among wireless units for collaborative distributed data analysis, and (6) an actuation interface that accommodates a variety of structural actuators. The key parameters of the prototype wireless sensing and actuation unit are summarized in Table 2.1. As shown in the table, the wireless unit provides deployment flexibility by using one of two different types of wireless transceivers: 900MHz MaxStream 9XCite and 2.4GHz MaxStream 24XStream. The rest

of this section describes in detail the hardware design of the wireless sensing and actuation unit, including the design for the auxiliary sensor signal conditioning and the actuation signal generation modules.

Table 2.1. Key performance parameters of the wireless sensing and actuation unit

Design Parameter	**Specification**	
Computing Core		
Microcontroller	8-bit RISC[1] architecture, up to 16MIPS[2] throughput at 16MHz	
Flash Memory	128K bytes	
Internal SRAM[3]	4K bytes	
External SRAM	128K bytes	
EEPROM[4]	4K bytes	
Power Consumption	30mA active, 55μA standby	
Wireless Transmission	*9XCite*	*24XStream*
Operating Frequency	ISM 902-928 MHz	ISM 2.4000 - 2.4835 GHz
Data Transfer Rate	38.4 kbps	19.2 kbps
Communication Range	Up to 300' (90m) indoor, 1000' (300m) at line-of-sight	Up to 600' (180m) indoor, 3 miles (5km) at line-of-sight
Power Consumption	55mA transmitting, 35mA receiving, 20μA standby	150mA transmitting, 80mA receiving, 26μA standby
Sensing Interface		
Sampling Precision and Rate	16bit, Up to 100kHz	
Analog Sensor Channels	4	
Actuation Interface		
Actuation Precision and Rate	16bit, Up to 1MHz	
Analog Output Channel	1	
Others		
Unit Size	10.2cm × 6.5cm × 4.0cm	
Unit Cost	About $150 using 9XCite	About $250 using 24XStream

[1] RISC: reduced instruction set computer.

[2] MIPS: million instructions per second.

[3] SRAM: static random access memory.

[4] EEPROM: electrically erasable programmable read-only memory.

2.1.1 Wireless Sensing Unit

As shown in Figure 2.1, the wireless sensing unit consists of three functional modules: sensor signal digitization, computational core, and wireless communication. The sensing interface converts analog sensor signals into digital data which is then transferred to the computational core through a high-speed Serial Peripheral Interface (SPI) port. Besides a low-power 8-bit Atmel ATmega128 microcontroller, external Static Random Access Memory (SRAM) is integrated with the computational core to accommodate local data storage and analysis. The computational core communicates with a wireless transceiver through a Universal Asynchronous Receiver and Transmitter (UART) interface. This subsection describes the three individual functional modules, analyzes the power consumption performance of the complete wireless sensing unit, and presents the final hardware packaging of the wireless sensing unit.

2.1.1.1 Sensor Signal Digitization Module

The main component of the sensor signal digitization module is a 4-channel 16-bit analog-to-digital (A/D) converter, Texas Instruments ADS8341. Each wireless sensing unit can accommodate signals from a heterogeneous set of up to four analog structural sensors (e.g. accelerometers, velocity meters, strain gages, among others). The 16-bit A/D resolution is sufficient for most applications in structural sensing. One requirement from the ADS8341 A/D converter is that the sensor signal should be between 0 and 5V. The highest sampling rate supported by this A/D converter is 100 kHz, which is much higher than the sampling frequency typically needed for monitoring civil structures. This rate determines that each sampling execution takes only 10 μs. Therefore, the A/D conversion can be finished swiftly through the timer interrupt service of the microcontroller (ATmega128) without disrupting the execution of wireless communication or data processing programs. This means that it is possible for the wireless sensing unit to keep its wireless communication module functioning, even when

the unit is sampling data from the sensing interface. Continuous wireless sensor data collection can thus be supported by this prototype wireless sensing system.

2.1.1.2 Computational Core

The computational core of the wireless sensing unit is responsible for executing embedded software instructions as required by an application. A low-cost 8-bit microcontroller, Atmel ATmega128, is selected for this purpose. The key objective for this selection is to balance the power consumption and hardware cost with the computation power needed by software applications (e.g. data interrogation algorithms). Running at 8MHz, the ATmega128 consumes about 15mA when it is active. Considering the energy capacity of normal batteries in the market, which is usually a few thousand milliamp-hours (mAh), normal AA batteries can easily support an active ATmega128 for hundreds of hours. If running in a duty cycle manner, with active and sleep modes interleaved, the ATmega128 microcontroller may sustain even longer before battery replacement is needed.

The ATmega128 microcontroller contains 128kB of reprogrammable flash memory for the storage of embedded software; based on laboratory and field experiments, this is sufficient for the incorporation of a wide variety of structural monitoring and control algorithms. The microcontroller also contains 4kB of nonvolatile Electronically Erasable Programmable Read-Only Memory (EEPROM) for data storage. One Serial Peripheral Interface (SPI) and two Universal Asynchronous Receiver and Transmitter (UART) interfaces are provided by the ATmega128 to facilitate communication with other hardware components. The timer and interrupt modules of the ATmega128 are employed to execute routines that need to be precisely timed, e.g. sampling sensor data or applying actuation signal on specified time intervals.

The microcontroller also contains 4kB Static Random Access Memory (SRAM) for storing stack and heap variables, which as it turns out, is often insufficient for the

execution of embedded data interrogation algorithms. To address this issue, an external 128kB memory chip, Cypress CY62128B, is incorporated within the wireless sensing unit design. Furthermore, hardware and software procedures are implemented to bypass the 64kB memory address space limitation of the ATmega128, to ensure that the full 128kB address space of the CY62128B can be utilized. The external memory is sufficient for executing many sophisticated damage identification algorithms on a large quantity of sensor data.

2.1.1.3 Wireless Communication Module

The wireless communication module provides an interface for the exchange of data with other wireless units. Sufficient communication reliability, range, and data transfer rate are needed to employ the wireless units in civil structures. On the other hand, due to stringent battery power constraints, the wireless module (which can be the most power-consuming component of a wireless sensing unit) should not be allowed to consume too much battery power while active. Therefore, certain trade-offs must be achieved to balance performance requirements with power consumption. Wireless frequency allocation regulated by the government is another factor that should be considered when selecting wireless transceivers. Operating in the 2.4GHz international ISM (Industrial, Science, and Medical) band, the 24XStream transceiver may be used in most countries in the world. However, the 9XCite transceiver may only be used in countries where the 900MHz band is open for unlicensed public usage, such as in the U.S., Canada, Mexico, and South Korea.

The wireless sensing unit is designed to be operable with two different wireless transceivers: 900MHz MaxStream 9XCite and 2.4GHz MaxStream 24XStream. Pin-to-pin compatibility between these two wireless transceivers makes it possible for the two modules to share the same hardware connections within the wireless unit design. Because of the different data rates, the embedded software implementation for wireless units using different transceivers is slightly different. This dual-transceiver support affords the

wireless sensing and actuation unit to be usable in different countries, and to have more flexibility in terms of data transfer rate, communication range, and power consumption. Table 2.2 summarizes the key performance parameters of the two wireless transceivers. As shown in the table, the data transfer rate of the 9XCite is double that of the 24XStream, while 24XStream provides a longer communication range but consumes much more battery power. Both transceivers support peer-to-peer and broadcasting communication modes that allow flexible information flow in the wireless sensor network.

Table 2.2. Key characteristics of the wireless transceivers

Specification	9XCite	24XStream
Operating Frequency	ISM 902-928 MHz	ISM 2.4000 – 2.4835 GHz
Channel Mode	7 frequency hopping channels, or 25 single frequency channels	7 frequency hopping channels
Data Transfer Rate	38.4 kbps	19.2 kbps
Communication Range	Up to 300' (90m) indoor, 1000' (300m) at line-of-sight	Up to 600' (180m) indoor, 3 miles (5km) at line-of-sight
Supply Voltage	2.85VDC to 5.50VDC	5VDC (±0.25V)
Power Consumption	55mA transmitting, 35mA receiving, 20μA standby	150mA transmitting, 80mA receiving, 26μA standby
Module Size	1.6" × 2.825" × 0.35" (4.06cm × 7.17cm × 0.89 cm)	1.6" × 2.825" × 0.35" (4.06cm × 7.17cm × 0.89 cm)
Network Topology	Peer to peer, broadcasting	Peer to peer, broadcasting

2.1.1.4 Power Consumption

Power consumption is another important issue to consider when selecting the hardware elements of a wireless sensing unit. While power consumption of each hardware component should be minimized, it must not be done at the expense of the functionalities required by structural monitoring applications. The energy consumed by the wireless sensing unit is a function of the voltage and the amount of electrical current supplied to each component. All the hardware components are internally referenced at 5V. Using

the 9XCite wireless transceiver, the active and standby electrical current for each component of the wireless sensing unit is listed in Table 2.3. When in active mode, the wireless sensing unit collects, interrogates or wirelessly transmits sensor data. In contrast, the hardware components consume minimal amount of electrical current when they are in standby mode.

Table 2.3. Approximate current consumption of the wireless sensing unit

Component	Active Current	Standby Current
A/D converter ADS8341 (at 100 Hz)	1mA	1μA
Micro-controller ATmega128 (at 8MHz)	15mA	40μA
SRAM CY62128B	15mA	15μA
Wireless transceiver 9XCite (TX/RX)	45mA*	20μA
Support electronics	1mA	24μA
Complete wireless sensing unit	77mA	100μA

* Assuming equal time transmitting (55mA) and receiving (35mA)

The wireless transceiver consumes the greatest amount of electrical power when active (45mA x 5V = 225mW), which indicates the importance of minimizing the use of the wireless communication channel as a means of preserving battery life. The total active current of the wireless sensing unit with the wireless transceiver in operation, I_{active}, as measured by a digital multi-meter in the laboratory, is found to be 77mA. The wireless sensing unit can operate on any power source providing at least 5.2V of voltage potential. In the current prototype, five lithium AA batteries (Energizer L91), providing a total voltage of 7.5V, are used. With the total energy capacity of a single L91 AA battery, $E_{battery}$, over 2,900mAh, the fully-active continuous life expectancy of the wireless sensing unit, T_{active}, is estimated to be:

$$T_{\text{active}} = \frac{E_{\text{battery}}}{I_{\text{active}}} = \frac{2,900\text{mAh}}{77\text{mA}} = 37.7\text{hrs} = 1.57\text{days} \tag{2.1}$$

This expected active life is conservative because the estimation assumes the unit is in continuous operation at all times. However, duty cycle usage of the battery allows for the

internal cell chemistries to attain equilibrium and can thus extend batteries' life expectancies. The standby lifetime of the wireless sensing unit, $T_{standby}$, is:

$$T_{\text{standby}} = \frac{E_{\text{battery}}}{I_{\text{standby}}} = \frac{2,900\text{mAh}}{100\mu\text{A}} = 29,000\text{hrs} = 1,208\text{days} \tag{2.2}$$

In all likelihood, wireless sensing units serving as part of a comprehensive structural health monitoring system would be operated on a duty-cycle schedule. For example, units might be programmed to turn on every day for 10 minutes to measure the ambient response of the instrumented structure. If it is assumed that on each day, the system is fully active for 10 minutes for data collection and transmission, the total operation time of the wireless sensing unit unattended in the field is estimated to be:

$$\begin{aligned} T_{10\,\text{min}-\text{active}-\text{per}-\text{day}} &= \frac{E_{\text{battery}}}{E_{0.17\text{hr}-\text{active-per-day}} + E_{23.83\text{hr}-\text{standby-per-day}}} \\ &= \frac{2,900\text{mAh}}{77\text{mA}\times 0.17\text{hr/day} + 100\mu\text{A}\times 23.83\text{hr/day}} \\ &= 190\text{days} \end{aligned} \tag{2.3}$$

If the unit is active for only 5 minutes every day, the life expectancy of the unit can last about one year.

The same life expectancy analysis can be conducted for a wireless sensing unit using the 24XStream transceiver. The different life expectancy results for wireless units using 9XCite and 24XStream transceivers are summarized in Table 2.4. Since the 24XStream transceiver consumes more power than the 9XCite transceiver, the life expectancies of a wireless unit using the 24XStream transceiver are shorter than a unit using the 9XCite transceiver.

Table 2.4. Estimated life expectancy (in days) of the wireless sensing unit

Life Expectancy	Unit with 9XCite	Unit with 24XStream
T_{active}	1.57	0.82
$T_{standby}$	1208	1140
$T_{10\,\mathrm{min-active-per-day}}$	190	107
$T_{5\,\mathrm{min-active-per-day}}$	329	197

2.1.1.5 Unit Packaging

A simple two-layer printed circuit board (PCB) is designed and fabricated. As shown in Figure 2.2(a), the PCB has a dimension of 9.7cm × 5.8cm, which may be further reduced using a multi-layer circuit design. Figure 2.2(b) shows that the PCB, wireless transceiver, and batteries can be stored within an off-the-shelf weatherproof plastic container, which has the dimensions of 10.2cm × 6.5cm × 4.0cm. Each packaged unit, including the five AA batteries, weighs about 0.38 kg.

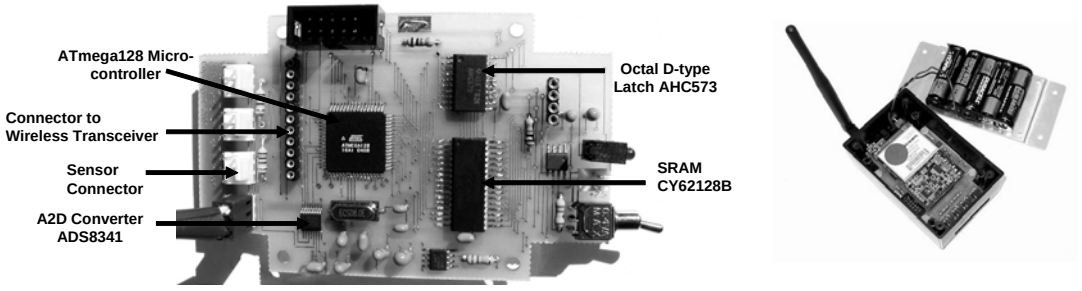

(a) PCB of the wireless sensing unit (9.7cm × 5.8 cm)

(b) Packaged unit (10.2cm × 6.5cm × 4.0 cm)

Figure 2.2. Pictures of the wireless sensing unit

2.1.2 Sensor Signal Conditioning Module

For field applications, a wireless sensing system must be capable of recording both ambient and forced structural vibrations. With ambient vibrations typically defined by small amplitudes, a high-resolution (16-bit or higher) A/D converter is normally needed by a structural sensing system. However, placement of the 16-bit ADS8341 A/D converter leaves it vulnerable to electrical noise present in the circuit. From experimental tests, the effective resolution for the A/D channels is found to be approximately 13-bit, which is likely insufficient for sampling low-amplitude vibration data in civil structures. Additionally, for the ADS8341 A/D converter, sensor signals must be within the 0 to 5V input range; hence, sensors outputting negative voltages are incompatible with the A/D converter. A signal conditioning module is thus designed to amplify signals, filter out electrical noise, and shift sensor signals within the 0 to 5V range. First, the amplified analog signal can be much less vulnerable to the quantization error of the A/D conversion; second, the anti-alias filtering eliminates the distortion artifacts resulted from low-frequency sampling to the high-frequency electrical noise; and third, the shifting functionality changes the mean value of the analog sensor signal to be around 2.5V.

Sensor signals are fed into the signal conditioning module prior to the A/D conversion, as illustrated in the lower left part of Figure 2.1. As shown in Figure 2.3(a), the filtering circuitry consists of a high-pass resistor-capacitor (RC) filter with a cutoff frequency of 0.02Hz and a low-pass fourth-order Bessel filter with a cutoff frequency of 25Hz. The linear-phase shift property of the Bessel filter ensures a constant time delay for signals in the pass band, thus maintaining the signal waveform in the time-domain. Figure 2.3(b) shows the complete signal conditioning board that includes hardware components for the filtering, offsetting, and amplification functions. In the current design, a three-position switch is mounted on the signal conditioning board, which provides three options for signal amplification factors: $\times 5$, $\times 10$, and $\times 20$.

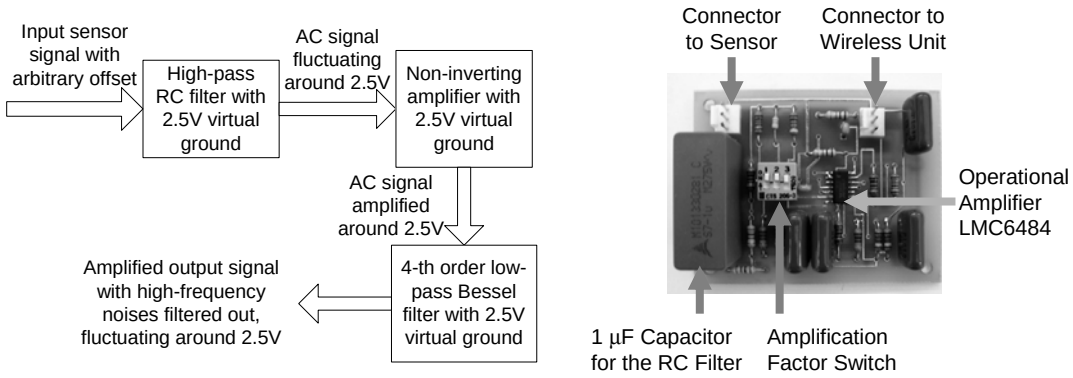

(a) Functional Diagram of the Circuits (b) PCB board (5.0cm × 6.5 cm)

Figure 2.3. Sensor signal conditioning module

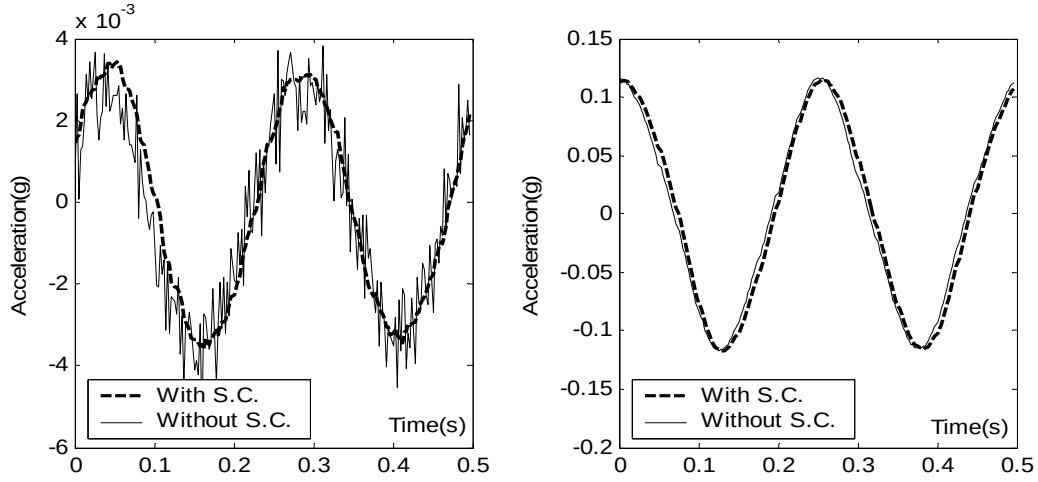

(a) Low vibration amplitude (b) High vibration amplitude

Figure 2.4. Acceleration data with and without signal conditioning (S.C.)

In order to illustrate the performance of the signal conditioning module, Figure 2.4 shows two acceleration time histories measured by two Crossbow CXL01LF1 accelerometers

placed side by side. The signal from one accelerometer is processed by the signal conditioning (S.C.) module before being fed into the A/D converter, while the signal from the other accelerometer is fed into the A/D converter directly. In this test, an amplification factor of 5 is selected for the signal conditioning module. As shown in Figure 2.4(a), when the vibration amplitude is low (about 4mg in this case), in which case the Signal-to-Noise-Ratio (SNR) is low, the sensor data with signal conditioning is much smoother than the data without signal conditioning. When the vibration amplitude is higher (about 0.1g), i.e. when the SNR is high, the difference between the data collected with and without signal conditioning is almost negligible with respect to the signal amplitude, as shown in Figure 2.4(b).

2.1.3 Actuation Signal Generation Module

A separate hardware module is designed to be connected with the wireless sensing unit, which permits the unit to generate analog voltage signals for commanding actuators. At the core of this actuation signal generation module is the single-channel 16-bit digital-to-analog (D/A) converter, the Analog Device AD5542. The AD5542 receives a 16-bit unsigned integer from the ATmega128 and converts the integer value to an analog voltage output spanning from -5 to 5V. Additional support electronics are included in the actuation signal generation module to offer stable zero-order hold (ZOH) voltage outputs at high sampling rates (1 MHz maximum). The wide voltage output range (-5 to 5V) of the actuation signal generation module, particularly the negative output range, is one of the key features of the module's design. With the wireless sensing unit designed to operate on 5V, the Texas Instruments PT5022 switching regulator is integrated in the signal generation module to convert the 5V regulated power supply into a stable -5V reference. Another auxiliary component required for the AD5542 to generate a bipolar -5 to 5V output signal is a rail-to-rail input and output operational amplifier, for which the National Semiconductor LMC6484 operational amplifier is selected. The typical slew rate of the LMC6484 is about 1.3V/μs, which means that the output voltage can swing for

a maximum of 1.3V within 1μs. This output gradient is compatible with the microsecond-level settling time of the AD5542 D/A converter. When operational, the actuation signal generation module draws about 70mA from the 5V power supply provided by the wireless sensing unit.

As shown in Figure 2.5(a), a separate double-layer printed circuit board (PCB) is designed to accommodate the D/A converter (AD5542) and its auxiliary electrical components. The actuation signal board is attached via two multi-line wires to the wireless sensor. To reduce circuit noise, two separate wires are used with one dedicated to analog signals and the other to digital signals. The analog signal cable transfers an accurate +5V reference voltage from the existing wireless sensing board to the signal generation module. The digital signal cable provides all the connections required to accommodate the serial peripheral interface (SPI) between the ATmega128 microcontroller and the AD5542. To command an actuator, a third wire is needed to connect the output of the actuation signal generation module with the structural actuator. The actuation signal generation module connected to the wireless sensing unit is shown in Figure 2.5(b).

2.2 Software Architecture of the Wireless Sensing and Actuation Unit

In order to achieve various functionalities for sensing and actuation, embedded software for the ATmega128 microcontroller is required. The embedded software can be written in a high-level programming language (such as C), compiled into binary instructions and preloaded into the nonvolatile flash memory of the microcontroller. When the wireless unit is powered on for normal operation, the microcontroller automatically starts executing the embedded instructions. The software design of the wireless sensing and actuation units follows the three-layer structure as shown in Figure 2.6. At the bottom

level are the software modules that manage the basic peripherals of the microcontroller. The middle layer consists of software modules that manage system-level functions. Application software modules for structural monitoring and control are implemented as the top level layer.

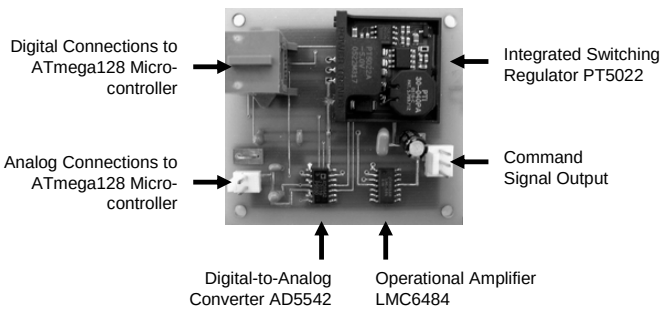

(a) PCB board (5.5cm × 6.0 cm)

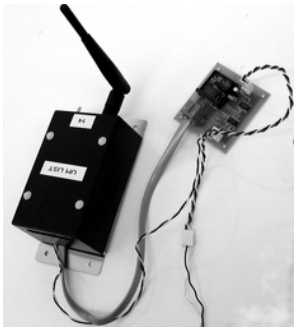

(b) Actuation signal module connected to wireless sensor

Figure 2.5. Pictures of the actuation signal generation module

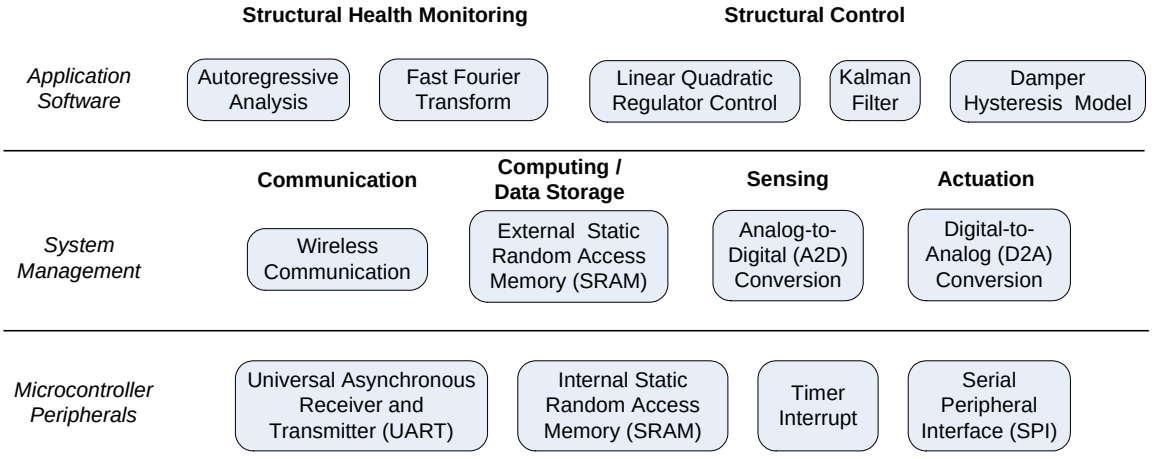

Figure 2.6. Three-layer software architecture for the ATmega128 microcontroller in the wireless sensing and actuation unit

2.2.1 Software Modules for Microcontroller Peripherals

As shown in Figure 2.6, the lowest level of the embedded software manages the peripherals of the ATmega128 microcontroller and serves as building blocks in developing system management modules for the wireless sensing unit. Embedded modules in this layer include byte-by-byte communication drivers through the UART (Universal Asynchronous Receiver and Transmitter) and SPI (Serial Peripheral Interface) ports, timer interrupt functions, and internal memory management.

2.2.1.1 UART Module

The UART interface is an asynchronous serial data link supporting full duplex operation. The sender and the receiver agree on transmission timing parameters in advance; special delimitation bits are added to each data byte in order to synchronize both the sending and the receiving devices. Figure 2.7 illustrates the hardware connections between two devices communicating through a UART interface. For example, when Device 1 needs to send a byte to Device 2, Device 1 first checks its CTS (Clear to Send) line to ensure that Device 2 is ready to receive data. If Device 2 is ready, the data byte is pushed bit by bit from the TX (Transmit) output of Device 1 to the RX (Receive) input of Device 2. The byte transfer must observe the pre-specified timing parameters and delimitation bits so that Device 2 can correctly recognize all the individual bits and reassemble the data byte. Operation procedures are symmetric when Device 2 transfers a byte to Device 1.

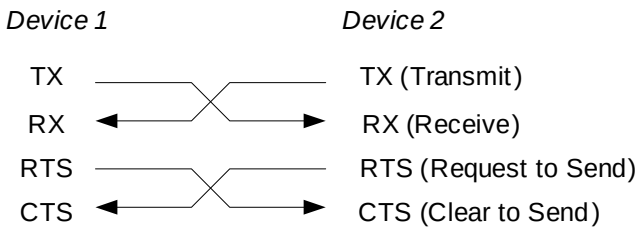

Figure 2.7. Hardware connections for a UART (Universal Asynchronous Receiver and Transmitter) interface

The ATmega128 microcontroller provides two UART ports: UART0 and UART1. UART1 is designed to be connected with the MaxStream wireless transceiver, while UART0 is used to print out debugging messages on a computer screen during the software development. A Kanda ATmega128 development board (Embedded Results Ltd. 2006) is used to provide the hardware conversion between the UART0 port of the microcontroller and the RS232 port of a computer. The ability to print out debugging messages helps reveal data stored in the memory space of the microcontroller when an embedded program is executing, which greatly facilitates software development. For each UART port, the following major functions are provided:

```
void InitUART(unsigned short baudrate);

void TransmitByteUART(unsigned char data);

unsigned char ReceiveByteUART(void);

unsigned char ReceiveByteUARTTimeOut(unsigned short TimeOut_Ticks,
    unsigned char *TimeOut_Flag);
```

The `InitUART` function initializes the UART port with a desired baudrate, such as 9,600 bps or 38,400 bps. The `TransmitByteUART` function transmits one data byte out from the microcontroller, while the `ReceiveByteUART` function allows the microcontroller to receive one data byte through the UART port. When executed, the `ReceiveByteUART` function waits until a data byte is received, so this function should only be used if a data byte is ensured to arrive. If there is any uncertainty that the data byte may not arrive, the `ReceiveByteUARTTimeOut` function should be used. This function provides a timeout threshold while waiting for the anticipated byte. If the byte does not arrive within certain time limit, the function sets the timeout flag, and exits immediately. This timeout detection is particularly useful for handling possible wireless transmission failures.

2.2.1.2 SPI Module

The SPI interface is a synchronous serial data link supporting full duplex operation. Figure 2.8 illustrates the hardware connections between two devices communicating

through an SPI interface. One device is assigned as the master, while the other device is assigned as the slave. The master device always initiates a transmission and manages the data frame through the SCLK (serial clock) line. When the master sends a byte to the slave through the MOSI (master output, slave input) line, the master expects to receive a byte from the slave through the MISO (master input, slave output) line simultaneously. Multiple slave devices are allowed to be connected with one master device, by assigning individual SS (slave select) lines for each slave device. At an instant of time, only one slave device communicates with the master device. Therefore, although the ATmega128 microcontroller provides only one SPI port, the port can be shared by the A/D converter (Texas Instruments ADS8341) and the D/A converter (Analog Device AD5542) operating as slave devices.

Two major functions are provided in the SPI module:

```
void SPI_MasterInit(void);

unsigned char SPI_MasterTransceive(unsigned char data);
```

The `SPI_MasterInit` function initiates the microcontroller as the master of the SPI communication at a data rate of 250 kbps in the current implementation. The `SPI_MasterTransceive` function takes one data byte as input, sends the byte to the slave device, receives a byte from the slave simultaneously, and then returns the received byte to the calling function.

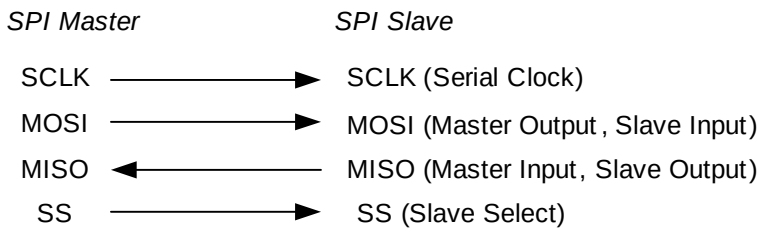

Figure 2.8. Hardware connections for an SPI (Serial Peripheral Interface) interface

2.2.1.3 Timer and Interrupt Services

The ATmega128 microcontroller provides two 16-bit timers and two 8-bit timers. Each timer contains an integer counter, incrementing by one after a specified number of clock cycles; the counter returns to zero after its maximum possible value is reached. For example, a 16-bit counter can only count up from 0 to an integer of $2^{16} - 1$, i.e. 65535. For higher timing precision, two 16-bit timers, denoted as Timer1 and Timer3, are employed in the current wireless sensing and actuation unit.

The Timer1 interrupt service is used to achieve a constant time step for sensor data sampling. For this purpose, Timer1 is set to increment after every 1μs. For example, if a sampling frequency of 100Hz is desired (sampling period is 0.01s), Timer1 would trigger an interrupt service for every 10,000 counts (i.e. 0.01s divided by 1μs). When the Timer1 interrupt is triggered, an interrupt handler function, `void Timer1Intrpt(void)`, is automatically executed to call the sensor data sampling routine. The interrupt service is a powerful feature that allows the software to momentarily pause an executing task (such as data processing or wireless communication) and to sample data from the sensing interface according to a precise timing schedule. Immediately after servicing the sensing interface, the paused task is resumed and the program continues its execution. This timer interrupt feature is utilized to implement continuous data streaming from multiple wireless sensing units, where sensor data sampling must occur at a constant sampling rate amidst the execution of the wireless communication or data interrogation program. In effect, the software supports concurrency by allowing multiple software tasks to execute at the same time.

Timer3 of the microcontroller is employed by the `ReceiveByteUARTTimeOut` function in the UART module. Incrementing by one after every 128μs, Timer3 is used to check for timeouts while waiting for a UART byte to arrive. For this purpose, a threshold value for the number of ticks in Timer3 counter is passed into the `ReceiveByteUARTTimeOut` function. For example, if the desired timeout period is 0.4 seconds, the threshold value

for Timer3 counter should be equal to 3125 (i.e. 0.4s divided by 128μs). When the `ReceiveByteUARTTimeOut` function is called, Timer3 starts counting from 0. The Timer3 hardware automatically sets a flag bit when the counter reaches the threshold value. While waiting for the arrival of a UART byte, the program keeps checking this flag bit to decide whether a timeout has occurred.

2.2.1.4 Internal SRAM

Figure 2.9 illustrates the memory space of the ATmega128. As shown in the figure, addresses from $0000 to $00FF (in hexadecimal) contain 32 general purpose working registers, 64 bytes of standard input/output (I/O) registers, and the 160 bytes of extended I/O registers. These registers provide access and control to the different services provided by the microcontroller, such as I/O ports, timers, serial ports, interrupt setups, etc.

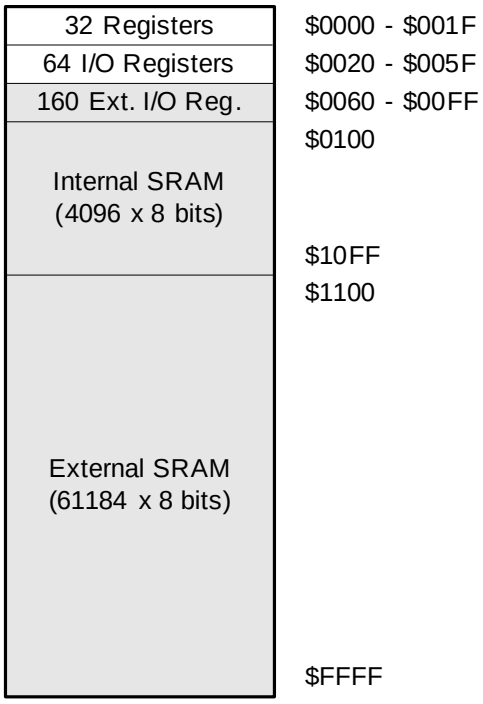

Figure 2.9. Memory map of the ATmega128 microcontroller

The ATmega128 microcontroller provides 4096 bytes of internal SRAM (Static Random Access Memory), which corresponds to the addresses $0100 to $10FF in Figure 2.9, inclusively. Addresses from $1100 to $FFFF (61184 bytes in total) are the optional address space mapped to external memory interfaced to the microcontroller. In the current implementation, the external memory is explicitly managed by the microcontroller program for storing data or analysis results. Therefore, the 4096 bytes of internal SRAM are used to store the stack and heap variables during program execution. Stack variables include the temporary and local variables for program routines, while heap variables are dynamically allocated in the program. One must ensure that during program execution, the stack and heap variables do not overflow the limited SRAM, otherwise the program execution will become unpredictable and lead to potential operational errors.

2.2.2 Software Modules for System Management

As shown in Figure 2.6, building on top of the microcontroller peripherals are the system management modules that organize other hardware components in the wireless unit. These include modules for the wireless transceiver, the external memory, the A/D, and the D/A converters.

2.2.2.1 Wireless Communication

While normally operating, the MaxStream transceiver transmits any bytes that are passed to it from the microcontroller; similarly, the transceiver passes bytes it receives from other wireless transceivers to the microcontroller. During wireless transmission, cyclic redundancy checking (CRC) of the data is automatically conducted by the MaxStream transceivers. CRC is important for ensuring that only complete, uncorrupted data packets are received by the transceiver and then passed to the microcontroller. The wireless communication module of the microcontroller utilizes the lower level UART driver to

communicate with the wireless transceiver. The software module provides the following functionalities: (1) reading or setting the internal parameters of the wireless transceiver, (2) sending or receiving data through the wireless transceiver, and (3) implementing the wireless communication protocol.

During runtime, two important transceiver parameters accessible to the microcontroller are the frequency channel and sequence numbers of the transceiver. As shown in Table 2.2, both the 9XCite and the 24XStream transceivers can operate on multiple frequency channels. Two transceivers must operate in the same frequency channel to communicate with each other. Within one channel, the wireless transceivers are identified by their sequence numbers. A sequence number can be preloaded into the wireless transceiver hardware. This sequence number can then be retrieved by the microcontroller software during runtime, so that the software can identify the wireless unit from other units in the same frequency channel.

In order to improve communication reliability, data packetization is employed while transmitting data through the wireless transceiver. Figure 2.10 illustrates the format of a standard wireless packet implemented in the current system. The packet design is intentionally simple to reduce communication overhead, which results in faster wireless communication. The first two bytes of a packet is a sentinel that marks the beginning of a packet. The selection of the sentinel bytes can be arbitrary and is chosen to be hexadecimal 0xAA55 in the current implementation. The third and fourth bytes are used for an unsigned integer that specifies the length of this packet. The fifth and the sixth byte contain the command ID as an unsigned integer, and the rest of the packet is the data payload associated with this command. The format within the payload should be designed specifically for each type of command. For example, if the command ID indicates that a packet contains sensor data, the payload may contain the sender sequence number, followed by the sensor data being transmitted.

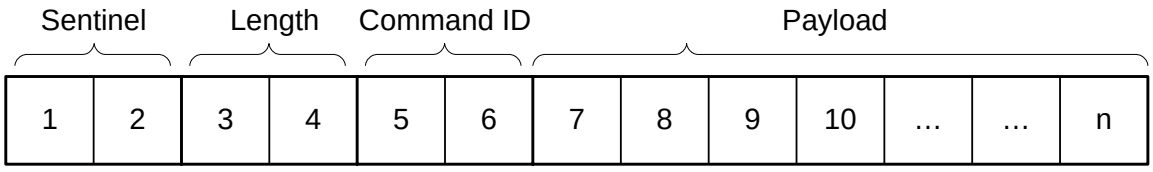

Figure 2.10. Format of a complete wireless packet (n-bytes long)

For a network of wireless units to operate efficiently, the units need to follow a specific communication protocol. The protocol specifies the proper communication sequence that should be observed to complete a communication task. In the design of a wireless communication protocol, the command IDs in each wireless packet can be employed to specify the purpose of each packet. After the receiver gets the packet, the receiver checks the command ID and payload data to decide how to properly handle the packet according to the protocol. Implementation of the wireless communication protocol is an important part of the wireless communication module. Different protocols are designed for different structural sensing and control applications. The protocols for wireless sensing and control applications will be described in Chapters 3 and 4, respectively.

2.2.2.2 External SRAM

A software module is implemented to manage the 128kB external Static Random Access Memory (SRAM). As shown in Figure 2.9, the memory space of the ATmega128 microcontroller is limited to 64kB, i.e. the microcontroller can only access half of the external memory at a time. To make full use of the 128kB external memory, a separate control line is employed to select the lower 64kB or upper 64kB of the Cypress CY62128B chip. Taking this into consideration, the external SRAM module includes the following functions:

```
void InitExSRAM(void);

void EnableLowHalfExSRAM(void);
```

```
void EnableHighHalfExSRAM(void);
```

The `InitExSRAM` function initializes the external memory by setting proper register entries of the microcontroller and enabling the chip-select pin of the CY62128B. The `EnableLowHalfExSRAM` and `EnableHighHalfExSRAM` allow access to the lower and upper half of the memory chip, respectively. The software developer must be cognizant of which half of the memory bank is being used at any point of the program.

2.2.2.3 A/D Module

The A/D module manages the interface between the wireless unit and the structural sensors. As introduced earlier, the A/D converter (Texas Instruments ADS8341) used for sensing and the D/A converter (Analog Device AD5542) used for actuation share the same SPI communication port of the ATmega128 microcontroller. The A/D module commands the ADS8341 chip to convert a 0 to 5V analog sensor signal to a 16-bit unsigned integer. Knowing the sensitivity and offset of the sensor signal, the microcontroller can then compute a floating-point number quantifying the physical parameter being measured by the sensor. The major functions provided by the A/D module are:

```
void InitA2D(void);

unsigned short A2DCh(unsigned int ch);

void StartA2DIntrpt(unsigned char freqID);

void StopA2DIntrpt(void);
```

The `InitA2D` function initializes the SPI port of the ATmega128 microcontroller as the master node in the communication and initializes the A/D converter as the slave node (Figure 2.8). The A/D converter is immediately disabled after initialization to avoid possible SPI communication conflict with the D/A converter. The `A2DCh` function takes an input integer that represents an A/D channel number (four channels in total),

commands the A/D converter to complete the conversion on this channel, receives the digitized sensor data through the SPI port, and returns the digitization result to the caller function. For the same reason of avoiding SPI conflict, the A/D converter is enabled at the beginning of the `A2DCh` function, and disabled at the end of the function. The `StartA2DIntrpt` function takes a sampling frequency ID as input, and activates the A/D timer interrupt. As soon as the timer interrupt is activated, the interrupt service function is called at the specified sampling frequency to sample and store sensor data. The current module implementation provides options for multiple sampling frequencies ranging from 50Hz up to 500Hz. Conversely, the `StopA2DIntrpt` function stops the A/D timer interrupt service.

2.2.2.4 D/A Module

The D/A module manages the interface between the wireless unit and structural actuators. According to the desired actuation force and the actuator property, the caller function to this module should decide the actuation command voltage in advance. Two functions are provided in this module:

```
void InitD2A (void);

void SetD2AVoltage (float voltage);
```

The `InitD2A` function initializes the D/A converter through the SPI communication driver. The D/A converter is immediately disabled after initialization, to avoid possible SPI communication conflict with the A/D converter. The `SetD2AVoltage` function takes a floating-point number between -5V and 5V as input, converts the number into a 16-bit integer, and pushes the integer to the D/A converter to output the corresponding actuation voltage signal. Again, to avoid SPI conflict, the D/A converter is enabled at the beginning of the `SetD2AVoltage` function, and disabled at the end of the function.

2.2.3 Application Software Modules

Utilizing the system management modules for communication, computing, sensing, and actuation, software programs can be implemented to support various structural health monitoring and control applications. A number of engineering algorithms, such as fast Fourier transform (FFT), autoregressive (AR) analysis, linear quadratic regulator (LQR) control, and Kalman filter estimation, have been implemented and embedded in the wireless units. These individual functions will be introduced in the forthcoming chapters on structural sensing and control applications. The importance of onboard data processing is that it helps save energy resources (i.e. preserving battery power) by reducing wireless transmission of large amount of raw sensor data. In addition, data reduction at the wireless unit allows for a scalable wireless sensing architecture that minimizes data glut. With application software executing in the wireless unit, each unit acts as an autonomous agent in a wireless sensing and control network. This architecture of distributed sensing and actuation represents a new paradigm in structural sensing and control, as opposed to traditional centralized systems, where raw data is localized at a central data repository for processing.

2.3 Summary

This chapter provided an overview of the integrated hardware and software design of a prototype wireless sensing and actuation unit. Commercial off-the-shelf hardware components are used to keep the cost of the wireless unit low. Power consumption of the entire wireless unit is minimized while allowing the hardware components to provide all of the necessary functionalities dictated by the sensing and control applications. A number of design features have been achieved by properly selecting the hardware components for the wireless unit:

1. Sensing: to ensure high-fidelity data collection, the combination of a high-resolution 16-bit A/D converter and a specially designed signal conditioning module is utilized.

2. Communication: wireless transceivers with communication ranges suitable for civil structure applications (ranges on the order of hundreds of feet) are selected. These transceivers support both peer-to-peer and broadcasting communication modes, allowing for different network topologies.

3. Computing: an external 128kB memory chip is utilized to enhance the computing power of the 8-bit low-cost microcontroller.

4. Actuation: an output analog signal ranging from -5V to 5V at a high actuation frequency is available for commanding structural actuators.

In order to capitalize on the rapidly evolving electronics market, new hardware components that consume less power while achieving similar or superior performance levels should be explored for developing future generations of the wireless sensing and actuation unit. Particularly, the market will continue to provide higher-speed, lower-power alternatives for the wireless transceiver and the microcontroller.

In addition to the hardware design of the wireless sensor prototype, embedded software for the microcontroller is developed in tandem. The embedded software design follows a three-layer architecture with microcontroller peripheral drivers, system management modules, and application software routines delineated on the bottom, middle, and upper layers, respectively. With one layer built upon another, this hierarchical software design allows for a scalable software architecture. For example, changes to a hardware component would only necessitate changes in its respective module in the lowest device driver layer. Furthermore, application software need not be concerned with tedious hardware implementation. The distributed processing capabilities in the wireless sensing

and actuation units will facilitate the implementation of structural monitoring and damage diagnosis algorithms, and support feedback structural control.

Chapter 3

Wireless Structural Sensing

A prototype wireless structural sensing system is constructed from a network of wireless sensing units introduced in the previous chapter. The prototype system assumes a single data server working with multiple wireless sensors in a star-topology network. To guarantee efficient and reliable system performance, a robust communication protocol featuring lossless data transfer is designed for the wireless structural sensing system. Implementation of the communication protocol includes software development for both the data server and the wireless sensing units. To verify the performance of the wireless structural sensing system, extensive laboratory and field validation tests have been conducted. These tests are particularly helpful in assessing the limitations of the system and providing valuable experience that can lead to further improvements in the system hardware and software design.

This chapter is organized as follows. Section 3.1 introduces the communication protocol designed for the prototype wireless structural sensing system. Section 3.2 presents the validation tests conducted in the National Center for Research on Earthquake Engineering (NCREE) in Taiwan. These laboratory tests are designed to validate the quality of the wireless sensor data and the computing capabilities of the wireless units. Section 3.3 presents the instrumentation of the wireless structural sensing system at

Geumdang Bridge, South Korea. The specially designed sensor signal conditioning module is tested for measuring vibration of the bridge deck. Section 3.4 presents the validation tests conducted at Voigt Bridge, San Diego, California. Flexibility of the wireless structural sensing system is validated by easily changing the network architecture during the tests. Section 3.5 summarizes the wireless structural sensing system and validation tests described in this chapter.

3.1 Communication Protocol Design for Wireless Structural Sensing

A simple star-topology network is adopted for the prototype wireless structural sensing system. The system includes a network server and multiple structural sensors, signal conditioning modules, and wireless sensing units (Figure 3.1). The server is used to organize the multiple wireless sensing units in the sensor network. The responsibilities of the server include: (1) commanding all the corresponding wireless sensing units to perform data collection or interrogation tasks, (2) synchronizing the internal clocks of the wireless sensing units, (3) receiving data or analysis results from the wireless sensing units, and (4) storing the data or results. Any desktop or laptop computer connected with a compatible wireless transceiver can be used as the network server. As shown in Figure 3.1, if the server is connected to the Internet, sensor data or analysis results can be viewed remotely from other computers on the Internet.

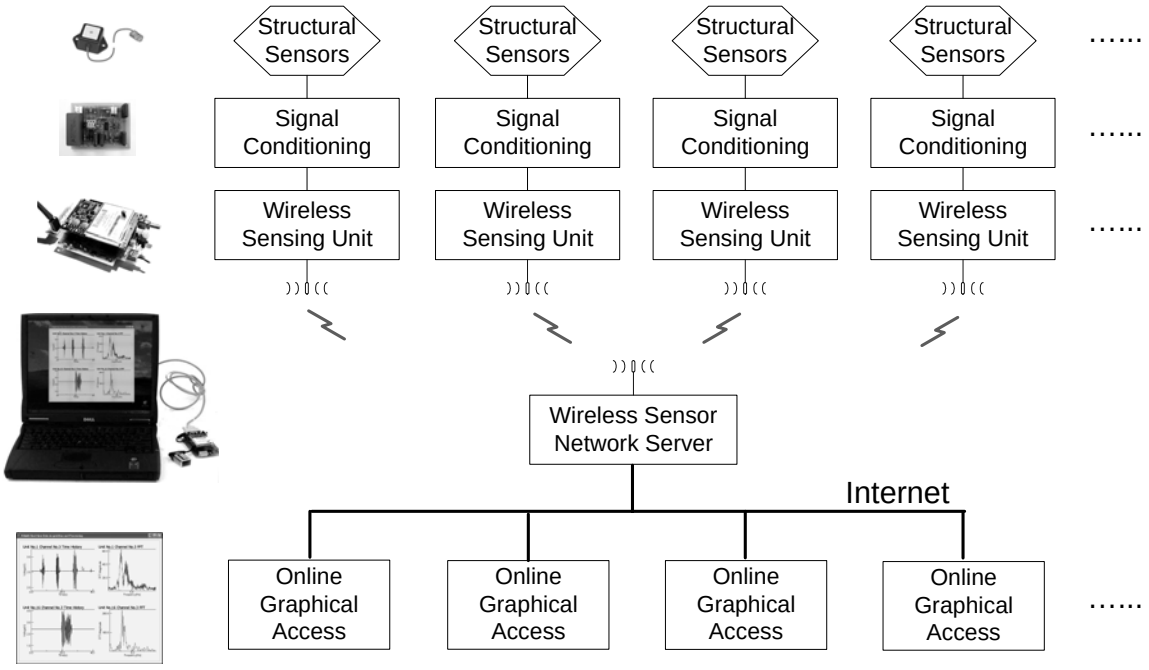

Figure 3.1. An overview of the prototype wireless structural sensing system

This section presents the communication protocol design for the wireless structural sensing system, including the protocols for data synchronization and collection. A dual-stack memory management scheme is implemented in the wireless sensing units to allow continuous sensor data collection. The software for the server and the wireless sensing units are designed in tandem to coordinate the communication between them. Finite state machine concepts are employed in designing the communication protocol for the wireless sensing units and the server (Tweed 1994). The state diagrams for data synchronization and collection are presented in this section.

The communication protocol is designed in such a manner that special characteristics of the structural sensing application are exploited. In structural sensing applications, the objective is normally to transmit sensor data or analysis results to the server. Therefore, the server is assigned the responsibility for ensuring reliable wireless communication, particularly since the server program normally runs on a desktop or a laptop computer,

which has much higher computing power than the microcontroller in a wireless unit. Communication is usually initiated by the server. After the server sends a command to the wireless sensing unit, if the server does not receive an expected response from the unit within a certain time limit, the server resends the command again until the expected response is received. However, after a wireless sensing unit sends a message to the server, the unit does not check whether the message arrives at the server, because the communication reliability is assigned to the server. The wireless sensing unit becomes aware of the lost data only when the server queries the unit for the same data. In short, the server plays an "active" role in the communication protocol while the wireless sensing unit plays more of a "passive" role. This concept of one-sided communication responsibility is implemented for both the synchronization and data collection protocols.

3.1.1 Synchronization of Wireless Sensing Units

For many damage and system identification procedures, measurement data collected by different sensors must be time synchronized. For example, modal analysis usually requires synchronized acceleration data from different locations of the structure (Ljung 1999, Ewins 2000). Figure 3.2 shows the communication procedures between the server and the wireless sensing units to ensure clock synchronization.

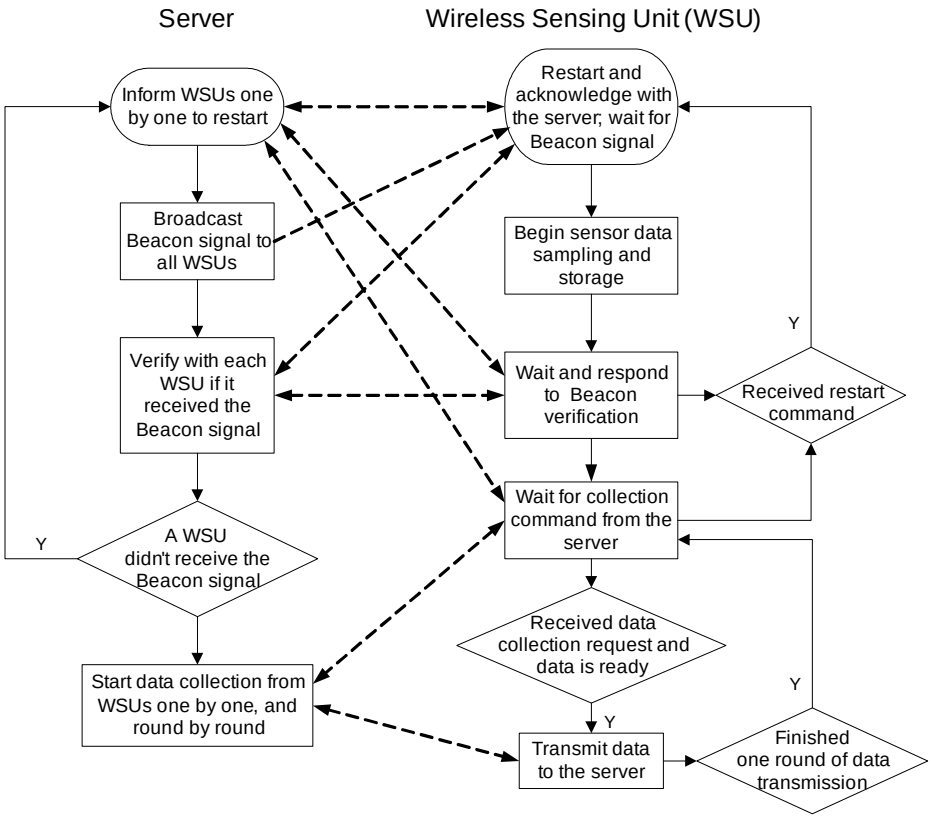

Figure 3.2. Communication procedures for the synchronization of wireless sensing units

The synchronization procedure utilizes the MaxStream wireless transceiver's broadcasting capability. This feature permits the data server's wireless transceiver to broadcast a beacon signal to which all wireless sensing units synchronize. Once the wireless sensing units receive the beacon signal from the server, each unit starts sampling the data at the requested sampling rate. To account for the situation where a wireless sensing unit might not receive the beacon signal, all wireless sensing units must confirm with the server that they have received the beacon signal successfully. As shown in Figure 3.2, when the server inquires with a unit whether the unit has received the beacon signal, the unit may be still waiting for the beacon signal which has never arrived. If this happens, the server restarts all the wireless sensing units by asking them to wait for

another beacon signal, and then re-broadcasts the new beacon signal. The synchronization procedure is iterated until the server has confirmed that the beacon signal has been received by all the wireless sensing units in the network.

Although all the units receive the beacon signal from the server, each wireless sensing unit may not receive the beacon at the same time. Therefore, some units may start collecting data slightly earlier than others. Because the propagation of the wireless radio-frequency (RF) signal takes only nano-seconds in this application, the synchronization error mainly originates from the difference in the time each wireless sensing unit takes to interpret the broadcasted beacon signal. Using precise timers in the laboratory, the beacon synchronization error between two sensing units is measured to be within 20μs of one another. This laboratory based timing of the synchronization error is intended to measure the expected error in a single-hop wireless sensor network where the server locates within a short range (about a few hundred meters) from the wireless sensors. Because all wireless sensing units are listening for the same beacon signal from the server, time synchronization across the entire wireless sensor network is represented by each unit-server pair. Since the units are independent of each other for time synchronization, the test results using two sensing units represents the synchronization error for an entire wireless network, irrespective of the number of wireless sensing units installed.

It should be noted that although the system synchronization error is around 20μs at the beginning of the data collection, the synchronization error may increase with time because of the natural time drift in the crystal clocks integrated with the wireless sensing unit. Current prototype unit employs a low-cost 8MHz crystal to provide system clock for the ATmega128 microcontroller. Laboratory tests show that the synchronization error between two units can accumulate up to 5ms in a 6-minute period. Thus, synchronization error is considered minimal and reasonable within a realistic time period for data collection. However, for long-term data collection, synchronization of the system should be performed periodically at a certain time interval. Crystals with higher precision may

be adopted in the wireless sensing units to reduce the synchronization error due to clock drift.

3.1.2 Design and Implementation of Synchronization Protocol

A robust data acquisition system should be sufficiently reliable and able to detect failures in the wireless communication channel and to recover from any communication failures encountered. The state machine concept is employed for designing the software architecture of both the wireless sensing units and the server to ensure the reliability of the wireless communication channel. A finite state machine consists of a set of states and definable transitions between the states. At any point in time, the state machine can only be in one of the possible states, or transiting between two states in response to different events. Figure 3.3 and Figure 3.4 show the abridged state diagrams for the server software and the wireless sensing unit software, respectively. Only the part of the communication state diagrams for synchronizing wireless sensing units is presented in these two figures (the rest part of the diagrams for data collection will be presented in Section 3.1.4). This part of communication state diagrams describes the program flow that realizes the synchronization procedure introduced in Section 3.1.1. In the state diagrams shown in Figure 3.3 and Figure 3.4, each rectangle or circle with bold boundary lines represents a possible state; lines with arrows represent state transitions. As shown in the legend, for each transition, the normal text above the horizontal line specifies the event/condition upon which the transition should take place, and the italic text below the horizontal line specifies the service/action to be executed during this transition.

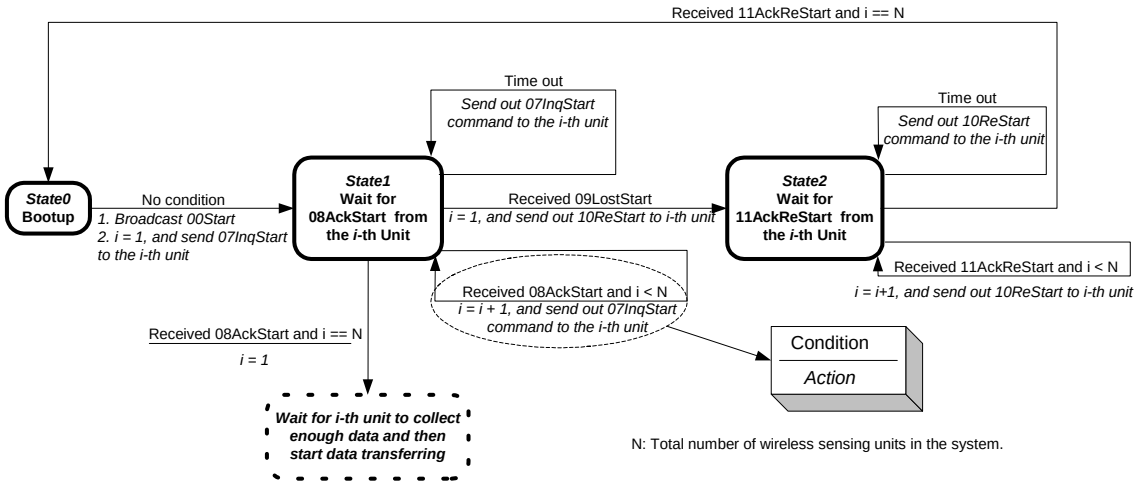

Figure 3.3. Communication state diagram of the server for data synchronization

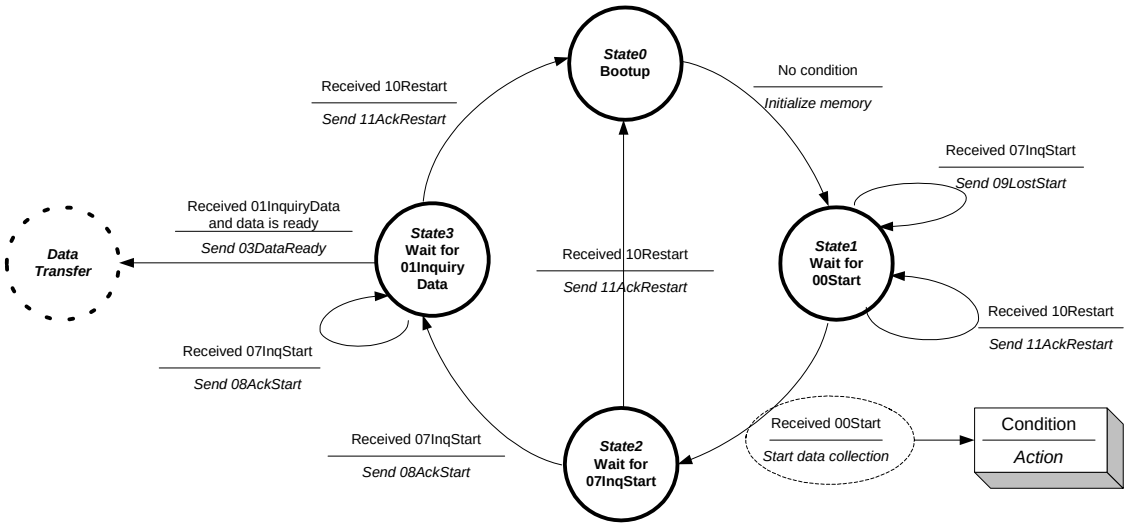

Figure 3.4. Communication state diagram of the wireless sensing units for data synchronization

When a wireless sensing unit is powered on, the unit starts from "State0" (Figure 3.4). Under "no condition", the unit automatically initializes the memory space, and transits into "State1" to wait for '00Start', where the '00Start' is the beacon signal that is broadcasted from the server to all the wireless sensing units, requesting all units to start data collection simultaneously. Accordingly, when the data collection program at the server starts, as shown in Figure 3.3, the server automatically broadcasts the '00Start' beacon signal to the wireless sensing units. As soon as a wireless sensing unit receives and recognizes the '00Start' beacon, the sensing unit starts collecting data from its sensors at a specified sampling rate, and saves the data temporarily into its external SRAM for later acquisition by the server. If it takes all the wireless units the same amount of time to receive and recognize the '00Start' signal, all the units should start recording data at the same time, i.e. the data acquisition is synchronized.

As shown in Figure 3.4, the wireless sensing unit transits into "State2" after receiving the '00Start' command. After the server broadcasts the '00Start' beacon signal, it sends the '07InqStart' command to each wireless unit, and waits until the '08AckStart' message is returned from the sensing unit to confirm receiving the '00Start' beacon. If a wireless sensing unit misses the '00Start' beacon, the unit will receive the '07InqStart' command when itself is in "State1" (instead of in "State2"). In this case, the wireless sensing unit will send '09LostStart' in response to the server's '07InqStart' inquiry. Knowing that the sensing unit has not properly received the '00Start' beacon, the server will ask all the units to restart and run the synchronization procedure, until the server confirms that all the units have received the broadcasted '00Start' signal correctly.

As mentioned earlier, the server is assigned the responsibility for ensuring the reliability of a wireless communication channel (e.g. no data loss). To illustrate, assume that when the wireless sensing unit transits from "State2" to "State3" in Figure 3.4, the '08AckStart' message sent from the unit to the server is lost. The server is now at its "State1" waiting for the '08AckStart'. However, because the server does not receive the '08AckStart' message within certain expected time, the server will resend '07InqStart' to

the unit. Therefore, when a wireless sensing unit is in its "State3", waiting for the data acquisition request from the server, the unit may still receive the '07InqStart' command because the '08AckStart' command was lost. In this case, the wireless sensing unit simply resends the '08AckStart' command to the server. This simple example illustrates the advantages inherent to the state machine concept when visualizing communication procedures. The development of the communication protocol demonstrates that the state machine concept provides the convenience for both designing and implementing program flow between the data server and the wireless sensing units.

3.1.3 Dual-stack Memory Allocation for Continuous Data Collection

After the server confirms that all the wireless sensing units have received the beacon signal, the server starts inquiring the units one by one for the data that have thus far been collected. Before the wireless sensing unit is queried for its data, the data is temporarily stored in the unit's onboard SRAM memory buffer. With over 128kB of space available in memory, the wireless sensing unit can effectively store up to 64,000 data points (at 16-bit resolution). Upon inquiry by the server, the wireless sensing unit transmits its most recently collected sensor data. A unique feature of the embedded wireless sensing unit software is that it can continue collecting data from interfaced sensors as the wireless sensing unit is transmitting data to the server.

At each time instant, the server can only communicate with one wireless sensing unit. To achieve real-time continuous data collection from multiple wireless sensing units with each unit having up to four analog sensors attached, a dual stack approach is designed to manage the SRAM memory. Essentially, the available memory bank of each unit is divided into four pairs of smaller memory stacks. When a wireless sensing unit starts collecting data, the embedded software establishes two memory stacks dedicated to each sensor channel for storing the sensor data. For each sensing channel, at any time instant,

only one of the stacks is used to store the incoming data stream. As new data is collected using one of the memory stacks, the data stored in the other stack is being sent out to the server. The role of the two memory stacks alternates as soon as one stack is filled with newly collected data. Figure 3.5 illustrates the embedded system's management of the external SRAM memory using a two-sensor example. The two memory stacks, labeled Stacks "X"-1 and "X"-2 for sensor channel "X" (X is 1 or 2 in this example), are shown in Figure 3.5. In the diagram, incoming data from each sensor channel is stored in the second stack (denoted as Stacks 1-2 and 2-2) while the system is wirelessly transferring data from the first stack (denoted as Stacks 1-1 and 2-1). Before Stacks "X"-2 are full, the wireless communication must be fast enough to transfer all the data from Stacks "X"-1. After Stacks "X"-2 are filled with the new data, the stacks alternate their roles, with the radio transmitting data from Stacks "X"-2 and microcontroller storing sensor data in Stacks "X"-1.

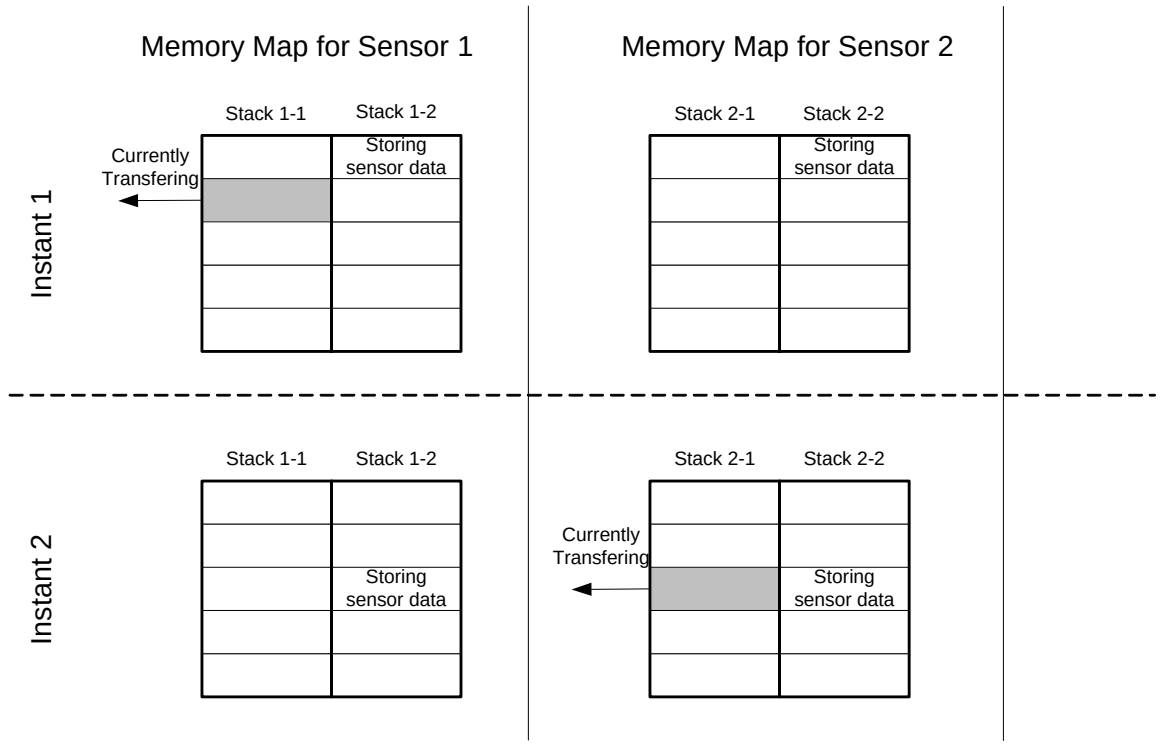

Figure 3.5. Dual-stack memory allocation for real-time continuous data collection

Limit to the bandwidth of continuous wireless data streaming is largely a function of the available wireless data transfer rate. In the current prototype system using the MaxStream 9XCite transceiver, the server is able to collect raw data from up to 24 wireless sensors continuously in real-time with a sampling frequency of 50Hz for each sensor, with the complete retry and acknowledgement communication protocols being followed. As the sampling rate increases, the number of sensors that can be utilized decreases. For example, if a sampling rate of 100 Hz is desired, then only 12 sensors can be accommodated for real-time data communication with a single data server. When the MaxStream 24XStream transceiver is used, the prototype system achieves about half of the data rate when using the 9XCite transceiver. If a high sampling rate and a large number of sensors are needed, then the system is not able to simultaneously collect data and wirelessly transmit at the same time. In such circumstances, the wireless sensing unit is first asked to collect a certain amount of data and to store the data temporarily in the local memory buffer. Upon completion, the wireless sensing unit can then send the data or the analysis results to the server.

It should be noted that when the wireless sensing units are commanded to collect data over a certain period of time and store the entire data set before transmitting, the capacity of the wireless sensor network can be increased to hundreds or even thousands of wireless units. In this mode, since the demand for real-time data transmission is not necessary, higher sampling rate can be used. The only limitation encountered in this mode of operation is the available on-board memory which controls the duration of time that the wireless sensor can collect data before exceeding its memory capacity. Using the current external SRAM of 128kB (as described in Section 2.1.1), each wireless sensing unit can store up to about 60,000 data points (every data point is two bytes using the 16-bit A/D converter with four A/D channels). Following the current communication protocol, it takes a wireless unit with the 9XCite transceiver about 46 seconds to transmit 60,000 data points to the server. For a wireless unit with the 24XStream transceiver, the transmission takes about 92 seconds.

3.1.4 Design and Implementation of Data Collection Protocol

Communication protocols are designed and implemented to reliably transmit sensor data or analysis results between the server and the wireless units. In a continuous data streaming example as shown in the last subsection, the communication protocol needs to ensure reliable data transfer from the dual memory stacks of the wireless sensing units to the server. The commonly used network communication protocol is the Transmission Control Protocol (TCP) standard (Stevens 1994). TCP is a sliding window protocol that handles both timeouts and retransmissions. It establishes a full duplex virtual connection between two sides of the communication. Although TCP is a reliable communication protocol, it is too general and cumbersome to be employed by the low-power and low data-rate wireless sensing network for structural applications. The relatively long latency of transmitting each wireless packet is another bottleneck that may slow down the communication throughput using TCP. A simpler communication protocol is designed to minimize transmission overhead for efficient application in a wireless structural sensing network. The protocol is designed to ensure reliable wireless transmission by properly addressing the issue of potential data loss.

The communication protocol designed for the prototype wireless sensing system inherits some useful features of TCP, such as data packetizing, sequence numbering, timeout checking, and retransmission. Based upon pre-assigned arrangement between the server and the wireless units, the sensor data stream is segmented into a number of packets, each containing a few hundred bytes. A sequence number is assigned to each packet so that the server can request the data sequentially. Similar to the protocol for synchronizing wireless sensing units (as introduced in Section 3.1.2), finite state machine concepts are employed in designing the communication protocol for transferring data between the wireless sensing units and the server. Figure 3.6 and Figure 3.7 show the communication state diagrams of the server and the wireless units, respectively, for one round of sensor

data collection. During each round of data collection, the server collects sensor data from all the wireless units. Note that the server and the units have separate sets of state definition.

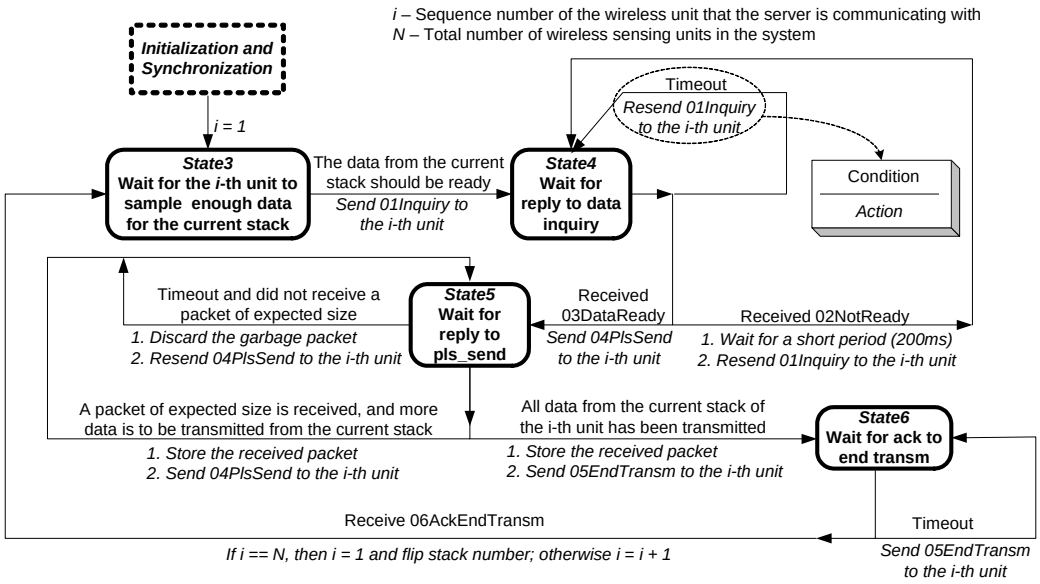

Figure 3.6. Communication state diagram of the server for data collection

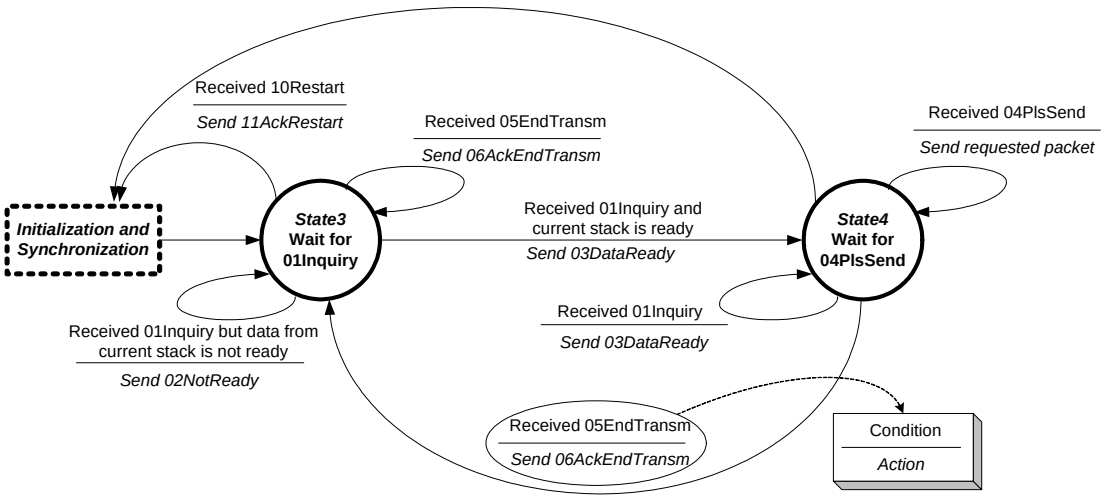

Figure 3.7. Communication state diagram of the wireless units for data collection

At the beginning of data collection, the server and all the wireless units are set in "State3" (see Figure 3.6 and Figure 3.7, respectively). Starting with the first wireless unit in the network, the server queries the unit for the availability of data in the current memory stack of that unit by sending '01Inquiry'. If the data is not ready, the unit replies '02NotReady', otherwise the unit replies '03DataReady' and transits to "State4". After the server is certain that the data from this wireless unit is ready for collection, the server transits to "State5". To request a data segment from a unit, the server sends a '04PlsSend' command that contains a packet sequence number. In case that the server does not receive the requested data segment within a prescribed time window, the server resends the same request until the data arrives successfully. One round of data collection from one wireless unit is ended with a two-way handshake, where the server and the unit exchanges '05EndTransm' and '06AckEndTransm'. The server then moves on to the next unit and continuously collects sensor data round-by-round.

3.2 Laboratory Validation Tests at NCREE, Taiwan

The wireless structural sensing system has undergone a number of laboratory and field validation tests to assess the performance and verify the prototype design and implementation (Wang, *et al.* 2005, Lu, *et al.* 2006, Lynch, *et al.* 2006a, Wang, *et al.* 2006b, Wang, *et al.* 2007b). This section describes a large-scale shake table test conducted at the National Center for Research on Earthquake Engineering (NCREE) in Taipei, Taiwan in June 2005. Quality of the wireless sensor data is verified using the data collected by a high-precision wire-based system. The embedded computing functionality of the wireless sensing units is also validated in the tests. Wireless sensor data collected in the test has also been used for damage identification purpose (Lynch, *et al.* 2006b).

3.2.1 Site Instrumentation

In collaboration with researchers at NCREE, Taiwan, the wireless sensing system is installed on a three-story steel frame structure mounted on a shake table. As shown in Figure 3.8, the three-story single-bay steel frame structure has a 3m-by-2m floor area and a 3m inter-story height. H150x150x7x10 I-section elements are used for all columns and beams with each beam-column joint designed as bolted connections. Each floor is loaded with concrete blocks and has a total mass of 6,000kg. The test structure is mounted on a 5m-by-5m shake table capable of applying base motion in 6 independent degrees-of-freedom.

As presented in Figure 3.8(a), the test structure is instrumented with a wireless network consisting of 6 wireless sensing units. Because of local frequency band requirements, the MaxStream 24XStream wireless transceiver operating at 2.4GHz spectrum is employed for the wireless sensing unit. The instrumentation strategy of the wireless sensing system is governed by an interest in both the acceleration response of the structure as well as the strain measurements at the base column. As shown in Figure 3.8(a), one wireless sensing unit is responsible for the three accelerometers instrumented on a floor. For example, wireless sensing unit WSU6 is used to record the data from three accelerometers on the top floor: A1, A2 and A3. This configuration of accelerometers is intended to capture both the longitudinal and lateral response of each floor, as well as any torsion behavior.

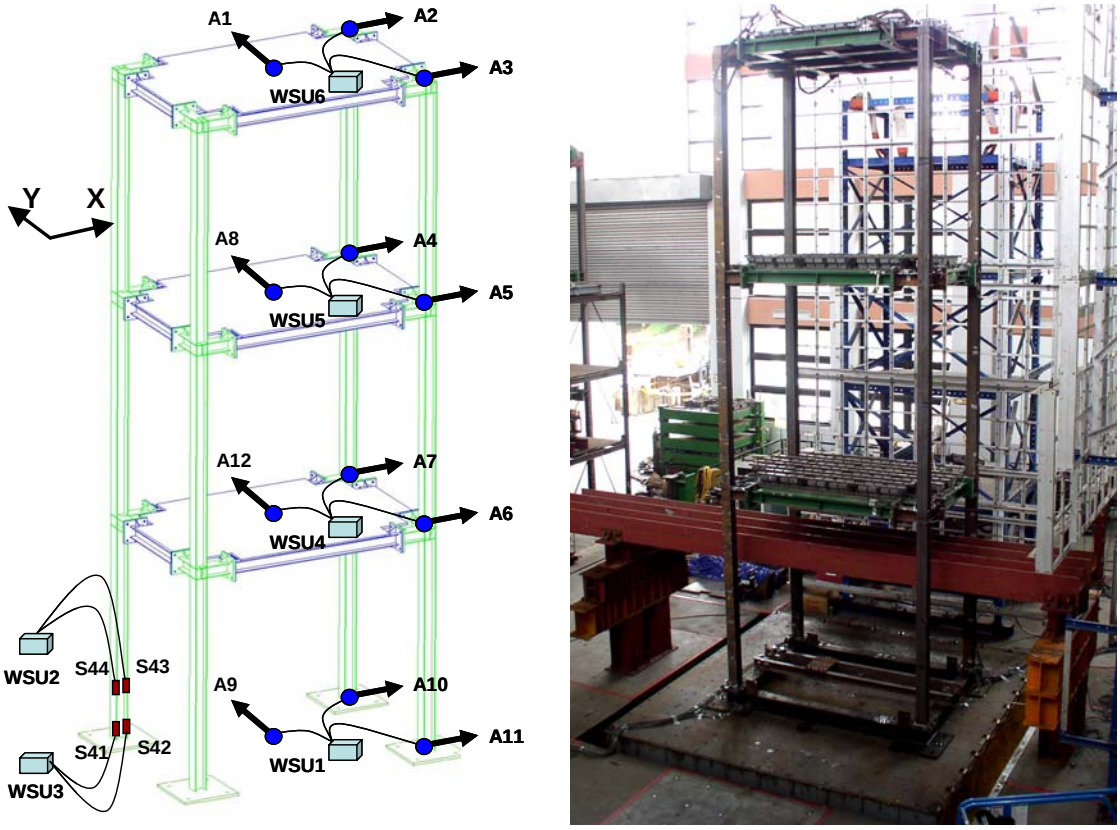

(a) Instrumentation layout (b) Shake table setup

Figure 3.8. Three-story steel-frame structure in NCREE

The accelerometers employed with the wireless sensing units are the Crossbow CXL01LF1, CXL02LF1, and CXL02LF1Z accelerometers (Table 3.1), which have acceleration ranges of ±1g, ±2g, and ±2g, respectively. The CXL01LF1 accelerometer has a noise floor of 0.5mg and a sensitivity of 2V/g, while the CXL02LF1 and CXL02LF1Z accelerometers have a noise floor of 1mg and a sensitivity of 1V/g. The only difference between the CXL02LF1 and CXL02LF1Z accelerometers is that the measurement axis of CXL02LF1 is parallel to the mounting plane, while the measurement axis of CXL02LF1Z is perpendicular to the mounting plane. Additionally, four metal foil strain gages with nominal resistances of 120Ω and a gage factor of two are mounted on two of the base columns. To measure the strain response, a Wheatstone

bridge amplification circuit is used to convert the changes in gage resistance into voltage signals (Horowitz and Hill 1989). Two wireless sensing units (WSU2 and WSU3) are dedicated to record the strain measurements with each unit connecting to two gages.

Table 3.1. Parameters of the accelerometers used by the wire-based and wireless systems in the NCREE laboratory test

Specification	**CXL01LF1**	**CXL02LF1 / CXL02LF1Z**	**Setra141-A**
Sensor Type	Capacitive	Capacitive	Capacitive
Maximum Range	±1 g	±2 g	±4 g
Sensitivity	2 V/g	1 V/g	0.125 V/g
Bandwidth	50Hz	50Hz	260Hz
RMS Resolution (Noise Floor)	0.5 mg	1 mg	0.4 mg
Minimal Excitation Voltage	5 VDC	5 VDC	5 ~ 15 VDC

In order to validate the performance of the wireless system, a set of wired sensors connecting to a cable-based data acquisition system are placed side-by-side to all the wireless accelerometers and strain gages shown in Figure 3.8(a). For the wired system, Setra141-A accelerometers (with acceleration range of ±4g and a noise floor of 0.4mg) and 120Ω metal foil strain gages are employed. Multiple Pacific Instrument Series 5500 data acquisition chassis are used in the wired system. Each chassis can sample 16 channels of sensor data at a maximum rate of 30 kHz. Throughout the validation tests, a sampling rate of 200Hz is used by the wired system.

3.2.2 Quality of the Wireless Sensor Data

Various ambient white noise and seismic excitations, including El Centro (1940), Kobe (1995), and Chi-Chi (1999) earthquake records, were applied to excite the test structure (Lynch*, et al.* 2006b). Both wired and wireless sensor data are collected in these tests. The results shown in Figure 3.9 are based on a 90-second bi-directional white noise

excitation of 1m/s and 0.5m/s standard deviation velocities in the X and Y directions respectively. The sampling rate for the wireless system is chosen to be 100Hz. The time history responses for both acceleration and strain measurements recorded (at locations A2, A5, A12, and S42) by the wireless sensing system are identical to those measured independently by the wire-based system. Similar results are also observed in other test runs, which indicate the high accuracy of the wireless sensor data. Due to the relatively high amplitude of the sensor signal, the signal conditioning module introduced in Section 2.1.2 is not necessary and has not been employed in these tests.

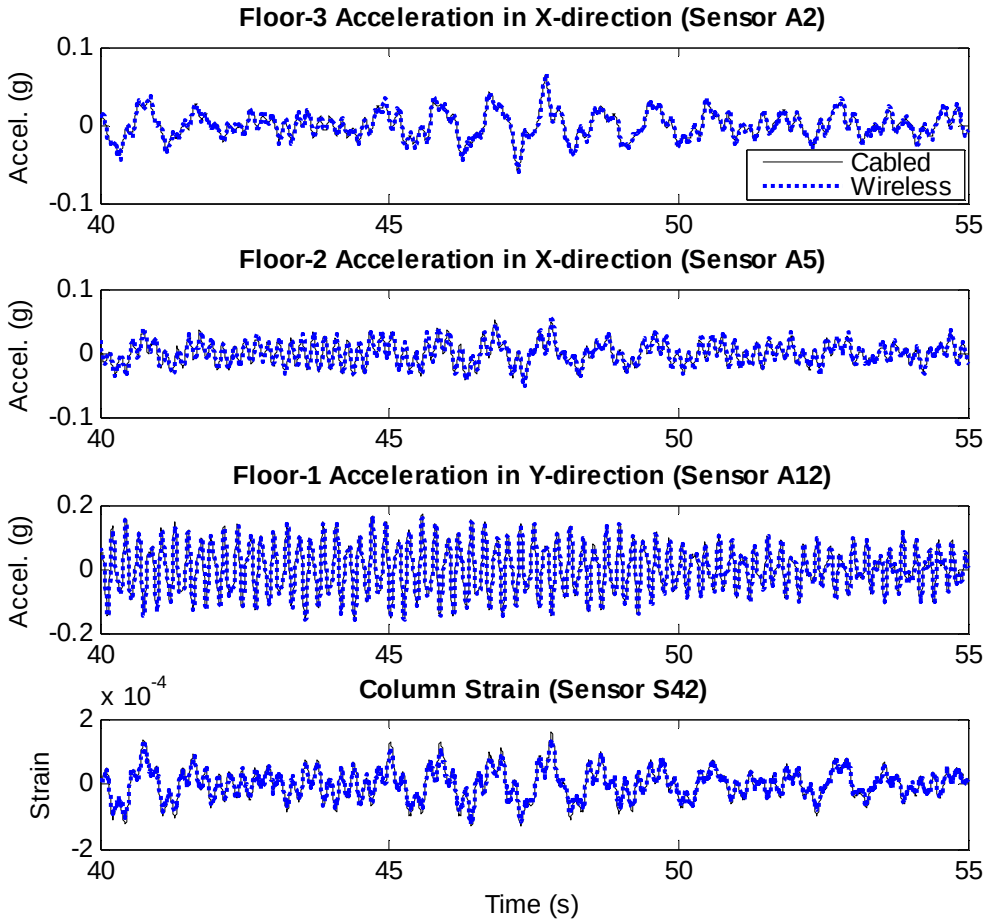

Figure 3.9. Comparison between wireless and wired sensor data for the NCREE 3-story structure

3.2.3 Embedded Autoregressive Analysis

In order to illustrate the utilization of the on-board microcontroller for data interrogation, an autoregressive (AR) time series model that is proposed for damage detection applications is implemented on each wireless sensing unit (Sohn and Farrar 2001, Nair*, et al.* 2006). At a sensor node, the AR model is computed to predict a discrete data sample *y(k)* using the weighted sum of previous data samples:

$$y(k) = \sum_{i=1}^{p} b_i \, y(k-i) + \varepsilon(k) \tag{3.1}$$

Here p is the order of the AR model, b_i (i = 1, …, p) are the AR coefficients, and $\varepsilon(k)$ is the residual error. The Burg algorithm is employed for estimating the coefficients of the AR process (Kay 1988). The algorithm starts by computing the AR coefficients of lower order models, and gradually increases the order from 1 to p. The Burg algorithm minimizes the expected norm of the prediction error vector. Implementation of the algorithm follows the procedure described by Press (1995).

The Burg algorithm is embedded in the microcontroller of the wireless sensing unit and demonstrated in a selected number of shake table tests at NCREE. The wireless sensing units are commanded to automatically determine the optimal AR model that fits the collected sensor data. Once the AR model is calculated, the model coefficients are then transmitted to the central server. As shown in Figure 3.10, the acceleration time history responses reconstructed using 20 AR model coefficients are compared with the directly recorded raw time history data at sensor locations A1, A4, and A6 (located on three different floors). As shown in the plots, the reconstructed time history using the AR model can accurately predict the response of the structure. That is, with the microcontroller, useful computations can be performed on the wireless sensing unit, and the amount of data (in this case, the AR coefficients) that need to be transmitted in real time can be significantly reduced.

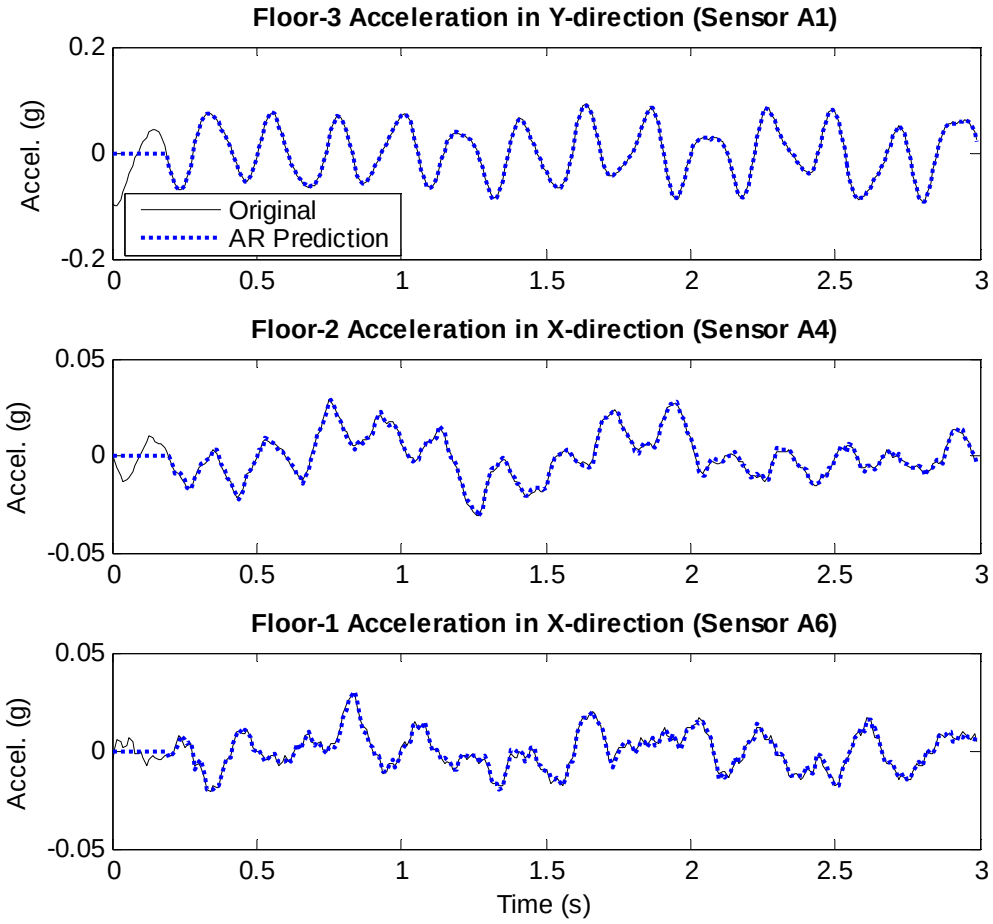

Figure 3.10. Comparison between original wireless sensor data and the AR predictions

3.3 Field Validation Tests at Geumdang Bridge, Icheon, South Korea

Field validation tests are also conducted to illustrate the use of the wireless units under real operating environments. Field tests can validate the long range communication of

the wireless sensors and reveal the potential problems in the propagation of wireless communication signals. Furthermore, ambient responses from normal daily operations in the field give very low signal amplitude, which could be difficult to measure with high precision. This section describes two field validation tests conducted at Geumdang Bridge in Icheon, South Korea, in collaboration with researchers at the Korea Advanced Institute of Science and Technology (KAIST). Sensor signal conditioning modules were employed during the second test. It is demonstrated that with the conditioned wireless sensor data, operating deflection shapes (ODS) of the bridge deck can be successfully extracted from the collected data.

3.3.1 Field Test 1 at Geumdang Bridge (December 2004)

Designed and managed by the Korea Highway Corporation (KHC), the two-lane test road at Geumdang Bridge is heavily instrumented to measure the performance of the pavement systems (Lee, *et al.* 2004). The pre-installed high precision wire-based system provides reliable baseline data for validating the performance of the wireless structural sensing system. The other convenient feature of this testing venue is that KHC has the ability to open or close the test road at will and to reroute traffic. The Geumdang Bridge has a total span of 273m, and is designed using two different section types. The northern portion is constructed with four independent spans (with span lengths of 31m, 40m, 40m and 40m respectively), each of which is designed using a 27cm concrete deck supported by four pre-cast concrete girders. The validation test is performed on the southern portion of the Geumdang Bridge. As shown in Figure 3.11, the southern portion of the bridge is constructed with a continuous 122m long post-tensioned box girder. The depth of the box girder is 2.6m, and the width of the bridge deck is about 12.6m. The southern portion is subdivided into three sections (38m, 46m, and 38m, respectively) which are supported by the abutment and the three piers.

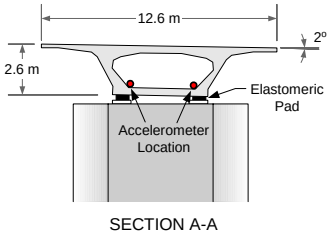

(a) Section view of the girder

(b) Side view picture of the bridge

(c) Outside perspective view of the bridge

(d) Interior of the box girder

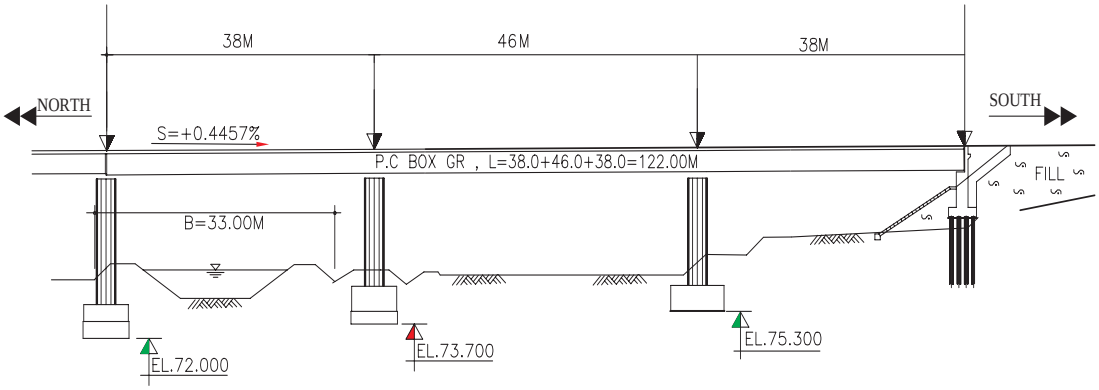

(e) Elevation view on the southern portion of the bridge

Figure 3.11. Illustration of Geumdang Bridge in Icheon, South Korea

The first field test was conducted in December 2004, without the sensor signal conditioning module (see Section 2.1.2). The wire-based system employs piezoelectric accelerometers to measure the vertical acceleration response of the bridge at the locations #1, 3, 4, 5, 6, 7, 8, 9, 10, 11, 13, 14, 15 and 16, as denoted in Figure 3.12(a). The piezoelectric accelerometers used by the wire-based monitoring system are PCB393

accelerometers manufactured by PCB Piezotronics. For direct comparison, the wireless sensing system also deploys accelerometers at these locations, with one accelerometer installed side-by-side to each PCB393 accelerometer (Figure 3.12b). However, for the wireless system, low-cost capacitive Piezotronics PCB3801 accelerometers are attached directly to the wireless sensing units at the 14 different sensor installation locations. Table 3.2 provides the performance comparison of the two accelerometers installed on the Geumdang Bridge. As illustrated in the table, PCB393 accelerometers used by the wire-based system have a very low noise floor of only 50μg and a high sensitivity of 10V/g. Therefore, the PCB393 accelerometers are well suited for use in ambient vibration applications, and they are expected to have better performance than the PCB3801 accelerometers used by the wireless system.

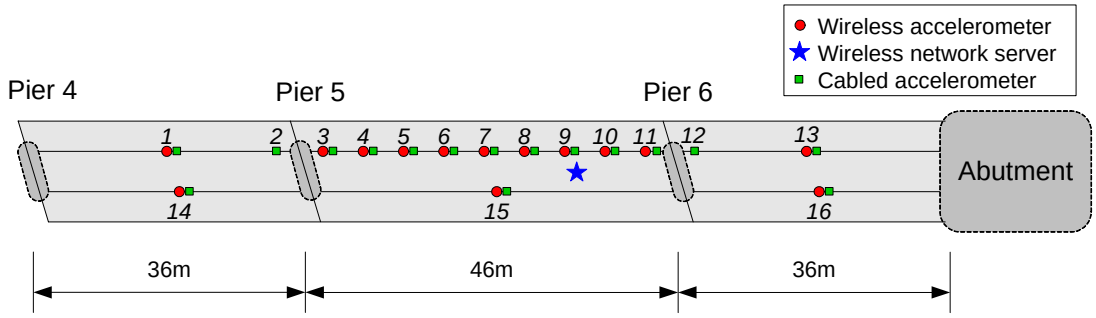

(a) Plan view showing wired and wireless accelerometers placed side-by-side for 14 locations

(b) Wired and wireless accelerometers

(c) Wireless sensing unit

(d) Truck excitation

Figure 3.12. Geumdang Bridge test in December 2004

Table 3.2. Parameters of the accelerometers used by the wire-based and wireless systems in the Geumdang Bridge test

Specification	PCB393 (Wired System)	PCB3801 (Wireless System)
Sensor Type	Piezoelectric	Capacitive
Maximum Range	± 0.5g	± 3g
Sensitivity	10 V/g	0.7 V/g
Bandwidth	2000 Hz	80 Hz
RMS Resolution (Noise Floor)	50 μg	500 μg
Minimal Excitation Voltage	18 ~ 30 VDC	5 VDC

While the interior of the box girder protects the wireless sensing units from harsh weather, there are a number of vertical stiffener diaphragms within the box girder that attenuate the wireless signal between the wireless sensing units. The wireless sensing units are installed with MaxStream 9XCite transceivers operating on the 900MHz frequency spectrum. The central server (a laptop connected with a 9XCite transceiver) is placed at the vicinity of sensor location #9, with a maximum distance between the central server and the furthest wireless sensing unit of about 60m. As opposed to the wire-based system, which takes over two days to install, the installation of the wireless sensing system takes only about couple hours.

For the wire-based monitoring system, the analog outputs of the PCB393 accelerometers are fed into a 16-channel PCB Piezotronics 481A03 signal conditioning unit. Before being sampled and digitized, the signals are filtered and amplified by a factor of 10 using an amplification circuit native to the Piezotronics 481A03 unit. A National Instruments' 12-bit data acquisition card (model number 6062E) is used by a standard laptop computer to sample and digitize the amplified accelerometer signals. The wire-based system is configured to sample the 14 sensor channels at 200Hz. For the wireless system, the PCB3801 accelerometers are connected directly to the sensing interface of each wireless sensing unit. Due to the limited wireless communication bandwidth and the large number of wireless sensing units that are streaming data simultaneously, the sampling rate of the wireless sensing system is selected at 70Hz. Over the course of two full days of testing,

the wireless sensing system never experiences any operational difficulties, and always successfully recovers from occasional data loss. The designed communication protocol for synchronized and continuous real-time data acquisition (see Section 3.1) proves to be highly reliable for the wireless sensor deployment on the bridge structure.

The Geumdang Bridge is kept closed to regular highway traffic while the bridge is excited using trucks of known weight and speed crossing the bridge (Figure 3.12d). Figure 3.13 illustrates the acceleration response of the bridge at sensor locations #8 and #13, when a 40-ton truck crosses the bridge at 60 km/hr. Sensor #8 is near the central server, while sensor #13 is among the farthest units from the central server. The figure plots the acceleration time histories collected by the two different systems. There exists a strong one-to-one correspondence in the acceleration response time history records collected by the two systems. As expected, the acceleration record measured by the wireless sensing system appears noisier than that collected by the wire-based system, due to the different accelerometers being used by the two systems and the signal conditioning in the wired system.

During the tests, the wireless sensing units were commanded to perform a 4096-point discrete Fourier transform (DFT) using the measured acceleration response. For a discrete signal h_k, the N-point DFT H_n is defined as:

$$H_n = \sum_{k=0}^{N-1} h_k e^{2\pi i k n / N}, n = 0, ..., N-1 \tag{3.2}$$

where i represents the imaginary unit. The corresponding frequency for each DFT point H_n depends on the sampling frequency f_s of the original discrete signal h_k:

$$f_n = \frac{n}{N} f_s \tag{3.3}$$

The complexity of computing DFT directly using the definition in Equation (3.2) is in general $O(N^2)$. When N is an integer power of two, Cooley-Tukey algorithm can be used

to compute the DFT more efficiently, with the complexity reduced to $O(N \log_2 N)$. The Cooley-Tukey algorithm, namely the fast Fourier transform (FFT), achieves its efficiency by recursively computing DFT of the odd-numbered points and even-numbered points of the signal h_k (Press 1995). When the length of the data is not an integer power of two, the data can be simply padded with zeros up to the next power of two.

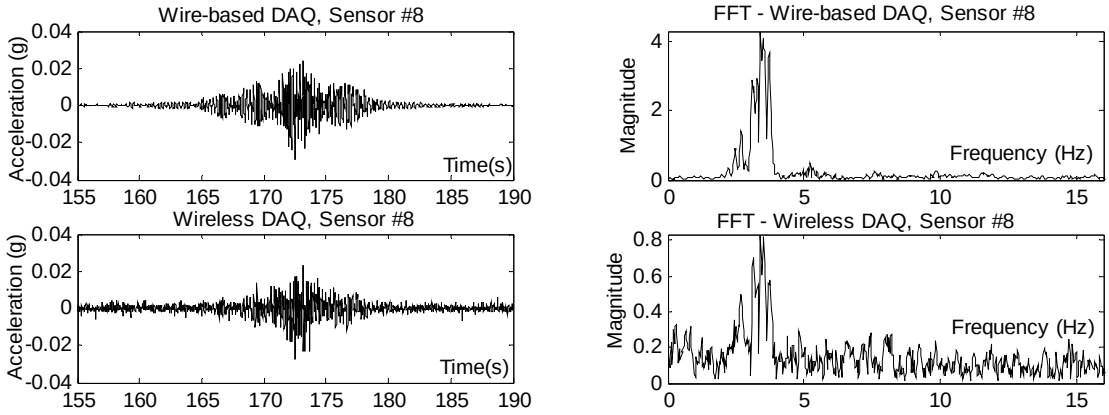

(a) Time-history responses and FFT results for sensor location #8

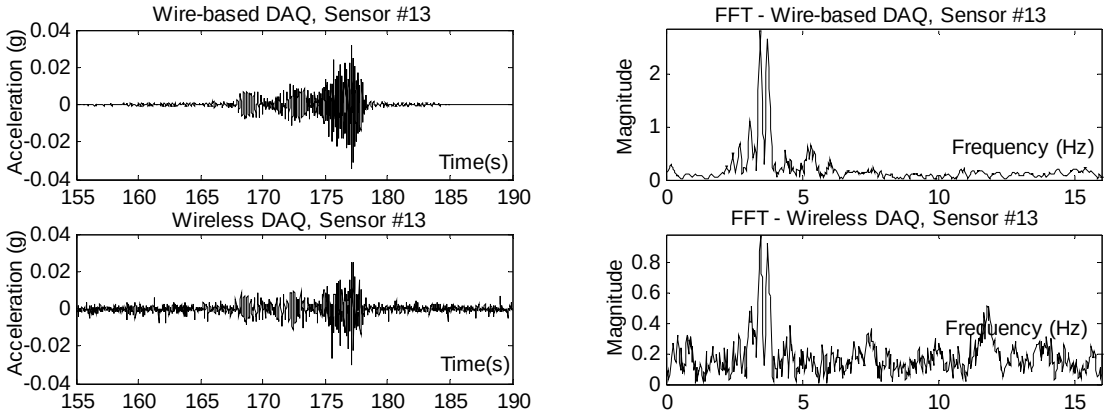

(b) Time-history responses and FFT results for sensor location #13

Figure 3.13. Measured acceleration time-history responses and the FFT results for the Geumdang Bridge test in December 2004

With the Cooley-Tukey algorithm embedded in the microcontrollers of the wireless sensing units, the frequency response calculated by the wireless units is shown in Figure 3.13. It can be seen that the frequency responses computed onboard by the wireless unit and off-line using the response data collected by the wire-based system are very close. The difference in the amplitude of the FFT results is mainly caused by the different sampling rate used in the two systems (70Hz in the wireless system and 200Hz in the wired system).

3.3.2 Field Test 2 at Geumdang Bridge (July 2005)

While the field test conducted at Geumdang Bridge in December 2004 successfully demonstrated the viability of the prototype wireless sensing system, the test results also show the discrepancy of using the wireless sensing units with low-cost sensors when measuring low-amplitude vibration signals in civil structures. A sensor signal conditioning module (see Section 2.1.2) was designed and fabricated after the Geumdang Bridge test in December 2004 to amplify sensor signals and filter signal noise. The signal conditioning module includes a low-pass fourth-order Bessel Filter with a cutoff frequency at 25Hz, which is designed to remove high-frequency sensor noises. The signal conditioning module can also amplify the sensor signal up to 20 times, so that the sensor signal is much stronger than circuitry noises before being digitized by the wireless sensing unit.

Using the sensor signal conditioning module, the second field test at the Geumdang Bridge was conducted in July 2005. In this second field test, a total of 14 accelerometers are deployed in the wireless system (Figure 3.14). A laptop connected with a MaxStream 9XCite transceiver, located at around the middle of the bridge, is employed to collect sensor data from all the 14 wireless sensing units. Furthermore, 13 accelerometers are instrumented with the wired system. The same set of accelerometers from the December 2004 test is employed by the wireless and wired systems (Table 3.2). The accelerometers

used in the wired system are high-precision piezoelectric accelerometers Piezotronics 393B12, and the accelerometers used in the wireless system are the MEMS accelerometers Piezotronics PCB3801 with lower precision. As in the December 2004 tests, PCB Piezotronics 481A03 signal conditioning unit and National Instruments' 12-bit data acquisition card (model number 6062E) are employed in the wired system.

Vibration tests are conducted by driving a 40-ton truck at set speeds to induce structural vibrations into the system. For all the tests conducted, the wireless sensing system proves to be highly reliable using the designed communication protocol and automatically recovers from occasional wireless transmission failures. The same sampling rate of 200Hz is employed by both the wired and the wireless system. Figure 3.15 shows the acceleration data recorded at sensor locations #2, #13, and #17 when the truck was crossing the bridge at 60km/h. Despite the difference in the accelerometer and signal conditioning devices, the recorded output by the wireless system has the precision identical to that offered by the commercial wired system. With the microcontroller, an embedded 4096 point FFT algorithm is used to determine the Fourier transform to the acceleration data. As shown in Figure 3.15, the first three dominant frequencies can easily be identified as 3.0, 4.3 and 5Hz, which are very close to the bridge natural frequencies previously published (Lee, *et al.* 2004).

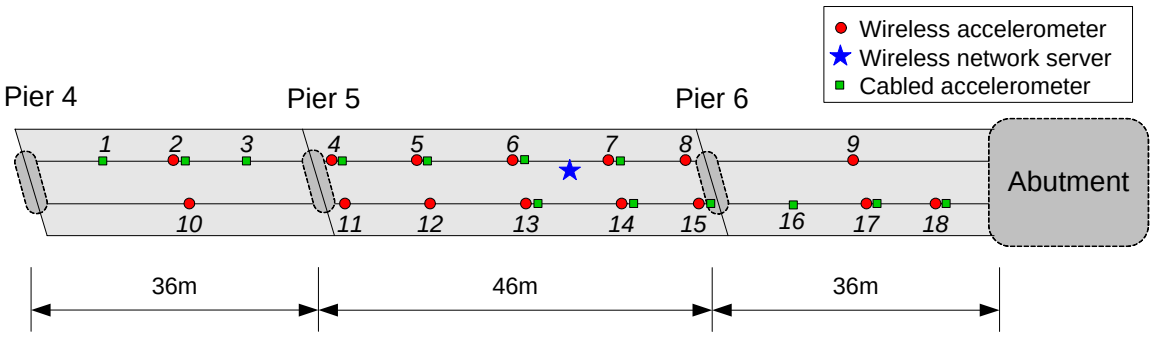

Figure 3.14. Deployment of wired and wireless accelerometers for the Geumdang Bridge test in July 2005

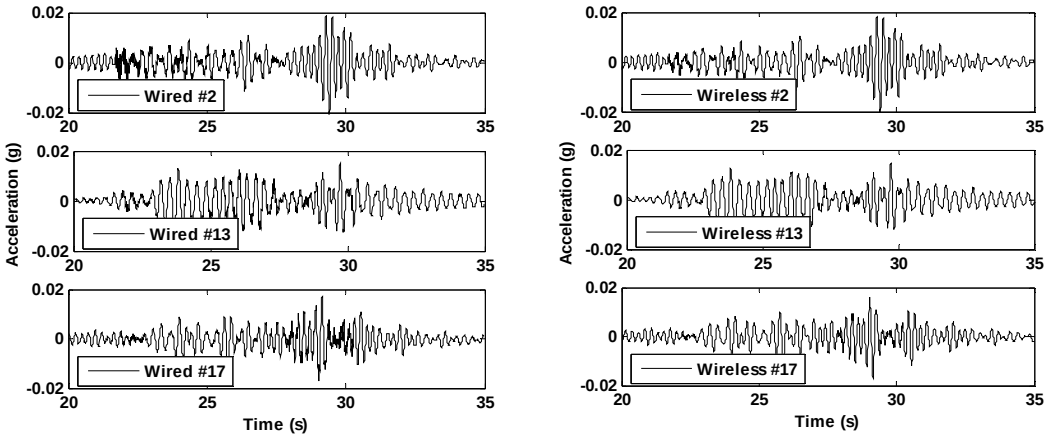

(a) Vertical acceleration of Geumdang Bridge when a 40 ton truck crossed at 60 km/hr

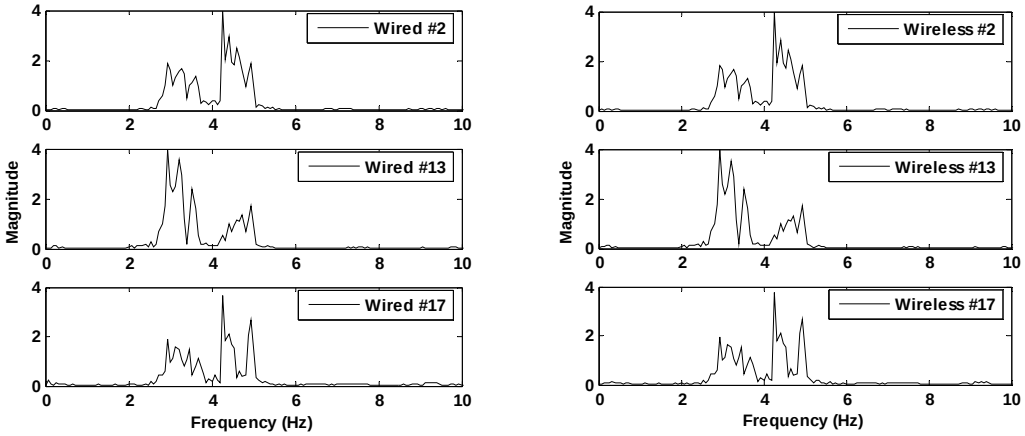

(b) FFT to the acceleration data

Figure 3.15. Measured acceleration time-history responses and the FFT results for the Geumdang Bridge test in July 2005

Once the dominant frequencies are determined, the complex numbers of the Fourier transform in the interested frequency range are wirelessly transmitted to the central server, so that the operating deflection shapes (ODS) of the bridge under the truck loading can be computed. Figure 3.16 illustrates the ODS for the first three dominant frequencies computed from the wireless sensor data. DIAMOND, a modal analysis software package, is used to extract the operating deflection shapes of the bridge deck

(Doebling, *et al.* 1997). Since the structure is excited by driving the truck along the bridge, the ODS shapes are not exactly the bridge mode shapes. Nevertheless, the ODS shapes are dominated by the corresponding modes and are typically good approximations to the mode shapes. The first three dominant frequencies are 2.93Hz, 4.27Hz, and 4.93Hz respectively. Both the dominant frequencies and ODS shapes agree with another set of analysis previously reported by Lynch *et al*. (2006a).

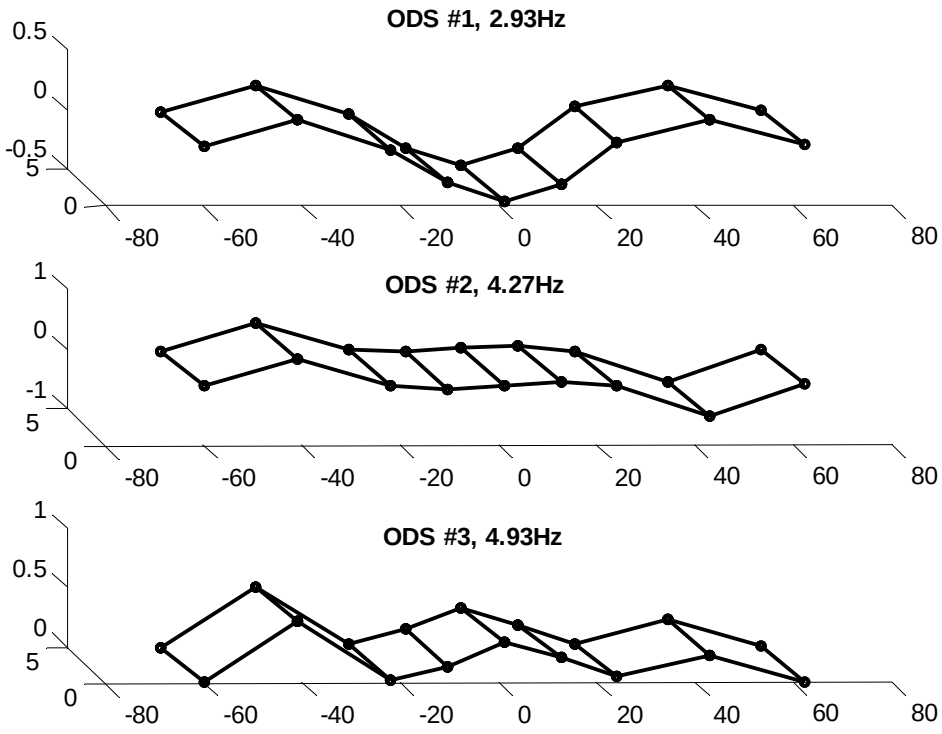

Figure 3.16. Operating deflection shapes (ODS) of the Geumdang Bridge

Utilizing the high quality of the wireless sensor data, the synchronization performance of the wireless sensor network can be evaluated. For each pair of wireless and wired measurement, the wireless sensor data can be shifted along the time axis so that the norm of the difference vector between the wireless and wired data is minimized. The time shift that achieves this minimized difference norm can be considered as the approximate time synchronization error. Analysis shows that for all the tests conducted in July 2005, the synchronization error is estimated to be less than or equal to 5ms at almost all the sensor locations. In each test, there is at most only one exceptional location where the estimated synchronization error is up to 10ms (Lynch*, et al.* 2006a).

3.4 Field Validation Test at Voigt Bridge, San Diego

Another field validation test for the wireless structural sensing system was conducted at Voigt Bridge, San Diego, CA, in March 2006. Up to 20 wireless sensing units were employed for the field test. A wire-based system was installed on the bridge, prior to the instrumentation of the wireless sensing system (Fraser*, et al.* 2006). An attractive feature of the wired system is the inclusion of a video camera that provides photographic data synchronized to bridge vibration data. This section describes the field instrumentation and test conducted at the Voigt Bridge. Comparison of the measurement results from the wired and wireless system is first presented. With the wireless system conveniently re-deployed to a different configuration, the operating deflection shapes (ODS) of the bridge deck are extracted from the wireless sensor data.

3.4.1 Instrumentation and Validation

Voigt Bridge is located on the campus of the University of California, San Diego. The bridge is a concrete box girder highway bridge that carries traffic over Interstate 5. The two-lane bridge is about 89.4m long and consists of four spans (Figure 3.17). The bridge deck has a skew angle of about 32º, with the concrete box-girder supported by three single-column bents. Over each bent, a concrete lateral diaphragm with a thickness of about 1.8m is located for stiffening the girder. The concrete lateral diaphragms could pose challenges for the transmission of wireless signals within the box girder. Longitudinally, the box girder is partitioned into five cells running the length of the bridge.

As a testbed project for structural health monitoring research, a sophisticated wire-based system has been installed in the northern-most cells of the Voigt Bridge by researchers at UCSD (Fraser*, et al.* 2006). The wire-based system includes accelerometers, strain gages, thermocouples, humidity sensors, and a video camera. Twenty capacitive accelerometers are installed in the northern most bridge cell, spaced about 4.5m apart, to measure the vertical vibration along the bridge. Data from the wired sensors are collected by a data acquisition system installed in the north-west corner of the bridge. Upon collection, the data can be accessed over the Internet using a Wi-Fi setup near the bridge. This wired data acquisition system serves as the baseline for validating the performance of the prototype wireless structural sensing system.

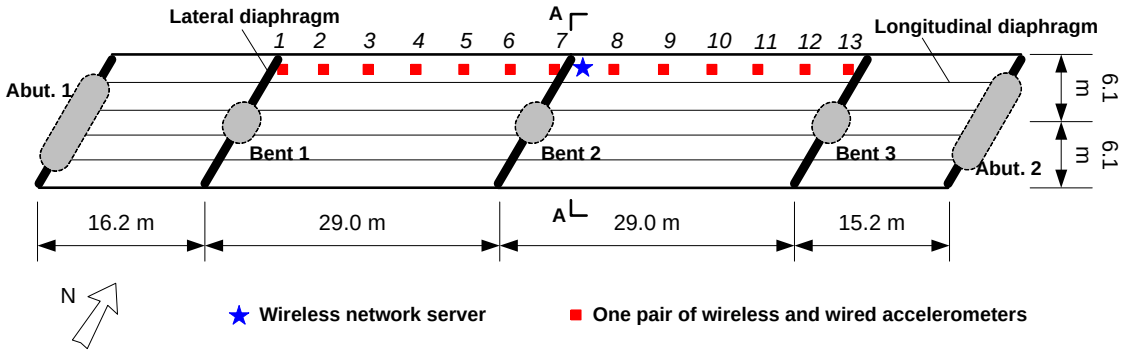

(a) Plan view of the bridge illustrating sensor locations of wired and wireless sensing systems

(b) View of the bridge deck

(c) Side view of the bridge over Interstate 5

Figure 3.17. Voigt Bridge on the campus of the University of California, San Diego

Girder cells along the north side of the bridge are accessible through four manholes on the bridge sidewalk. For the purpose of validating the proposed wireless structural sensing system, thirteen accelerometers interfaced to wireless sensing units are installed within the two middle spans of the bridge to measure vertical vibrations. One wireless sensing unit (associated with one signal conditioning module and one accelerometer) is placed immediately below the accelerometer associated with the permanent wired monitoring system (Figure 3.18). While the wired accelerometers are mounted to the cell walls, wireless accelerometers are simply mounted on the floor of the girder cells to expedite the installation process. The installation and calibration of the wireless sensing system, including the placement of the 13 wireless sensors, takes about an hour. The MaxStream 9XCite wireless transceiver operating at 900MHz (allowed by US government regulations) is integrated with each wireless sensing unit.

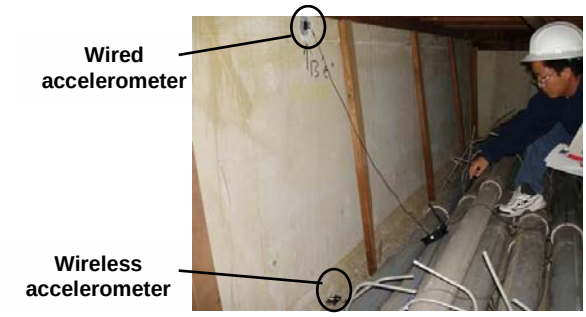

(a) Picture of one pair of wired and wireless accelerometers

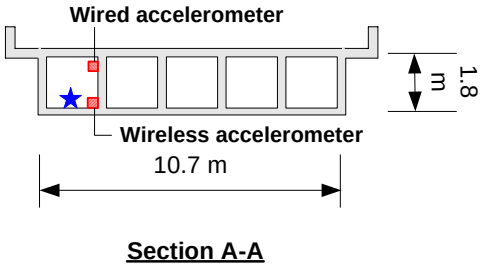

(b) Figure illustrating the deployment the accelerometers

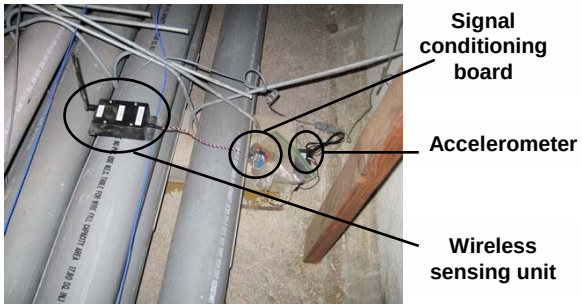

(c) One set of wireless sensing unit, signal conditioning board, and accelerometer

(d) Data acquisition unit of the wired monitoring system

Figure 3.18. Voigt Bridge test comparing the wireless and wired sensing systems

Accelerometers are instrumented for the Voigt Bridge test. At locations #3, 4, 5, 9, 10, and 11 as shown in Figure 3.17a, PCB Piezotronics 3801 accelerometers are used for both the wired and the wireless systems. At the other seven locations, Crossbow CXL01LF1 accelerometers are used with the wired system, while Crossbow CXL02LF1Z accelerometers are used with the wireless system. Table 3.3 summarizes the key parameters of the three types of accelerometers. Signal conditioning modules are used for filtering noise, amplifying and shifting signals for the wireless accelerometers. The signals of the wired accelerometers are directly digitized by a National Instruments PXI-6031E data acquisition board. Sampling frequencies for the wire-based system and the wireless system are 1,000 Hz and 200 Hz, respectively.

Table 3.3. Parameters of the accelerometers used by the wire-based and wireless systems in the Voigt Bridge test

Specification	PCB3801	CXL01LF1	CXL02LF1Z
Sensor Type	Capacitive	Capacitive	Capacitive
Maximum Range	± 3g	± 1g	± 2g
Sensitivity	0.7 V/g	2 V/g	1 V/g
Bandwidth	80 Hz	50Hz	50Hz
RMS Resolution (Noise Floor)	0.5 mg	0.5 mg	1 mg
Minimal Excitation Voltage	5 ~ 30 VDC	5 VDC	5 VDC

The bridge is under normal traffic operation during the tests. Figure 3.19(a) shows the time history data at locations #6 and #12, collected by the wire-based and wireless sensing systems when a vehicle passes over the bridge. A close match is observed between the data collected by the two systems. The minor difference between the two data sets can be mainly attributed to two sources: (1) the signal conditioning modules are used in the wireless system but not in the wired system; (2) the wired and wireless accelerometer locations are not exactly adjacent to each other, as previously described. Figure 3.19(b) shows the Fourier spectrum results determined from the time history data. The FFT results using the data collected by the wired system are computed offline, while the FFT results corresponding to the wireless data are computed online in real-time by each wireless sensing unit. After each wireless sensing unit executes its FFT algorithm, the FFT results are wirelessly transmitted to the network server. Strong agreement between the two sets of FFT results validates the computational reliability of the wireless sensing units. Because the sampling frequency of the wired system is five times higher than that of the wireless system, the magnitude of the Fourier spectrum for the wired system is also about five times higher than those for the wireless system.

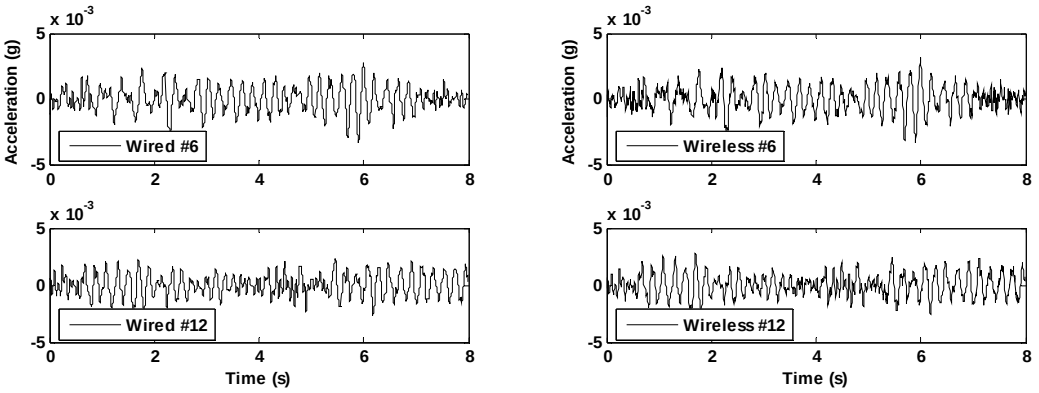

(a) Comparison between wired and wireless time history data

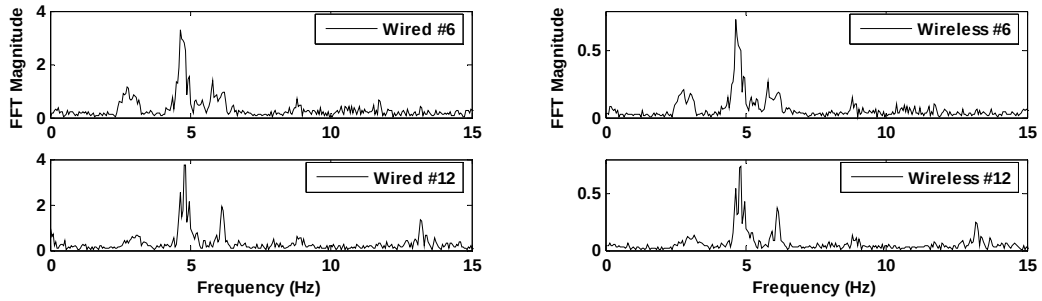

(b) Comparison between FFT to the wired data, as computed offline by a computer, and FFT to the wireless data, as computed online by the wireless sensing units

Figure 3.19. Comparison between wired and wireless data for the Voigt Bridge test

3.4.2 Operating Deflection Shape Analysis

One attractive feature of the wireless sensing system is that the locations of the sensors can be re-configured easily. To determine the operating deflection shapes of the bridge deck, the configuration of the original wireless sensing system is changed to attain a more suitable spatial distribution. Twenty wireless accelerometers and the wireless network server can be easily mounted to the bridge sidewalks (Figure 3.20). The communication distance between the server and the farthest-away wireless sensing unit is close to the full length of the bridge.

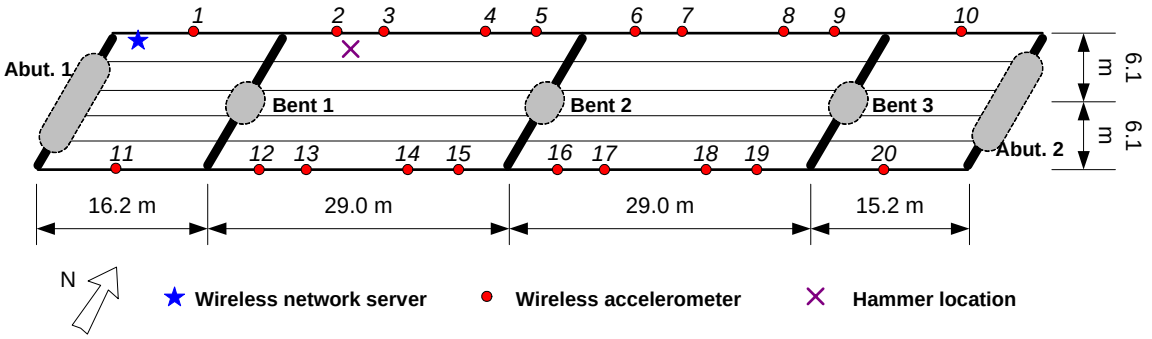

(a) Plan view of the bridge illustrating the deployment of wireless accelerometers

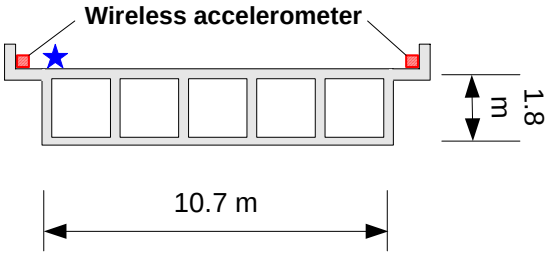

Section A-A

(b) View of section A-A

(c) One side of bridge deck with wireless accelerometers mounted

Figure 3.20. Wireless accelerometer deployment for the operating deflection shape analysis to Voigt Bridge

Hammer excitations are employed during the test. The excitation is applied during intervals of no passing vehicles. The operating deflection shape (ODS) analysis presented herein is based on the data collected during a hammer excitation test. The hammering location is shown in Figure 3.20(a). DIAMOND, a modal analysis software package, is used to extract the operating deflection shapes of the bridge deck (Doebling, *et al.* 1997). Under hammer excitation, the operating deflection shapes at or near a resonant frequency should be dominated by a single mode shape (Richardson 1997). Figure 3.21 presents the first four dominant operating deflection shapes of the bridge deck using wireless acceleration data. The ODS #1, #2, and #4 show primarily flexural bending modes of the bridge deck; a torsional mode is observed in ODS #3.

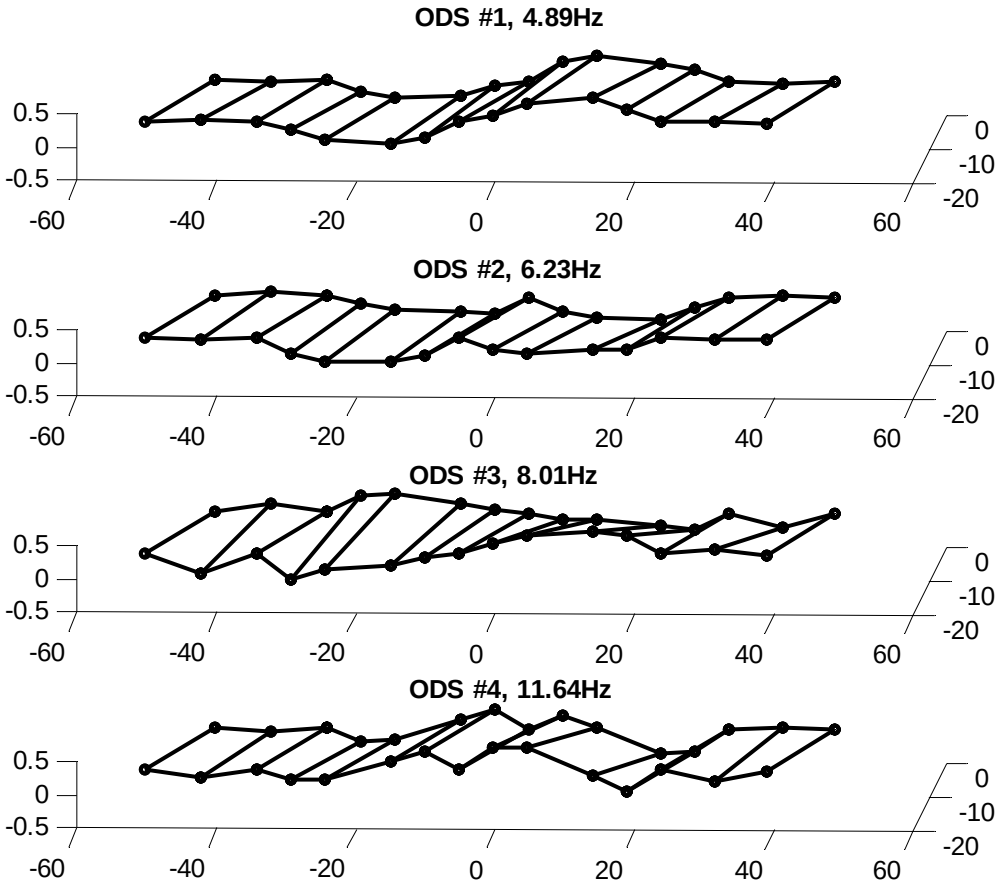

Figure 3.21. Operating deflection shapes of Voigt Bridge extracted from wireless sensor data

3.5 Summary

In this chapter, the design, implementation, and validation of a wireless sensing system have been described. The prototype wireless sensing system includes a single data server and multiple wireless sensing units that can be distributively deployed in a large-scale

civil structure. To avoid the overhead of off-the-shelf protocols, such as the Transmission Control Protocol (TCP) standard, a simple and efficient communication protocol is specially designed for the wireless structural sensing network. The protocol ensures synchronized and robust wireless sensor data collection. Using a dual-stack memory management scheme, the system also supports continuous data streaming from a network of wireless sensors. State machine concept proves to be effective in representing and designing communication program flows between the data server and the wireless sensing units.

This chapter has presented three large-scale laboratory and field validation tests for the prototype wireless sensing system:

1. The half-scale 3-story structural test at NCREE, Taiwan, illustrates the system robustness and the fidelity of wireless sensor data when deployed in a laboratory environment. The embedded computing capability of the wireless sensing units has also been successfully validated.

2. The Geumdang Bridge tests demonstrate the reliable performance of the wireless system in a real environment. The specially designed sensor signal conditioning module proves to be valuable for measuring low-amplitude vibration signals in civil structures. Engineering analyses, such as the determination of operating deflection shapes, have been successfully demonstrated using the conditioned wireless sensor data.

3. The test at Voigt Bridge again validates the performance of the wireless sensing system deployed on a boxed-girder bridge. Re-configurability of the wireless sensor network topology is illustrated by using two completely different deployment schemes.

Besides the validation tests reported in this chapter, the prototype wireless structural sensing system has also been tested on a number of other structures. On Gi-Lu Bridge, a

240m-span cable-stay bridge in Chi-Chi, Taiwan, 9 wireless sensing units were instrumented to measure the vertical velocity of the bridge deck (Lu, *et al.* 2006); on Grove Street Bridge in Ypsilanti, Michigan, 18 wireless sensing units were deployed to measure the dynamic acceleration and static strain measurements of the bridge deck (Hou and Lynch 2006); in Fox Theatre, Detroit, 21 wireless sensing units were mounted to measure the vertical acceleration of the balcony (Zimmerman, *et al.* 2007). The performance of the wireless structural sensing system has been successfully validated and enhanced through these tests. Future developments of the wireless sensing system may include multi-hopping multi-layer wireless sensor networks densely deployed in civil structures. Distributed intelligence in the wireless sensing nodes is yet to be better harnessed so that the wireless sensing nodes can collaboratively monitor structural condition and detect possible damage.

Chapter 4

Wireless Structural Control

In traditional structural control systems, coaxial wires are normally used to provide communication links between sensors, actuators and controllers. For a large scale structure, wired control systems require high instrumentation cost, are difficult to reconfigure, and potentially suffer from a single-point failure at the controller. With the rapid emergence of wireless communication and embedding computing technologies, a natural extension of the wireless sensing technology is to explore its applicability for semi-active or active control devices by eradicating cables associated with traditional control systems. The replacement of wired communication with wireless communication may result in substantial reduction in installation time and expense. Wireless control architectures can offer an attractive alternative, particularly for instrumenting large-scale civil structures.

As described in Chapter 2, an actuation module can be appended to the wireless sensing unit for structural control applications. In a wireless feedback structural control system, the wireless units not only collect structural response data in real time, but also communicate with other units, make optimal control decisions, and issue commands to structural actuators. Compared with wired control systems, the difficulties faced by a wireless feedback control system include the shorter communication range and longer

communication latency. To overcome these constraints in wireless communication, a decentralized control paradigm is being investigated when a sensing and control unit may not be able to acquire all the necessary information for control decisions based on full state feedback. In decentralized control strategies, structural response information is distributively collected and transmitted to the control units directly. Specifically, this research develops decentralized structural control algorithms for embedment in the wireless units. Experimental tests and numerical simulations have been conducted to verify the performance of the wireless sensing and control system.

This chapter presents the design of the wireless structural sensing and control system, a decentralized structural control algorithm, and the experimental and simulation results. Section 4.1 describes the architecture and implementation of the wireless control system. Section 4.2 presents the centralized and decentralized optimal structural control algorithms that are developed based on the classical linear quadratic regulator (LQR) control design. The effect of communication time delay is considered in the formulation of the control problem. Numerical simulations using a 3-story example structure are conducted to validate the efficacy and reliability of the control algorithms. Section 4.3 first analyzes the feedback time delay resulted from wireless communication latency, and then presents the laboratory validation experiments to the wireless structural control system using a 3-story half-scale steel frame instrumented with three magnetorheological (MR) dampers. Section 4.4 further investigates, through numerical simulations, the performance of decentralized measurement feedback control strategies for large scale structures. The effects of different decentralization strategies and communication time delays are examined.

4.1 A Prototype Wireless Structural Control System

In order to illustrate the architecture of the prototype wireless control system, Figure 4.1 shows a 3-story structure controlled by three actuators. Wireless sensors and controllers are mounted on the structure for measuring structural response data and commanding the actuators in real-time. To mimic the control tests to be described in the next section, besides the wireless sensing and control units for data collection and the operation of the actuators, the discussion herein assumes that a remote command server with a wireless transceiver is included in the system. The command server is employed to initiate the operation of the control system and to log the flow of wireless data. At the beginning of a wireless control test, the command server first broadcasts a start signal to all the wireless sensing and control units, which initiates the operation of the control system. Once the start command is received, the wireless units that are responsible for collecting sensor data start acquiring and broadcasting data at a preset time interval. Consequently, the wireless units responsible for commanding the actuators receive the sensor data, compute control decisions, and dispatch control commands within the specified time interval allotted at each time step. According to the control commands, the actuators apply forces to the structure to mitigate excessive vibration.

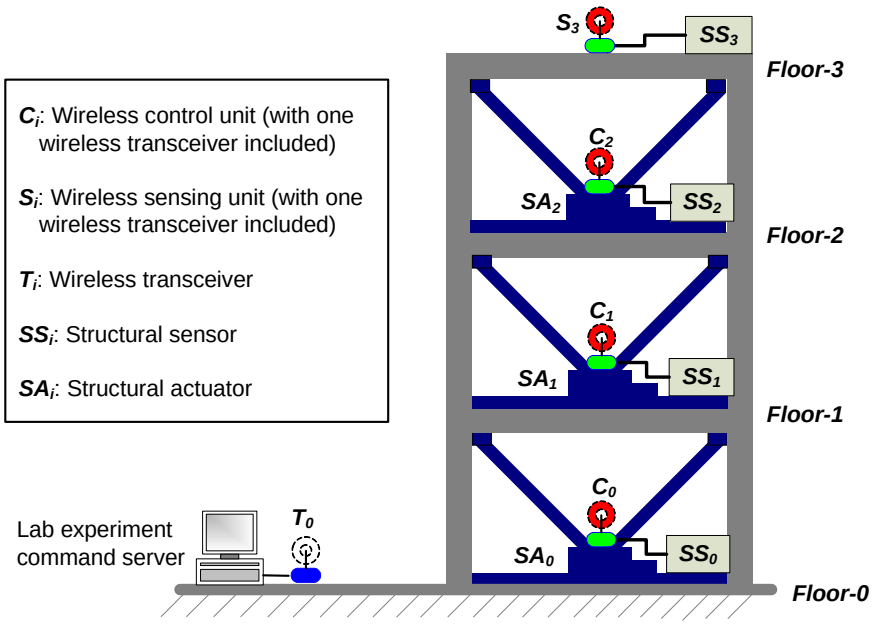

Figure 4.1. Illustration of the prototype wireless sensing and control system using a 3-story structure controlled by three actuators

Figure 4.2 illustrates the communication patterns in a traditional centralized control system and a decentralized control system. In a centralized control system, one centralized controller collects data from all the sensors in a structure, computes control decisions, and then dispatches actuation signals to actuators. In a decentralized control system, multiple sensors and controllers are distributively placed in a structure, and the control decisions are made with or without the full set of response data. The controller nodes can be closely collocated with system actuators. Compared with wired control systems, wireless control systems generally suffer from shorter communication range and longer communication time delay. Therefore, decentralized control is necessary in a wireless control system. In a decentralized control system, since each controller communicates with sensors and actuators in its vicinity, the requirement on communication range can be significantly reduced, and communication latency decreases by reducing the number of sensors or actuators that each controller has to communicate with. As the control decisions are computed and executed distributively by individual

controllers, system redundancy and reliability can also be improved using decentralized control. On the other hand, since each controller may only have limited information and longer time delay using wireless communication, the stability and optimality of decentralized control strategies need to be examined carefully.

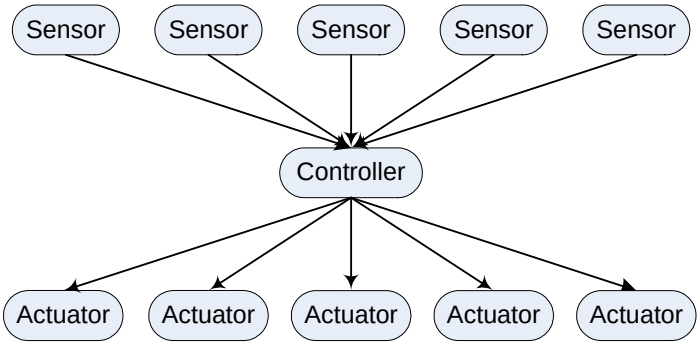

(a) A centralized control system

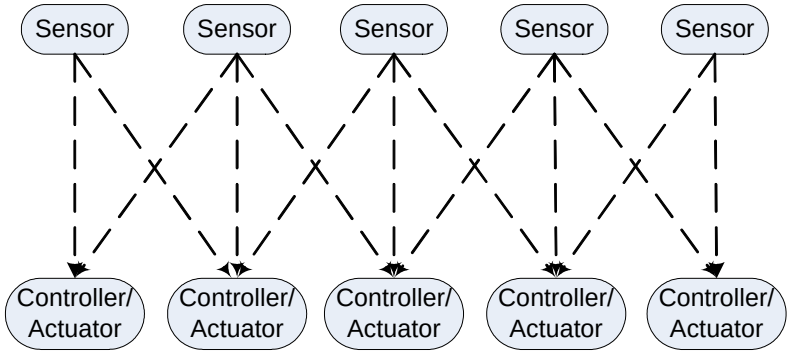

(b) A decentralized control system

Figure 4.2. Centralized and decentralized control systems

The feedback control loop designed for the prototype wireless sensing and control system is illustrated in Figure 4.3a, and the pseudo code implementing the feedback loop is presented in Figure 4.3b. As shown in the figure, sensing is designed to be clock-driven, while control and actuation are designed to be event-driven. The wireless sensing nodes collect sensor data at a preset sampling rate and transmit the data during an assigned time slot. Upon receiving the required sensor data, the control/actuation nodes immediately compute control decisions and apply the corresponding actuation signals to the actuators. If a control/actuation node does not receive the expected sensor data at one time step, it may use a previous data sample for control decisions, or does not take any action.

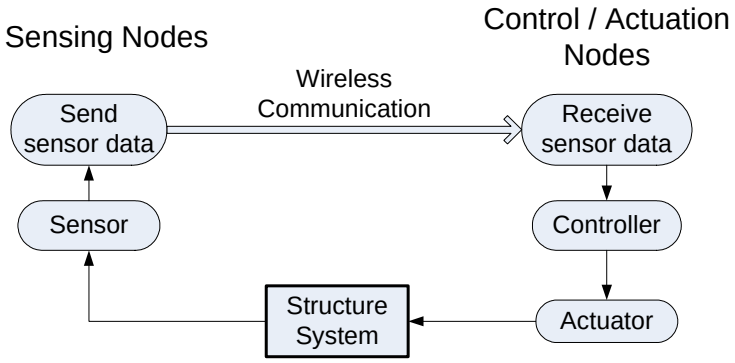

(a) Feedback control loop between the sensing nodes and control/actuation nodes

```
    Sensing Nodes (Clock-driven)          Control / Actuation Nodes (Event-driven)
ITERATE {                                 ITERATE {
                                            IF (sensor data arrived on time)
  Wait for the assigned time slot.            Compute control decisions.
                                              Apply actuation signal.
  Sample sensor data.                       ELSE
                                              Use old data sample or no action.
  Wirelessly transmit sensor data. ------>  Wait for new wireless sensor data.
}                                         }
```

(b) Pseudo code for the feedback control loop

Figure 4.3. Illustration of the feedback control loop in a wireless sensing and control system

Similar to the wireless structural sensing system, state machine concept is used for designing and implementing the wireless structural control system. For each wireless subnet, one wireless unit is designed to coordinate the communication sequence at every control sampling time step. Figure 4.4 and Figure 4.5 illustrate the communication state diagrams of a coordinator wireless unit and other non-coordinator units, respectively. To initiate the system operation, the coordinator unit first broadcasts a start command '01StartCtrl' to all other sensing and control units in the subnet. Once the start command and its acknowledgement '03AcknStartCtrl' are received, the system starts the real-time feedback control operation, i.e. both the coordinator and other units are in "State2". At every sampling time step, the coordinator unit broadcasts a beacon signal '02BeaconData' together with its own sensor data, announcing the start of a new time step. Upon receiving the beacon signal, other sensing units broadcast their sensor data following a preset transmission sequence, so that transmission collision is avoided. The wireless control units responsible for commanding the actuators receive the sensor data, calculate desired control forces, and apply control commands at each time step. To guarantee a constant sampling time step and to minimize feedback latency, timeout checking and data re-transmission are not recommended during the feedback control operation. Instead, if a control/actuation node does not receive the expected sensor data at one time step, it may use a previous data sample, or take no action. This design is applicable for both centralized control (where the coordinator unit and all other sensing/control units are all within a single network) and decentralized control (where each wireless subnet includes one coordinator and a number of sensing/control units).

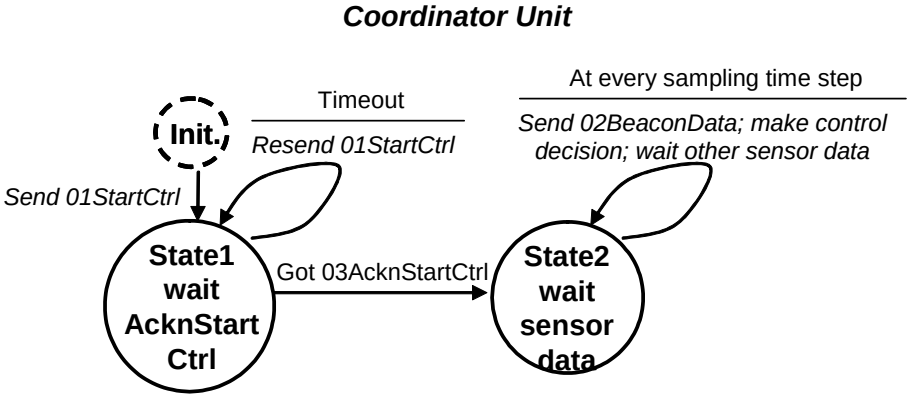

Figure 4.4. Communication state diagram of a coordinator unit in a wireless structural control subnet

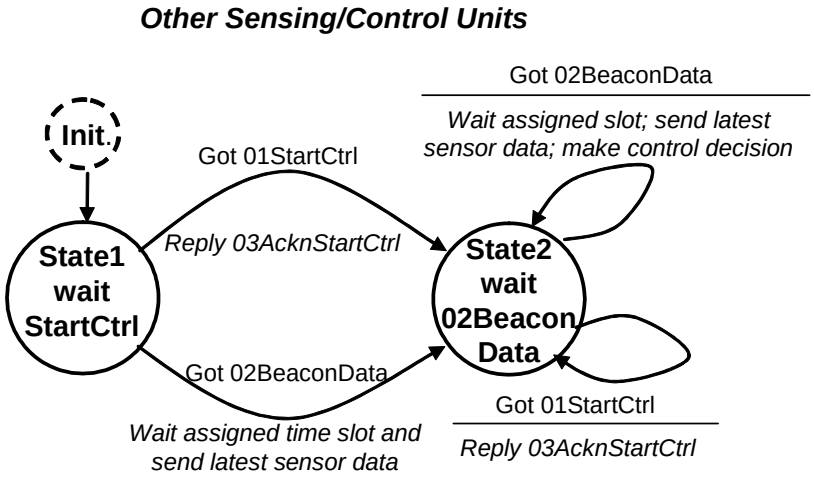

Figure 4.5. Communication state diagram of non-coordinator units in a wireless structural control subnet

4.2 Centralized and Decentralized Structural Control Algorithms

In a feedback structural control system, optimal control decisions need to be made according to the measured sensor data in real time. This section introduces an optimal structural control algorithm that is developed based on the classical Linear Quadratic Regulator (LQR) control design (Franklin, *et al.* 1998). The effect of feedback time delay is considered in the formulation of the control problem. Centralized and decentralized control solutions are developed for the time-delayed measurement feedback control problem. Numerical simulations using a 3-story example structure are conducted to illustrate the efficacy and reliability of the control algorithms.

4.2.1 Formulation of the Structural Control Problem

For a lumped-mass model with n degrees-of-freedom (DOF), the system equation of motion of a controlled structural system can be formulated as:

$$\mathbf{M}\ddot{\mathbf{q}}(t)+\mathbf{C}\dot{\mathbf{q}}(t)+\mathbf{K}\mathbf{q}(t)=\mathbf{T}_{\mathbf{u}}\mathbf{u}(t)+\mathbf{T}_{\mathbf{w}}\mathbf{w}(t) \tag{4.1}$$

where $\mathbf{q}(t)$ is the $n \times 1$ displacement vector relative to the ground; $\mathbf{M}$, $\mathbf{C}$, $\mathbf{K}$ are the $n \times n$ mass, damping, and stiffness matrices; $\mathbf{w}(t)$ and $\mathbf{u}(t)$ are the $m_1 \times 1$ external excitation and $m_2 \times 1$ control force vectors, respectively; and $\mathbf{T_u}$ and $\mathbf{T_w}$ are the control force and external excitation location matrices, respectively.

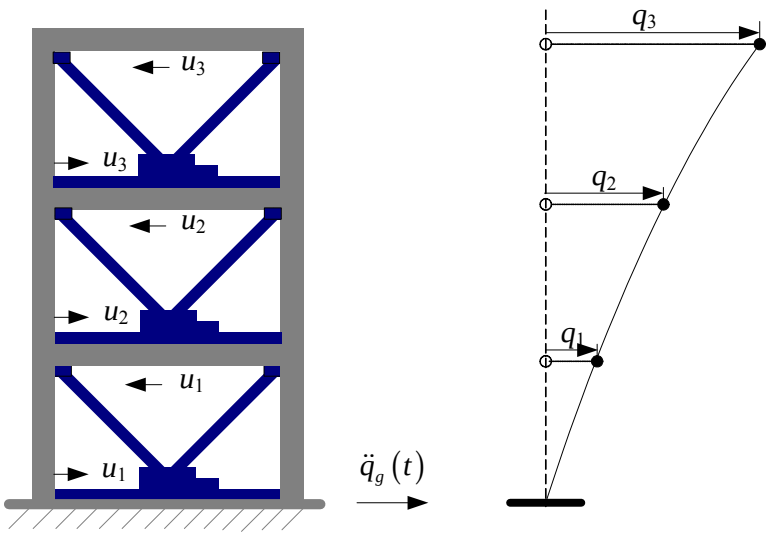

Figure 4.6. A three-story controlled structure excited by unidirectional ground motion

For simplicity, the discussion is based on a 2-D shear frame structure subject to unidirectional ground excitation. In the example structure shown in Figure 4.6, when the external excitation is unidirectional ground motion, $\mathbf{w}(t)$ is a scalar ($m_1 = 1$) containing the ground acceleration history $\ddot{q}_g(t)$ and the spatial load pattern $\mathbf{T_w}$ is equal to $-\mathbf{M}\{\mathbf{1}\}_{n\times 1}$. Entries in $\mathbf{u}(t)$ are the actuator forces between neighboring floors. For the 3-story structure, if a positive actuator force is defined to be moving the floor above the actuator towards the left direction, and moving the floor below the actuator towards the right direction (as shown in Figure 4.6), the control force location matrix $\mathbf{T_u}$ can be defined as:

$$\mathbf{T_u} = \begin{bmatrix} -1 & 1 & 0 \\ 0 & -1 & 1 \\ 0 & 0 & -1 \end{bmatrix} \tag{4.2}$$

The state-space representation of the structural system can be written as (Soong 1990):

$$\dot{\mathbf{x}}(t) = \mathbf{A}\mathbf{x}(t) + \mathbf{B}\mathbf{u}(t) + \mathbf{E}\mathbf{w}(t) \tag{4.3}$$

where $\mathbf{x} = \left[\mathbf{q}(t); \dot{\mathbf{q}}(t)\right]$ is the state vector, and the state space system matrices are defined as:

$$\mathbf{A} = \begin{bmatrix} \mathbf{0}_{n\times n} & \mathbf{I}_{n\times n} \\ -\mathbf{M}^{-1}\mathbf{K} & -\mathbf{M}^{-1}\mathbf{C} \end{bmatrix},\ \mathbf{B} = \begin{bmatrix} \mathbf{0}_{n\times m_2} \\ \mathbf{M}^{-1}\mathbf{T}_{\mathbf{u}} \end{bmatrix},\ \mathbf{E} = \begin{bmatrix} \mathbf{0}_{n\times m_1} \\ \mathbf{M}^{-1}\mathbf{T}_{\mathbf{w}} \end{bmatrix} \tag{4.4}$$

For convenient implementation using digital controllers, such as the microcontrollers in the wireless sensing and actuation nodes, a discrete system equivalent to the continuous system in Equation (4.3) can be formulated. A typical approach in formulating an approximate discrete system equivalent to the continuous system is to assume a zero-order hold (ZOH) (Franklin, *et al.* 1998). Using ZOH, the control force is assumed to be piece-wise constant during each sampling time step:

$$\mathbf{u}(t) = \mathbf{u}(kT), kT \le t < (k+1)T \tag{4.5}$$

where T is the sampling time period, and k is an integer representing the sampling step number (k = 0, 1, 2, …). With the ZOH assumption, the discrete state-space system is found to be (Franklin, *et al.* 1998):

$$\mathbf{x}_{\mathbf{d}}[k+1] = \mathbf{A}_{\mathbf{d}}\mathbf{x}_{\mathbf{d}}[k] + \mathbf{B}_{\mathbf{d}}\mathbf{u}_{\mathbf{d}}[k] + \int_0^T e^{\mathbf{A}(T-\tau)}\mathbf{E}\mathbf{w}(kT+\tau)\,d\tau,\ k = 0,1,2... \tag{4.6}$$

where the discrete system matrices $\mathbf{A_d}$ and $\mathbf{B_d}$ are defined as:

$$\begin{aligned} \mathbf{A}_{\mathbf{d}} &= e^{\mathbf{A}T} \\ \mathbf{B}_{\mathbf{d}} &= \int_0^T e^{\mathbf{A}\tau}\mathbf{B}\,d\tau = \mathbf{A}^{-1}\left(e^{\mathbf{A}T} - \mathbf{I}\right)\mathbf{B},\ \text{when } \mathbf{A}^{-1} \text{ exists} \end{aligned} \tag{4.7}$$

For the above equations, the matrix exponential, $e^{\mathbf{J}}$, where $\mathbf{J}$ is a square matrix, is defined as:

$$e^{\mathbf{J}} = \mathbf{I} + \mathbf{J} + \frac{\mathbf{J}^2}{2!} + \frac{\mathbf{J}^3}{3!} + \cdots = \sum_{k=0}^{\infty} \frac{\mathbf{J}^k}{k!} \tag{4.8}$$

The state vector of the discrete system in Equation (4.6) is equivalent to the state vector of the continuous system in Equation (4.3) at each k^{th} discrete time step:

$$\mathbf{x}(t) = \mathbf{x}_{\mathbf{d}}[k], t = kT \tag{4.9}$$

When implementing a control system, time delay is often encountered in sensing, communication, or actuation. Assuming feedback time delay of l steps (i.e. a time delay of lT) for each sampling step, the discrete system can be formulated by modifying Equation (4.6) as:

$$\mathbf{x}_{\mathbf{d}}[k+1] = \mathbf{A}_{\mathbf{d}}\mathbf{x}_{\mathbf{d}}[k] + \mathbf{B}_{\mathbf{d}}\mathbf{u}_{\mathbf{d}}[k-l] + \int_0^T e^{\mathbf{A}(T-\tau)}\mathbf{E}\mathbf{w}(kT+\tau)\,d\tau \tag{4.10}$$

Since the objective of feedback control is essentially to improve the stabilization properties of the closed-loop system, the excitation $\mathbf{w}(t)$ is omitted. Thus, the simplified state-space representation considering time delay becomes:

$$\mathbf{x}_{\mathbf{d}}[k+1] = \mathbf{A}_{\mathbf{d}}\mathbf{x}_{\mathbf{d}}[k] + \mathbf{B}_{\mathbf{d}}\mathbf{u}_{\mathbf{d}}[k-l] \tag{4.11}$$

In order to effectively mitigate excessive structural response, the control force vector $\mathbf{u_d}$ needs to be decided appropriately at each sampling time step. Centralized and decentralized control solutions that can be used to optimally decide the control force vector $\mathbf{u_d}$ are presented in the next subsection.

4.2.2 Centralized and Decentralized Control Algorithm Considering Time Delay

For the state-space representation of the time-delayed structural control system as defined in Equation (4.11), the objective of the classical linear quadratic regulator (LQR) control is to minimize a quadratic cost function J:

$$J\Big|_{\mathbf{u_d}} = \sum_{k=l}^{\infty}\left(\mathbf{x_d}^T[k]\mathbf{Q}\mathbf{x_d}[k] + \mathbf{u_d}^T[k-l]\mathbf{R}\mathbf{u_d}[k-l]\right),\ \mathbf{Q}_{2n\times 2n} \geq 0 \text{ and } \mathbf{R}_{m_2\times m_2} > 0 \qquad (4.12)$$

by selecting an optimal control force trajectory $\mathbf{u_d}$. Let the measurement vector be denoted by a $p_2 \times 1$ vector $\mathbf{y_d}[k]$ measured at time k. The state-space vector $\mathbf{x_d}[k]$ and the measurement vector $\mathbf{y_d}[k]$ can be related by a $p_2 \times 2n$ linear transformation, $\mathbf{C_y}$, as:

$$\mathbf{y_d}[k] = \mathbf{C_y}\mathbf{x_d}[k] \qquad (4.13)$$

For example, if the relative velocities on all floors are measurable but the relative displacements are not measurable, $\mathbf{C_y}$ can be defined as:

$$\mathbf{C}_{\mathbf{y}I} = \left[\mathbf{0}_{n\times n} \quad \vdots \quad \mathbf{I}_{n\times n}\right] \qquad (4.14)$$

In another example, if only inter-story velocities between adjacent floors are measurable, the following measurement matrix $\mathbf{C_y}$ can be used for the 3-story structure shown in Figure 4.6:

$$\mathbf{C}_{\mathbf{y}II} = \left[\begin{array}{c|ccc} & 1 & 0 & 0 \\ \left[\mathbf{0}_{3\times 3}\right] & -1 & 1 & 0 \\ & 0 & -1 & 1 \end{array}\right] \qquad (4.15)$$

Assuming static measurement feedback, the optimal feedback control force $\mathbf{u_d}$ is computed using an $m_2 \times p_2$ gain matrix $\mathbf{G_d}$ as:

$$\mathbf{u_d}[k] = \mathbf{G_d}\mathbf{y_d}[k] \qquad (4.16)$$

where the gain matrix $\mathbf{G_d}$ is designed so that the cost function J is minimized. The information structure for decentralized feedback can be represented by appropriate sparsity patterns in the gain matrix $\mathbf{G_d}$. For example, the following equation illustrates the patterns of two decentralized and one centralized gain matrices for the 3-story lumped-mass shear structure:

$$\mathbf{G}_{\mathbf{d}I} = \begin{bmatrix} \blacksquare & 0 & 0 \\ 0 & \blacksquare & 0 \\ 0 & 0 & \blacksquare \end{bmatrix}, \quad \mathbf{G}_{\mathbf{d}II} = \begin{bmatrix} \blacksquare & \blacksquare & 0 \\ 0 & \blacksquare & \blacksquare \\ 0 & \blacksquare & \blacksquare \end{bmatrix} \text{ and } \mathbf{G}_{\mathbf{d}III} = \begin{bmatrix} \blacksquare & \blacksquare & \blacksquare \\ \blacksquare & \blacksquare & \blacksquare \\ \blacksquare & \blacksquare & \blacksquare \end{bmatrix} \tag{4.17}$$

When combined with the measurement matrix $\mathbf{C}_\mathbf{y}$ defined in Equations (4.14) and (4.15), the pattern in $\mathbf{G}_{\mathbf{d}I}$ specifies that when computing control decisions, the actuator at each floor only needs the entry in the measurement vector $\mathbf{y}_\mathbf{d}$ corresponding to that floor. The pattern in $\mathbf{G}_{\mathbf{d}II}$ specifies that the control decisions require information from a neighboring floor. Finally, the pattern in $\mathbf{G}_{\mathbf{d}III}$ indicates all entries in the measurement vector participate in the control decisions, thus, equivalent to a centralized control scheme.

For the feedback control problem with l steps of time delay, Chung *et al*. (1995) propose a solution by introducing a modified first-order difference equation:

$$\overline{\mathbf{x}}_\mathbf{d}[k+1] = \overline{\mathbf{A}}_\mathbf{d}\overline{\mathbf{x}}_\mathbf{d}[k] + \overline{\mathbf{B}}_\mathbf{d}\overline{\mathbf{u}}_\mathbf{d}[k] \tag{4.18}$$

This modified first-order difference system is equivalent to the original system by proper definitions of the augmented matrices and vectors:

$$\overline{\mathbf{A}}_\mathbf{d} = \begin{bmatrix} \mathbf{A}_\mathbf{d} & \mathbf{0} & \cdots & \mathbf{0} & \mathbf{0} \\ \mathbf{I} & \mathbf{0} & \cdots & \mathbf{0} & \mathbf{0} \\ \mathbf{0} & \mathbf{I} & \cdots & \mathbf{0} & \mathbf{0} \\ \vdots & \vdots & \ddots & \vdots & \vdots \\ \mathbf{0} & \mathbf{0} & \cdots & \mathbf{I} & \mathbf{0} \end{bmatrix}, \quad \overline{\mathbf{B}}_\mathbf{d} = \begin{bmatrix} \mathbf{B}_\mathbf{d} \\ \mathbf{0} \\ \mathbf{0} \\ \vdots \\ \mathbf{0} \end{bmatrix}, \quad \overline{\mathbf{x}}_\mathbf{d}[k] = \begin{bmatrix} \mathbf{x}_\mathbf{d}[k] \\ \mathbf{x}_\mathbf{d}[k-1] \\ \vdots \\ \mathbf{x}_\mathbf{d}[k-l] \end{bmatrix}, \quad \overline{\mathbf{u}}_\mathbf{d}[k] = \mathbf{u}_\mathbf{d}[k-l] \tag{4.19}$$

where $\mathbf{0}$ and $\mathbf{I}$ represent, respectively, the zero and identity submatrices of proper dimensions. Correspondingly, the weighting matrix $\mathbf{Q}$ and the measurement matrix $\mathbf{C}_\mathbf{y}$ are also augmented and denoted by $\overline{\mathbf{Q}}$ and $\overline{\mathbf{C}}_\mathbf{y}$, respectively, as:

$$\bar{\mathbf{Q}} = \begin{bmatrix} \mathbf{Q} & \mathbf{0} & \cdots & \mathbf{0} & \mathbf{0} \\ \mathbf{0} & \mathbf{0} & \cdots & \mathbf{0} & \mathbf{0} \\ \mathbf{0} & \mathbf{0} & \cdots & \mathbf{0} & \mathbf{0} \\ \vdots & \vdots & \ddots & \vdots & \vdots \\ \mathbf{0} & \mathbf{0} & \cdots & \mathbf{0} & \mathbf{0} \end{bmatrix}, \quad \bar{\mathbf{C}}_{\mathbf{y}} = \begin{bmatrix} \mathbf{0} & \mathbf{0} & \cdots & \mathbf{0} & \mathbf{C}_{\mathbf{y}} \end{bmatrix} \tag{4.20}$$

To make the optimization problem independent of the initial state of the structure, $\bar{\mathbf{x}}_{\mathbf{d}}[l]$, which contains the state space vectors $\mathbf{x_d}[0]$, …, $\mathbf{x_d}[l]$, is considered as a random vector. The design objective is altered to minimize the expected value of the original cost J:

$$\bar{J} = E\{J\} \tag{4.21}$$

where $E\{\bullet\}$ denotes the expectation of a random variable. Let $\bar{\mathbf{X}}_{\mathbf{d}l}$ represent the second statistical moment of the augmented initial state:

$$\bar{\mathbf{X}}_{\mathbf{d}l} = E\left\{\bar{\mathbf{x}}_{\mathbf{d}}[l]\bar{\mathbf{x}}_{\mathbf{d}}^{T}[l]\right\} \tag{4.22}$$

It can be shown that by introducing an auxiliary matrix $\mathbf{H}$,

$$\mathbf{H} = \sum_{k=0}^{\infty}\left[\left(\bar{\mathbf{A}}_{\mathbf{d}} + \bar{\mathbf{B}}_{\mathbf{d}}\mathbf{G}_{\mathbf{d}}\bar{\mathbf{C}}_{\mathbf{y}}\right)^{k}\right]^{T}\left(\bar{\mathbf{Q}} + \bar{\mathbf{C}}_{\mathbf{y}}{}^{T}\mathbf{G}_{\mathbf{d}}{}^{T}\mathbf{R}\mathbf{G}_{\mathbf{d}}\bar{\mathbf{C}}_{\mathbf{y}}\right)\left(\bar{\mathbf{A}}_{\mathbf{d}} + \bar{\mathbf{B}}_{\mathbf{d}}\mathbf{G}_{\mathbf{d}}\bar{\mathbf{C}}_{\mathbf{y}}\right)^{k} \tag{4.23}$$

the expected cost is equivalent to (Chung, *et al.* 1995):

$$\bar{J} = E\left\{\bar{\mathbf{x}}_{\mathbf{d}}^{T}[l]\mathbf{H}\bar{\mathbf{x}}_{\mathbf{d}}[l]\right\} = trace\left(\mathbf{H}\bar{\mathbf{X}}_{\mathbf{d}l}\right) \tag{4.24}$$

where $trace(\bullet)$ denotes the trace of a square matrix. In practice, it is generally assumed that initial state $\bar{\mathbf{x}}_{\mathbf{d}}[l]$ is a random variable uniformly distributed on the surface of the unit sphere, i.e. $\bar{\mathbf{X}}_{\mathbf{d}l} = \mathbf{I}$. Finally, the control problem with time delay can be posed as solving the following nonlinearly coupled matrix equations:

$$\left(\bar{\mathbf{A}}_{\mathbf{d}} + \bar{\mathbf{B}}_{\mathbf{d}}\mathbf{G}_{\mathbf{d}}\bar{\mathbf{C}}_{\mathbf{y}}\right)^{T}\mathbf{H}\left(\bar{\mathbf{A}}_{\mathbf{d}} + \bar{\mathbf{B}}_{\mathbf{d}}\mathbf{G}_{\mathbf{d}}\bar{\mathbf{C}}_{\mathbf{y}}\right) - \mathbf{H} + \left(\bar{\mathbf{Q}} + \bar{\mathbf{C}}_{\mathbf{y}}{}^{T}\mathbf{G}_{\mathbf{d}}{}^{T}\mathbf{R}\mathbf{G}_{\mathbf{d}}\bar{\mathbf{C}}_{\mathbf{y}}\right) = \mathbf{0} \tag{4.25a}$$

$$\partial \bar{J} / \partial \mathbf{H} = \left(\bar{\mathbf{A}}_{\mathbf{d}} + \bar{\mathbf{B}}_{\mathbf{d}}\mathbf{G}_{\mathbf{d}}\bar{\mathbf{C}}_{\mathbf{y}}\right)\mathbf{L}\left(\bar{\mathbf{A}}_{\mathbf{d}} + \bar{\mathbf{B}}_{\mathbf{d}}\mathbf{G}_{\mathbf{d}}\bar{\mathbf{C}}_{\mathbf{y}}\right)^{T} - \mathbf{L} + \bar{\mathbf{X}}_{\mathbf{d}l} = \mathbf{0} \tag{4.25b}$$

$$\partial \bar{J} / \partial \mathbf{G}_{\mathbf{d}} = 2\bar{\mathbf{B}}_{\mathbf{d}}{}^{T}\mathbf{H}\left(\bar{\mathbf{A}}_{\mathbf{d}} + \bar{\mathbf{B}}_{\mathbf{d}}\mathbf{G}_{\mathbf{d}}\bar{\mathbf{C}}_{\mathbf{y}}\right)\mathbf{L}\bar{\mathbf{C}}_{\mathbf{y}}{}^{T} + 2\mathbf{R}\mathbf{G}_{\mathbf{d}}\bar{\mathbf{C}}_{\mathbf{y}}\mathbf{L}\bar{\mathbf{C}}_{\mathbf{y}}{}^{T} = \mathbf{0} \tag{4.25c}$$

where $\mathbf{G}_{\mathbf{d}}$ is the optimal feedback gain matrix, $\mathbf{H}$ is the auxiliary matrix, and $\mathbf{L}$ is a Lagrangian multiplier matrix. Details on the derivation of the above procedures have been described by Chung *et al*. (1995).

In this study, an iterative algorithm described by Lunze (1992) is modified for computing the solutions to the discrete-time control problem considering time delay. The original algorithm is proposed for a continuous-time control problem without time delay, where the derivation results in a similar set of matrix equations as in Equation (4.25). The algorithm computes for a decentralized control gain matrix $\mathbf{G}_{\mathbf{d}}$ by constraining the structure of $\mathbf{G}_{\mathbf{d}}$ to be consistent with the decentralized information structure. As shown in Figure 4.7, the modified iterative algorithm starts from an initial estimate for the gain matrix $\mathbf{G}_{\mathbf{d}}$. Within each iteration step *i*, the matrix $\mathbf{H}_{\boldsymbol{i}}$ and $\mathbf{L}_{\boldsymbol{i}}$ are solved respectively using the current estimate of the gain matrix $\mathbf{G}_{\mathbf{d}i}$. Based on the $\mathbf{H}_{\boldsymbol{i}}$ and $\mathbf{L}_{\boldsymbol{i}}$ matrices computed, a search gradient $\mathbf{\Delta}_i$ is calculated and the new gain matrix $\mathbf{G}_{\mathbf{d}i+1}$ is computed by traversing along the gradient from $\mathbf{G}_{\mathbf{d}i}$. An adaptive multiplier, *s*, is used to dynamically control the search step size. At each iteration step, two conditions are used to decide whether $\mathbf{G}_{\mathbf{d}i+1}$ is an acceptable estimate. The first condition is *trace*($\mathbf{H}_{i+1}\bar{\mathbf{X}}_{\mathbf{d}l}$) < *trace*($\mathbf{H}_{i}\bar{\mathbf{X}}_{\mathbf{d}l}$) which guarantees that $\mathbf{G}_{\mathbf{d}i+1}$ is a better solution than $\mathbf{G}_{\mathbf{d}i}$. The second condition is that the maximum magnitude of all the eigenvalues of the matrix $\left(\bar{\mathbf{A}}_{\mathbf{d}} + \bar{\mathbf{B}}_{\mathbf{d}}\mathbf{G}_{\mathbf{d}i+1}\bar{\mathbf{C}}_{\mathbf{y}}\right)$ needs to be less than one to ensure the stability of the augmented system. To find the gain matrix $\mathbf{G}_{\mathbf{d}}$ that is consistent with the decentralized architectural constraints, the gradient matrix $\mathbf{\Delta}_i$ computed using Equation (4.25c) is modified by zeroing out those entries which correspond to the zero terms in the decentralized

feedback gain matrix. The iteration then proceeds to compute the next estimate $\mathbf{G}_{\mathbf{d}i+1}$ by traversing along this constrained gradient. The iteration ends when the 2-norm of the difference between $\mathbf{G}_{\mathbf{d}i}$ and $\mathbf{G}_{\mathbf{d}i+1}$ is less than a preset threshold value.

$\mathbf{G}_{\mathbf{d}1} = [\mathbf{0}]_{m_2 \times p_2}$;

s = 1;

for i = 1,2,…

Solve Eq. (4.25a) for $\mathbf{H}_i$;

Solve Eq. (4.25b) for $\mathbf{L}_i$;

Find gradient by Eq. (4.25c): $\boldsymbol{\Delta}_i = -\left(2\overline{\mathbf{B}}_{\mathbf{d}}{}^T \mathbf{H}\left(\overline{\mathbf{A}}_{\mathbf{d}} + \overline{\mathbf{B}}_{\mathbf{d}}\mathbf{G}_{\mathbf{d}}\overline{\mathbf{C}}_{\mathbf{y}}\right)\mathbf{L}\overline{\mathbf{C}}_{\mathbf{y}}{}^T + 2\mathbf{R}\mathbf{G}_{\mathbf{d}}\overline{\mathbf{C}}_{\mathbf{y}}\mathbf{L}\overline{\mathbf{C}}_{\mathbf{y}}{}^T\right)$;

Apply shape constraint to $\boldsymbol{\Delta}_i$;

iterate {

$\mathbf{G}_{\mathbf{d}i+1} = \mathbf{G}_{\mathbf{d}i} + s \cdot \boldsymbol{\Delta}_i$;

Solve equation (4.25a) again for $\mathbf{H}_{i+1}$ using $\mathbf{G}_{\mathbf{d}i+1}$;

if $trace(\mathbf{H}_{i+1}\overline{\mathbf{X}}_{\mathbf{d}l})$ < $trace(\mathbf{H}_i\overline{\mathbf{X}}_{\mathbf{d}l})$ and $\max\left(\left|eigen\left(\overline{\mathbf{A}}_{\mathbf{d}} + \overline{\mathbf{B}}_{\mathbf{d}}\mathbf{G}_{\mathbf{d}i+1}\overline{\mathbf{C}}_{\mathbf{y}}\right)\right|\right)$ < 1

exit the **iterate** loop;

else

s = s / 2;

If (s < machine precision), then **exit** the **iterate** loop;

end

};

s = s × 2;

If $\left\|\mathbf{G}_{\mathbf{d}i+1} - \mathbf{G}_{\mathbf{d}i}\right\|$ < acceptable error, then **exit** the **for** loop;

End

Figure 4.7. Heuristic algorithm solving the coupled nonlinear matrix equations (4.25a-c) for centralized and decentralized optimal time-delayed feedback control (Lunze, 1990).

It should be noted that for both centralized and decentralized control schemes, the above algorithm is heuristic and may yield a local minimum in the solution space. In fact, for the static measurement feedback control problem, mathematical conditions for the existence and global uniqueness of the solutions are not yet known (Syrmos, *et al.* 1997). There may be more than one local minimum, and the gradient search may not find the global minimum. Nevertheless, as shown by the simulation and experimental results that will be presented later, the optimal gain matrices generated by the heuristic algorithm in Figure 4.7 prove to be offering good control performance.

4.2.3 Evaluation of the Heuristic Algorithm for Computing Optimal Control Gain Matrices

When a heuristic algorithm is employed for an engineering problem, it is important to examine the applicability and limitations. To evaluate the performance of the heuristic algorithm shown in Figure 4.7, the algorithm is first employed to solve a classical state-feedback LQR control problem without time delay. The purpose is to compare the gain matrix computed by the heuristic algorithm against the optimal LQR gain matrix computed by functions implemented in the Matlab Control System Toolbox (MathWorks Inc. 2005). This comparison study is presented in Section 4.2.3.1. Using the numerical simulations performed with a 3-story example structure, Section 4.2.3.2 discusses the importance of considering time delay while solving for the optimal gain matrices. The importance of the iterative procedure for constraining the search gradient while solving for decentralized gain matrices is discussed in Section 4.2.3.3. Finally, the control performance when the gain matrices are properly solved using the heuristic algorithm is illustrated in Section 4.2.3.4.

4.2.3.1 Utilization of the Heuristic Algorithm for State-Feedback LQR Control without Time Delay

Assuming that the system is linear time invariant (LTI), a discrete-time control problem can be formulated as:

$$\mathbf{x_d}[k+1] = \mathbf{A_d}\mathbf{x_d}[k] + \mathbf{B_d}\mathbf{u_d}[k],\ k = 0,1,2,... \tag{4.26}$$

Note that the difference between Equations (4.26) and (4.11) is that no feedback time delay exists here. As defined in Section 4.2.1, the $\mathbf{x_d}$ and $\mathbf{u_d}$ vectors are the state and control force vectors, respectively. The definitions of $\mathbf{x_d}$, $\mathbf{u_d}$, and system matrices $\mathbf{A_d}$ and $\mathbf{B_d}$ are given in Section 4.2.1. The objective of the classical infinite-horizon linear quadratic regulator (LQR) control is to minimize a cost function J, which is similar to the function shown in Equation (4.12), with the number of time delay steps, l, equal to 0:

$$J\Big|_{\mathbf{u_d}} = \sum_{k=0}^{\infty}\left(\mathbf{x_d}^T[k]\mathbf{Q}\mathbf{x_d}[k] + \mathbf{u_d}^T[k]\mathbf{R}\mathbf{u_d}[k]\right),\ \mathbf{Q}_{2n\times 2n} \geq 0 \text{ and } \mathbf{R}_{m_2\times m_2} > 0 \tag{4.27}$$

The optimal control strategy to the classical LQR control problem is defined by a linear state-feedback control law:

$$\mathbf{u_d}[k] = \mathbf{G_d}\mathbf{x_d}[k] \tag{4.28}$$

To compute the optimal gain matrix $\mathbf{G_d}$, the discrete-time Algebraic Riccati Equation (ARE) is first solved for the Riccati matrix $\mathbf{P}$ (Franklin, *et al.* 1998):

$$\mathbf{P} = \mathbf{Q} + \mathbf{A_d}^T\mathbf{P}\mathbf{A_d} - \mathbf{A_d}^T\mathbf{P}\mathbf{B_d}\left(\mathbf{R} + \mathbf{B_d}^T\mathbf{P}\mathbf{B_d}\right)^{-1}\mathbf{B_d}^T\mathbf{P}\mathbf{A_d} \tag{4.29}$$

The optimal control gain matrix is then computed as:

$$\mathbf{G_d} = -\left(\mathbf{R} + \mathbf{B_d}^T\mathbf{P}\mathbf{B_d}\right)^{-1}\mathbf{B_d}^T\mathbf{P}\mathbf{A_d} \tag{4.30}$$

The Riccati matrix **P** is a positive definite matrix. If the initial state of the system is denoted as $\mathbf{x_d}[0]$, the minimum of the cost function achieved by the optimal control strategy is determined by **P** and $\mathbf{x_d}[0]$:

$$\min J = \mathbf{x}_\mathbf{d}^T[0]\mathbf{P}\mathbf{x}_\mathbf{d}[0] \tag{4.31}$$

It can be observed that the classical state-feedback LQR control problem is a special case of the measurement-feedback time-delayed control problem discussed in Section 4.2.2. Specifically, the measurement-feedback time-delayed control problem is equivalent to the traditional LQR control problem under the following conditions:

1. The measurement vector $\mathbf{y_d}$ is the same as the state vector $\mathbf{x_d}$, i.e. the measurement matrix $\mathbf{C_y}$ in Equation (4.13) is an identity matrix of size $2n \times 2n$.

2. There is no feedback time delay, i.e. the number of time delay steps, l in Equation (4.11), is equal to zero.

Under these two conditions, the augmented matrices defined in Equations (4.19) and (4.20) degenerate to their counterparts in the original system. Furthermore, the LQR indexes defined in Equations (4.12) and (4.27) are equivalent. As a result, under the two conditions given above, the optimal control gain matrix computed by the algorithm in Figure 4.7 should converge to the optimal control matrix generated by classical discrete-time LQR control, as shown in Equation (4.30). To validate this equivalence, the 3-story structural model shown in Figure 4.6 is employed. The system matrices of this example structure are:

$$\mathbf{M} = \begin{bmatrix} 6\times10^3 & & \\ & 6\times10^3 & \\ & & 6\times10^3 \end{bmatrix} \text{kg} \tag{4.32a}$$

$$\mathbf{C} = \begin{bmatrix} 1.24\times10^{4} & -5.16\times10^{3} & \\ -5.16\times10^{3} & 1.24\times10^{4} & -4.59\times10^{3} \\ & -4.59\times10^{3} & 7.20\times10^{3} \end{bmatrix} \text{ N/(m/s)} \tag{4.32b}$$

$$\mathbf{K} = \begin{bmatrix} 3.4\times10^{6} & -1.8\times10^{6} & \\ -1.8\times10^{6} & 3.4\times10^{6} & -1.6\times10^{6} \\ & -1.6\times10^{6} & 1.6\times10^{6} \end{bmatrix} \text{ N/m} \tag{4.32c}$$

The three undamped natural frequencies of the structure are 1.18Hz, 3.26Hz, and 4.84Hz, respectively. Rayleigh damping is adopted when computing the damping matrix **C**, and a 4% damping is assigned for the first two vibration modes. When the external excitation is unidirectional ground motion, the discrete-time system matrices $\mathbf{A_d}$ and $\mathbf{B_d}$ can be formulated as in Equation (4.7). For the results presented in this subsection, a control sampling period of 0.005s is used, and the weighting matrices for the quadratic index *J* in Equation (4.27) are defined as:

$$\mathbf{Q} = \begin{bmatrix} \mathbf{Q}_I & \mathbf{0}_{3\times3} \\ \mathbf{0}_{3\times3} & \mathbf{0}_{3\times3} \end{bmatrix} \text{ and } \mathbf{R} = 10^{-9}\mathbf{I}_{3\times3} \tag{4.33}$$

where the submatrix $\mathbf{Q}_I$ is defined as:

$$\mathbf{Q}_I = 5\times10^{3}\mathbf{C}_\mathbf{z}^T\mathbf{C}_\mathbf{z} \text{ and } \mathbf{C}_\mathbf{z} = \begin{bmatrix} 1 & & \\ -1 & 1 & \\ & -1 & 1 \end{bmatrix} \tag{4.34}$$

Note that

$$\mathbf{x}_\mathbf{d}^T[k]\mathbf{Q}\mathbf{x}_\mathbf{d}^T[k] = \mathbf{q}^T[k]\mathbf{Q}_I\mathbf{q}[k] = 5\times10^{3}\left\|\mathbf{C}_\mathbf{z}\mathbf{q}[k]\right\|_2^2 \tag{4.35}$$

which is proportional to the sum of the squares of the inter-story drifts at time step *k*. The pattern in matrix **Q** indicates that the first part of the quadratic index *J* is decided by the sum of the squares of inter-story drifts over all time steps. To attain adequate control performance, the entries in the **Q** matrix, which represent the weighting for the structural response $\mathbf{x_d}$, are chosen to be orders of magnitude higher than the entries in the **R** matrix, which represent the weighting for the control forces.

The system matrices $\mathbf{A_d}$ and $\mathbf{B_d}$, and the weighting matrices $\mathbf{Q}$ and $\mathbf{R}$ together uniquely determine the optimal gain matrix for classical LQR control, which is illustrated in Equations (4.29) and (4.30). The `dlqr` command in the Matlab Control System Toolbox (MathWorks Inc. 2005) is employed to compute the optimal control gain matrix:

$$\mathbf{G_d} = 10^5 \times \begin{bmatrix} -9.6511 & -0.6502 & -0.1328 & -0.9213 & -0.4374 & -0.3318 \\ 8.8166 & -8.8735 & -0.3073 & 0.4834 & -0.7937 & -0.4068 \\ 0.5068 & 9.2529 & -9.8614 & 0.1055 & 0.4929 & -0.9292 \end{bmatrix} \tag{4.36}$$

On the other hand, the time-delayed measurement feedback control algorithm presented in Figure 4.7 is executed under the conditions that $\mathbf{C_y}$ is an identity matrix and the number of time delay steps, l, is zero. As expected, the gain matrix computed by the algorithm is the same as the matrix shown in Equation (4.36) when rounded to the same number of decimal digits. This comparison shows that when time delay is ignored and full state feedback is available, the heuristic algorithm presented in Figure 4.7 is equivalent to the discrete LQR control.

4.2.3.2 Time Delay Effects on the Control Solution

In order to illustrate the importance of considering time delay in the problem formulation, numerical simulations are conducted for decentralized and centralized control strategies. For the simulations, the control gain matrices are solved without considering time delay. However, during the time history integration, delayed information is used for making control decisions, since the time delayed information is what the controller has at that time instant. In other words, when using the algorithm in Figure 4.7 to compute the gain matrix, the number of time delay steps, l in Equation (4.11), is set to be zero. For the results presented herein, average acceleration time integration method (Chopra 2001) is employed for simulating the dynamic response of the controlled structure. The simulations employ a 3-story example structure, whose mass, damping, and stiffness matrices are given in Equation (4.32). For simplicity, ideal structural actuators that are

capable of producing any desired force under the maximum limit of 20kN is deployed between each pair of adjacent floors using the V-braces, as shown in Figure 4.6.

Three control architectures are employed: (1) decentralized, (2) partially decentralized, and (3) centralized. Different patterns of the gain matrices, $\mathbf{G_d}$, and the measurement matrices, $\mathbf{C_y}$, for these three control architectures are summarized in Table 4.1. As defined by these matrices, one centralized and two decentralized velocity feedback patterns are adopted. An LQR weighting matrix **Q** denoting the minimization of inter-story drifts over time and a diagonal weighting matrix **R** (as defined in Equation (4.33)) are used when computing the optimal gain matrices. Various combinations of centralization degrees (1: fully decentralized; 2: partially decentralized; 3: centralized) and sampling time steps ranging from 0.005s to 0.1s (at a resolution of 0.005s) are simulated. The time delay for information feedback is set to be equal to one sampling time step during the simulation, i.e. the number of time delay steps, *l*, is equal to one. This setup reflects the scenario for the wireless sensing and control system, where the feedback time delay primarily consists of the wireless communication latency.

Table 4.1. Different decentralization patterns for controlling the 3-story example structure

Degree of Centralization	#1 Fully Decentralized	#2 Partially Decentralized	#3 Centralized
Gain Matrix Pattern	$\mathbf{G}_{dI}$ in Eq. (4.17)	$\mathbf{G}_{dII}$ in Eq. (4.17)	$\mathbf{G}_{dIII}$ in Eq. (4.17)
Measurement Matrix	$\mathbf{C}_{yII}$ in Eq. (4.15)	$\mathbf{C}_{yII}$ in Eq. (4.15)	$\mathbf{C}_{yI}$ in Eq. (4.14)

To assess the performance of each control scheme, three ground motion records are used for the simulation: 1940 El Centro NS (Imperial Valley Irrigation District Station), 1999 Chi-Chi NS (TCU-076 Station), and 1995 Kobe NS (JMA Station) earthquake records. Performance indexes proposed by Spencer, *et al*. (1998) are adopted. In particular, two representative performance indexes employed are:

$$PI_1 = \max_{\text{Earthquakes}} \left\{ \frac{\max_{t,i} d_i(t)}{\max_{t,i} \hat{d}_i(t)} \right\}, \text{ and } PI_2 = \max_{\text{Earthquakes}} \left\{ \frac{J_{LQR}}{\hat{J}_{LQR}} \right\} \tag{4.37}$$

where PI_1 and PI_2 are the indexes corresponding to inter-story drifts and LQR cost indexes, respectively. In the above equation, $d_i(t)$ represents the inter-story drift between floor i (i = 1, 2, 3) and its lower floor at time t, and $\max_{t,i} d_i(t)$ is the maximum inter-story drift over the entire time history and among all three floors. The maximum inter-story drift is normalized by its counterpart $\max_{t,i} \hat{d}_i(t)$, the maximum response of the uncontrolled structure. The largest normalized ratio among the simulations for the three different earthquake records is defined as the performance index PI_1. Similarly, the performance index PI_2 is defined for the LQR control index J_{LQR}, as given in Equation (4.12). When computing the LQR index over time, a uniform time step of 0.001s is used to collect the structural response, regardless of the sampling time step of the control scheme; this allows one control strategy to be compared to another without concern for the different sampling time steps used in the control solution.

The values of the two control performance indexes are plotted in Figure 4.8 for different combinations of centralization degrees and sampling time steps, which are equal to the feedback time delays. The plots shown in Figure 4.8(a) and Figure 4.8(b) illustrate that centralization degree and sampling step have significant impact on the performance of the control system. In general, the performance index is desired to be less than one, i.e. the controlled structure response should be less than the uncontrolled response. To better review the simulation results, the performance indexes for the three different control schemes are re-plotted as a function of sampling time in Figure 4.8(c) and Figure 4.8(d). As shown in the plots, the control performance degrades rapidly as the control time delay increases. The results also show that the control system actually destabilizes the structure when the time delay is over 0.02s for the decentralized case, or over 0.025s for the centralized and partially decentralized cases. When the time delay gets longer, which is equivalent to the condition that the sampling time step grows larger, the numerical

simulations generate structural responses that are unrealistically large (i.e. the performance indexes are much greater that one). The simulation results show that if the effect of time delay is not considered in the problem formulation, the performance of the control system with feedback time delay is likely to degrade and the structure may even be destabilized by the control system.

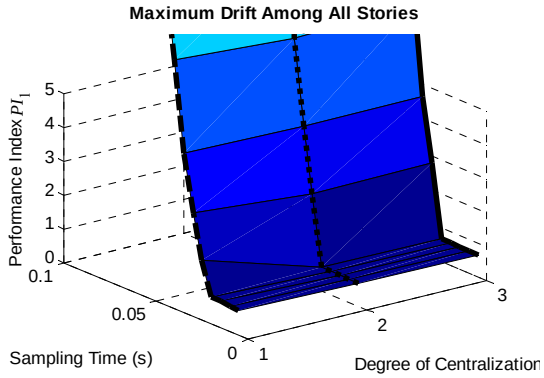

(a) 3D plot for performance index PI_1

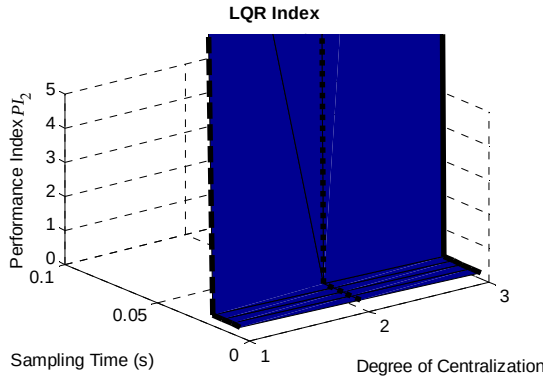

(b) 3D plot for performance index PI_2

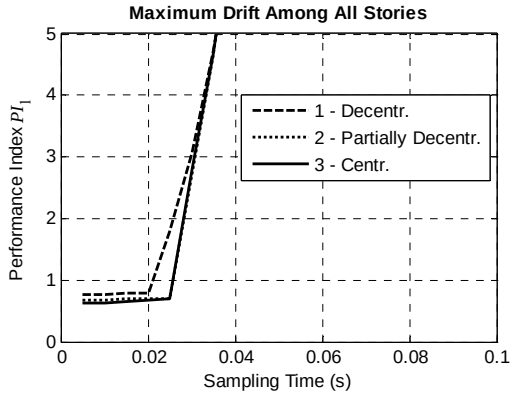

(c) Condensed 2D plot for PI_1

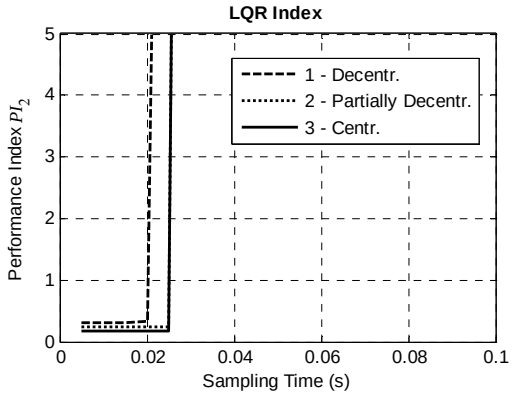

(d) Condensed 2D plot for PI_2

Figure 4.8. Simulation results illustrating control performance indexes for different sampling time steps and centralization degrees, when gain matrices are computed without considering time delay in the control formulation

4.2.3.3 Effects of Constrained Gradient Search for Decentralized Control Solution

In the heuristic algorithm shown in Figure 4.7, the shape constraints are applied to the search gradient at each iteration step for computing the decentralized gain matrices. One naive way of computing decentralized gain matrices is to compute the centralized gain matrix first, and then apply the shape constraint directly to the centralized gain matrix. This subsection presents the simulation results when the decentralized gain matrices are obtained in such a manner, i.e. simply zeroing out corresponding entries of centralized gain matrices. Time delay is considered in the problem formulation for computing the gain matrices. During the time history integration, the measurement information with one step of time delay is used for making the control decisions.

The simulations presented in this subsection employ the same 3-story structure and centralized/decentralized control schemes as introduced in Section 4.2.3.2. The same performance indexes as defined in Equation (4.37) are computed for the three scaled earthquake records. Figure 4.9 illustrates the performance index plots for different sampling time steps and degrees of centralization. Similar to the results shown in Figure 4.8, the structural system is destabilized when the sampling time step grows larger for the decentralized case and partially decentralized cases. This shows that the naive way of obtaining decentralized gain matrices by simply zeroing out the entries in centralized gain matrices is not desirable, and may even destabilize the structure. Note that for the centralized case, the results represent the proper use of the algorithm in Figure 4.7, since no entries of the gain matrix are set to be zeros.

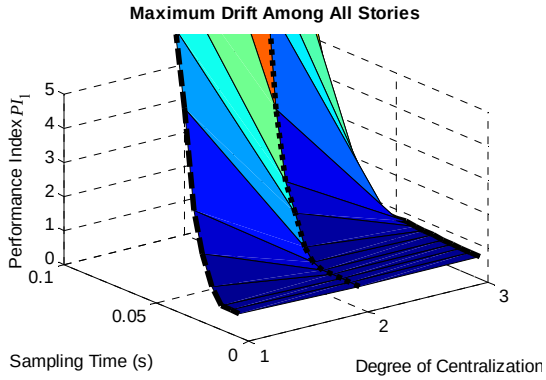

(a) 3D plot for performance index PI_1

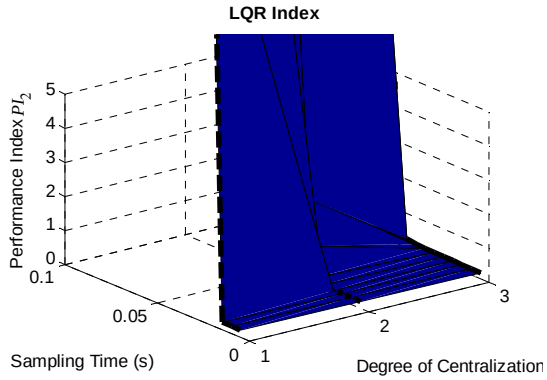

(b) 3D plot for performance index PI_2

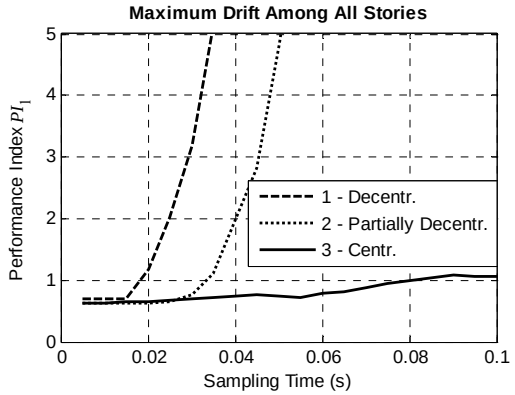

(c) Condensed 2D plot for PI_1

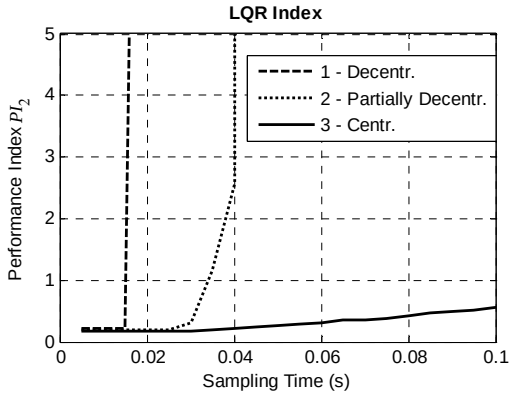

(d) Condensed 2D plot for PI_2

Figure 4.9. Simulation results illustrating control performance indexes for different sampling time steps and centralization degrees, when decentralized control gain matrices are computed by zeroing-out entries in the centralized gain matrices

4.2.3.4 Control Strategies with Time Delays and Constrained Gradient Search

For the results presented in this subsection, the control gain matrices are computed by properly following the algorithm in Figure 4.7. Feedback time delay is considered during the problem formulation, and the decentralized gain matrices are obtained by shape-constrained gradient search. Similar to the last two subsections, simulations are conducted upon the 3-story structure using different sampling time steps and degrees of

centralization. Values of the two control performance indexes are plotted in Figure 4.10 for different combinations of centralization degrees and sampling time steps. The plots shown in Figure 4.10(a) and Figure 4.10(b) illustrate that centralization degree and the sampling time step have significant impact on the performance of the control system. Generally speaking, control performance is better for higher degrees of centralization and shorter sampling times. To better review the simulation results, the performance indexes for the three different control schemes are re-plotted as a function of sampling time in Figure 4.10(c) and Figure 4.10(d). As shown in Figure 4.10(c), if the partially decentralized control system can achieve a sampling step of 0.04s and a centralized system can only achieve 0.08s due to additional communication latency, the partially decentralized system can result in lower maximum inter-story drifts. Similar trends are observed in Figure 4.10(d), although for a given sampling time step, the performance index PI_2 for the centralized case is always lower than the indexes for the two decentralized cases. The destabilization shown in Figure 4.8 and Figure 4.9 no longer exists here. The comparison between the three figures illustrate the importance of considering time delay effect in the control formulation, and the importance of applying the iterative constrained gradient search scheme when computing the decentralized control gain matrices. The results presented in Figure 4.10 also illustrate that although the heuristic algorithm in Figure 4.7 does not guarantee to yield the global optimum, adequate control performance can still be achieved in the example.

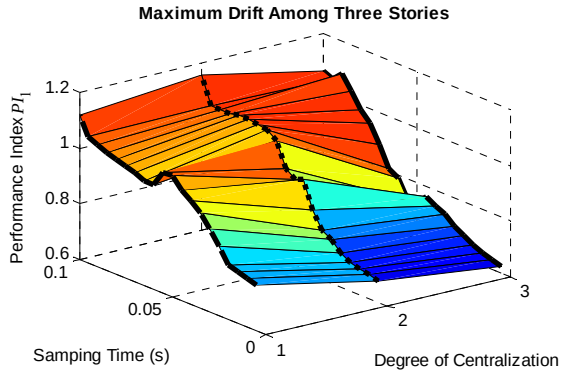

(a) 3D plot for performance index PI_1

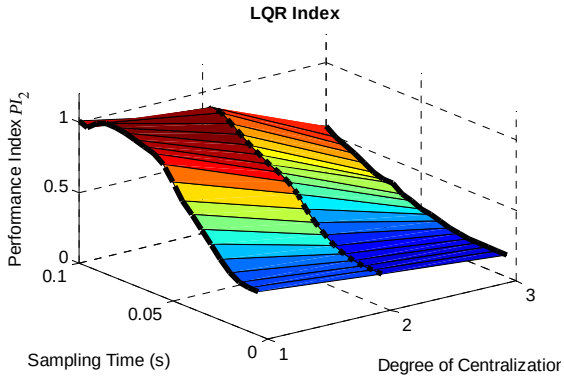

(b) 3D plot for performance index PI_2

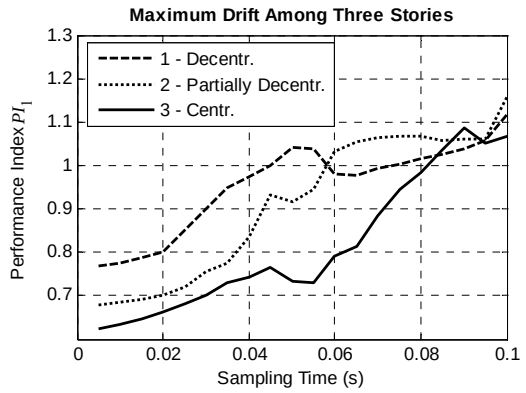

(c) Condensed 2D plot for PI_1

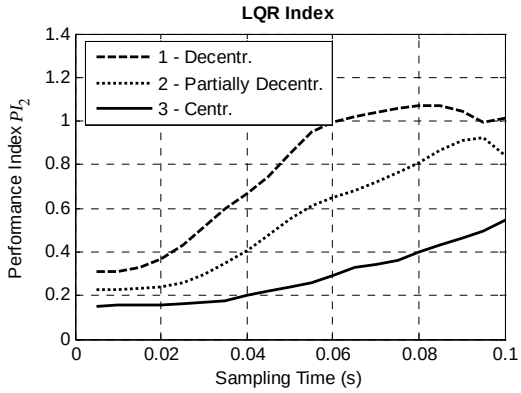

(d) Condensed 2D plot for PI_2

Figure 4.10. Simulation results illustrating control performance indexes for different sampling time steps and centralization degrees, when time delay is considered in the formulation and decentralized gain matrices are computed by iterative gradient search

4.3 Validation Experiments for Wireless Structural Sensing and Control

Validation tests for the wireless sensing and control system are conducted at the National Center for Research on Earthquake Engineering (NCREE) in Taipei, Taiwan. Centralized and decentralized control schemes are adopted in the experiments. Both a baseline wired control system and a wireless control system are employed to implement

the real-time feedback control of a 3-story steel frame instrumented with three magnetorheological (MR) dampers. This section first analyzes the communication time delay of the wireless control system, and then introduces the test setup of the control experiments. The modified Bouc-Wen numerical models for the MR dampers employed in this study are described. Results of the centralized and decentralized control experiments are presented and compared with numerical simulation results.

4.3.1 Wireless Communication Latency

One critical issue in adopting wireless communication technology for real-time feedback structural control systems is the communication latency encountered when transmitting sensor data from the wireless sensing units to the wireless control units. Using the MaxStream 24XStream transceiver as an example, the anticipated transmission time for a single data packet is illustrated in Figure 4.11. The transmission time consists of the communication latency, $T_{Latency}$, of the transceivers and the time to transfer data between the microcontroller and the transceiver using the universal asynchronous receiver and transmitter (UART) interface, T_{UART} (see Section 2.1.1). Assume that the data packet to be transmitted contains N bytes and the UART data rate is T_{UART} bps (bits per second), which is equivalent to R_{UART} /10 bytes per second, or R_{UART} /10000 bytes per millisecond. It should be noted that the UART is set to transmit 10 bits for every one byte (8 bits) of sensor data, including one start bit and one stop bit. The communication latency in a single transmission of this data packet can be estimated as:

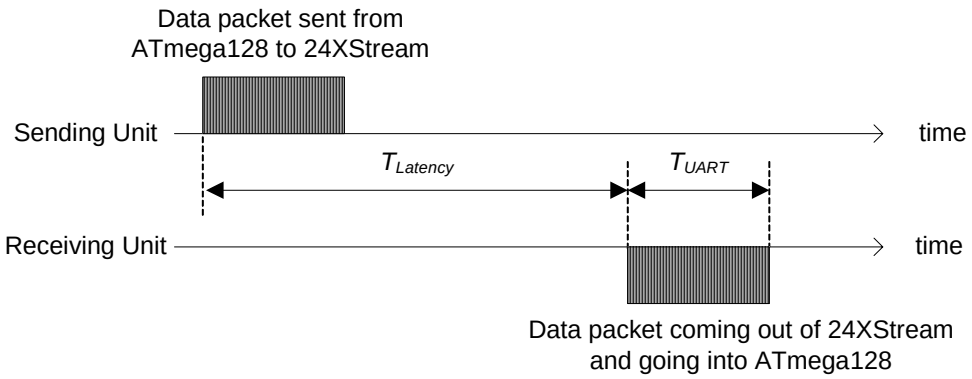

Figure 4.11. Communication latency of a single wireless transmission

$$T_{SingleTransm} = T_{Latency} + \frac{10000N}{R_{UART}} \text{ (ms)} \tag{4.38}$$

In the prototype wireless sensing and control system, the setup parameters of the 24XStream transceiver are first tuned to minimize the transmission latency, $T_{Latency}$. Then experiments are conducted to measure the actual achieved $T_{Latency}$, which turns out to be around 15±0.5ms. The UART data rate of the 24XStream radio, R_{UART}, can be selected among seven different options, ranging from 1200 bps to 57600 bps. After considering the UART performance of the ATmega128 microcontroller operating at 8MHz, R_{UART} is selected as 38400 bps in the implementation. For example, if a data packet sent from a sensing unit to a control unit contains 11 bytes, the total time delay for a single transmission is estimated to be:

$$T_{SingleTransm} = 15 + \frac{10000 \times 11}{38400} \approx 17.86 \text{ (ms)} \tag{4.39}$$

This single-transmission delay represents one communication constraint that needs to be considered when calculating the upper bound for the maximum sampling rate for the control system. Another deciding factor for the sampling rate is the number of wireless transmissions needed at each control sampling step. A few milliseconds of safety cushion time at each sampling step are a prudent addition that allows a certain amount of

randomness in the wireless transmission latency without undermining the reliability of the communication system. Although the achievable transmission latency, $T_{Latency}$, is around 15ms for the MaxStream 24XStream transceiver, it can be as low as 5ms for the 9XCite transceiver. This lower latency makes the 9XCite transceiver more suitable for real-time feedback control applications compared with the 24XStream transceiver. However, the 9XCite transceiver may only be used in countries where the 900MHz band is for free public usage, such as the U.S., Canada, Mexico, and South Korea. In this experimental study conducted in Taiwan, the 24XStream transceiver is employed.

4.3.2 Test Setup

A three-story steel frame structure is designed and constructed by researchers affiliated with NCREE. Figure 4.12 shows the 3-story test structure and its dimensions. The three-story structure is mounted on a 5m × 5m 6-DOF shake table. The shake table can generate ground excitations with frequencies spanning from 0.1Hz to 50Hz. For this study, only longitudinal excitations are used. Along this direction, the shake table can excite the structure with a maximum acceleration of 9.8m/s^2. The excitation has a maximum stroke and force of ±0.25m and 220kN, respectively. The test structure and shake table are heavily instrumented with accelerometers, velocity meters, and linear variable displacement transducers (LVDT) to measure their dynamic response. These sensors are interfaced to a high-precision wire-based data acquisition (DAQ) system permanently installed in the NCREE facility; the DAQ system is set to a sampling rate of 200 Hz. A separate set of wireless sensors are installed as part of the wireless control system.

(a) The 3-story test structure mounted on the shake table

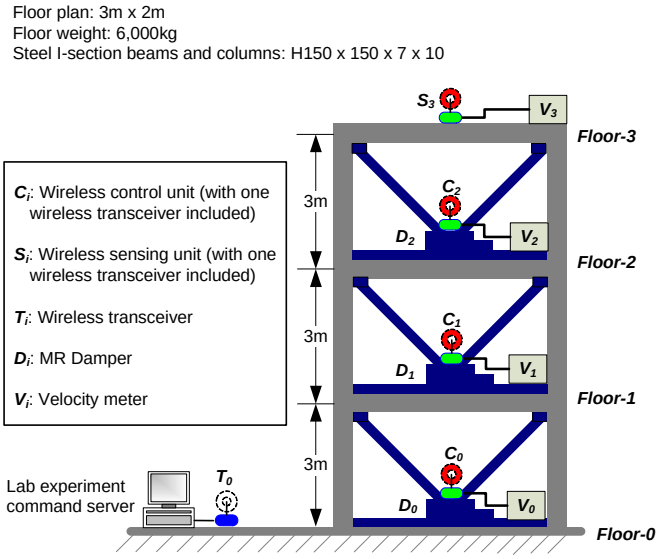

(b) Deployment of the wireless sensors, controllers, and actuators

Figure 4.12. Laboratory setup for wireless structural sensing and control experiments

The basic architecture of the prototype wireless sensing and control system is schematically shown in Figure 4.12b, where a total of four wireless sensing units are installed. Each wireless sensing unit is interfaced to a Tokyo Sokushin VSE15-D velocity meter to measure the absolute velocity response for each floor of the structure as well as the base. The sensitivity of this velocity meter is 10V/(m/s) with a measurement limit of ±1 m/s. The three wireless units on the first three levels of the structure (C_0, C_1, and C_2) are also responsible for commanding the MR dampers. Besides the wireless control system, a traditional wire-based control system is installed in the structure for comparative tests.

Centralized and decentralized velocity feedback control schemes are used for the wired and the wireless control systems. For the centralized control tests, the measurement vector includes the relative velocities (but not the relative displacements) on all floors with respect to the ground; the measurement matrix, $\mathbf{C}_y$, thus has the form in Equation

(4.14). For decentralized control tests, the inter-story velocities between adjacent floors are defined as the measurement vector, and the measurement matrix $\mathbf{C}_y$ is set to have the form in Equation (4.15). Furthermore, to represent a fully decentralized, partially decentralized and centralized control schemes, the feedback gain matrices for the 3-story test structure are constrained to the sparsity patterns shown in Equation (4.17). When combined with the measurement matrix $\mathbf{C}_y$ defined in Equations (4.14) and (4.15), the pattern in $\mathbf{G}_{dI}$ specifies that when computing control decisions, the actuator at each floor only needs the entry in the measurement vector $\mathbf{y}_d$ corresponding to that floor. The pattern in $\mathbf{G}_{dII}$ specifies that the control decisions require information from a neighboring floor. Finally, the pattern in $\mathbf{G}_{dIII}$ indicates all entries in the measurement vector participate in the centralized control decisions.

For this test structure, the wire-based system can achieve a sampling rate of 200Hz, or a time step of 0.005s. Because of the local frequency band requirements in Taiwan, the MaxStream 24XStream wireless transceiver operating at the 2.4GHz spectrum is employed for the experimental tests. If all three wireless control units need velocity data from all the floors to compute control decisions, a communication sequence illustrated in Figure 4.13 can be adopted by the prototype system. The control sampling step, which is 80ms in this example, is mostly decided by the total time required for transmitting all four data packets. For the 24XStream wireless transceiver adopted in the system, wireless transmission of each velocity measurement takes about 18ms, as calculated in Equation (4.39). During every control time step, the wireless unit C_0 first samples the velocity data V_0 at its own floor, and then sends out the data together with a beacon signal to other wireless units. Upon receiving the beacon signal, units C_1, C_2, and S_3 sequentially broadcast their sensor data. A time lag of 8ms is designed as a safety cushion for each control sampling time step, allowing certain randomness in the wireless transmission time. The control units C_0, C_1, and C_2 compute control decisions and apply actuation signals during the intervals of wireless transmissions concurrently.

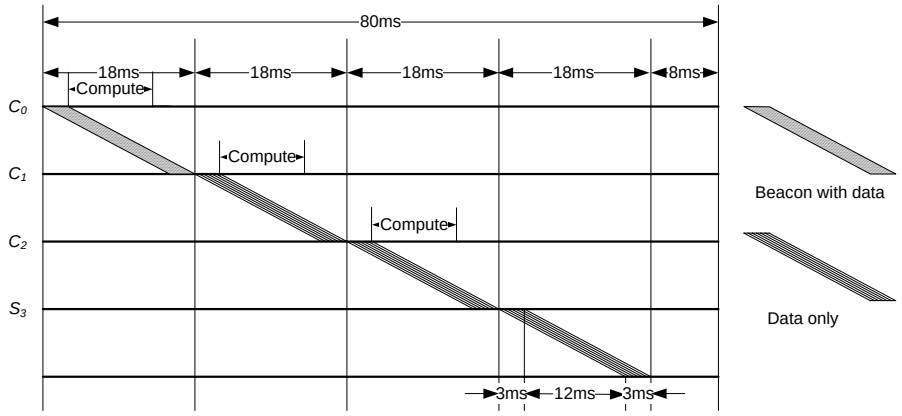

Figure 4.13. Communication sequence in a wireless structural control network

Table 4.2 summarizes the different patterns of the gain matrix $\mathbf{G}_{\mathbf{d}}$, the measurement matrices $\mathbf{C}_{\mathbf{y}}$, and the achievable sampling periods for the wireless and wired control strategies. Compared with the wireless centralized scheme, an advantage of the decentralized architecture is that fewer communication steps are needed, thereby reducing the time for wireless communication. As shown in Table 4.2, the wireless system can achieve a sampling rate of 16.67Hz for partially decentralized control and 50Hz for fully decentralized control.

Table 4.2. Different decentralization patterns and sampling period/rate for the wireless and wire-based control experiments

	Wireless System			Wired System
Degree of Centralization	#1	#2	#3	#3
Gain Matrix Pattern	$\mathbf{G}_{\mathbf{d}I}$ in Eq. (4.17)	$\mathbf{G}_{\mathbf{d}II}$ in Eq. (4.17)	$\mathbf{G}_{\mathbf{d}III}$ in Eq. (4.17)	$\mathbf{G}_{\mathbf{d}III}$ in Eq. (4.17)
Measurement Matrix	$\mathbf{C}_{\mathbf{y}II}$ in Eq. (4.15)	$\mathbf{C}_{\mathbf{y}II}$ in Eq. (4.15)	$\mathbf{C}_{\mathbf{y}I}$ in Eq. (4.14)	$\mathbf{C}_{\mathbf{y}I}$ in Eq. (4.14)
Sampling Period/Rate	0.02s / 50Hz	0.06s / 16.67Hz	0.08s / 12.5Hz	0.005s / 200Hz

4.3.3 Hysteresis Model of the Magnetorheological (MR) Dampers

For this experimental study, three 20 kN MR dampers are installed with V-braces on each story of the steel structure (Figure 4.14a). The damping coefficients of the MR dampers can be changed in real-time by the wireless control units (Figure 4.14b) by issuing a command voltage between 0 to 1.2V. A separate power module is needed to provide 24V of power to each MR damper. In addition, this power module takes the command voltage as an input and converts this command signal to a regulated current from 0 to 2A. This command voltage determines the electric current of the electromagnetic coil in the MR damper, which in turn, generates a magnetic field that sets the viscous damping properties of the MR damper. Therefore, the axial force required to move the damper piston against the cylinder is adjustable through the command voltage. Calibration tests are first conducted on the MR dampers before mounting them to the structure so that modified Bouc-Wen damper models can be formulated for each damper (Lin et al., 2005).

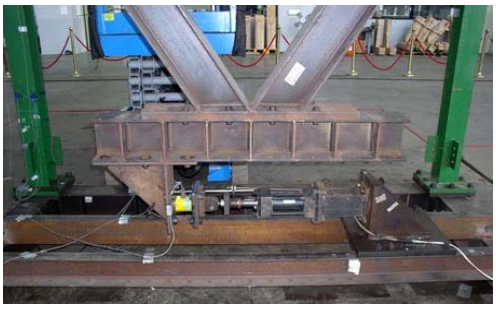

(a) MR damper installed between the 1st floor and the base floor

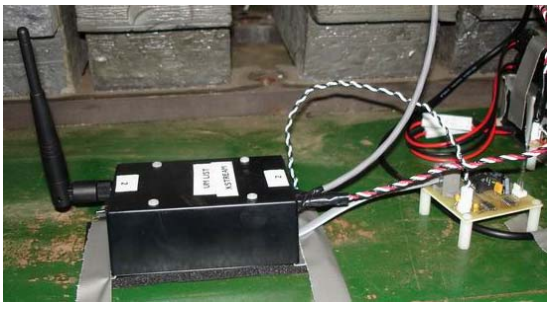

(b) Wireless control unit and an off-board control signal generation module

Figure 4.14. MR damper controlled by a wireless control unit

The nonlinear force-velocity relationship for this modified Bouc-Wen model is defined as:

$$u(t) = C(V)\Delta\dot{q}(t) + u_h(t) \tag{4.40}$$

where $u(t)$ is the force provided by the MR damper, $C(V)$ is the damping coefficient adjustable through the damper command voltage V, $\Delta\dot{q}(t)$ is the relative velocity of the damper piston against the cylinder, and $u_h(t)$ is the hysteresis restoring force of the damper. The hysteresis restoring force, $u_h(t)$, evolves according to the following differential equation (Lin, *et al.* 2005):

$$\dot{u}_h(t) = A\Delta\dot{q}(t) + \sum_{n=1}^{N} a_n \left[\beta \left|\Delta\dot{q}(t)\right| \left|u_h(t)\right|^{n-1} u_h(t) + \gamma \Delta\dot{q}(t) \left|u_h(t)\right|^n \right] \tag{4.41}$$

where A, β, γ, a_n, and N are parametric constants of the Bouc-Wen model. The higher the order N, the more accurate the model is in describing the complicated hysteresis behavior of the semi-active damper. In this study, it was found that an order of $N = 2$ provides fairly accurate modeling to the damper hysteresis forces. The hysteresis restoring force in discrete-time form at step k is then rewritten as:

$$u_h[k] = u_h[k-1] + \mathbf{\Phi}^T[k-1]\mathbf{\Theta}(V) \tag{4.42a}$$

$$\mathbf{\Theta}(V) = \left\{\theta_1(V) \quad \theta_2(V) \quad \theta_3(V) \quad \theta_4(V) \quad \theta_5(V)\right\}^T \tag{4.42b}$$

$$\begin{aligned} \mathbf{\Phi}[k] = \Delta t \Big\{ & \Delta\dot{q}[k] \quad \left|\Delta\dot{q}[k]\right| u_h[k] \quad \Delta\dot{q}[k] \left|u_h[k]\right| \quad \cdots \\ & \left|\Delta\dot{q}[k]\right| \left|u_h[k]\right| u_h[k] \quad \Delta\dot{q}[k] \left|u_h[k]\right|^2 \Big\}^T \end{aligned} \tag{4.42c}$$

The five parameters in vector $\mathbf{\Theta}(V)$ are modeled as low-order polynomial functions of the damper voltage V. Similarly, the damping coefficient, $C(V)$, is modeled as a linear function of the damper voltage V. For each MR damper, the constant coefficients in the polynomial functions $\mathbf{\Theta}(V)$ and $C(V)$ are pre-determined and validated through a series of calibration experiments with the damper (Lin, *et al.* 2005). For example, if the damper

force unit is MN and the piston velocity unit is m/s, constant coefficients in the following equations are determined for the MR damper on the base floor:

$$\begin{aligned} C(V) &= 0.0083V + 0.005 \\ \theta_1(V) &= -13.3V^3 + 23.0V^2 + 1.0V + 1.1 \\ \theta_2(V) &= -161.6V^2 - 88.7V - 389.3 \\ \theta_3(V) &= -5.0V^2 - 169.2V - 160.4 \\ \theta_4(V) &= -0.643V^2 - 8.028V - 0.776 \\ \theta_5(V) &= 0.35V^2 - 6.8V - 0.32 \end{aligned} \tag{4.43}$$

In these experiments, a displacement-controlled actuator is employed to command displacements to the damper piston while the damper cylinder is fixed to a reaction frame. A load cell is then used to measure the damper force, so that the force-displacement time histories of the damper can be recorded. To compute the constant coefficients in the modified Bouc-Wen model, sinusoidal and random displacement are first applied to the damper with the damper command voltage fixed at multiple levels. Then the model is validated through experiments when random displacement time histories are applied to the damper with the command voltage randomly varied.

In the real-time feedback control tests, hysteresis status updating for the MR dampers is an integral part of calculating the command voltages for the dampers. At each sampling time step, a wireless control unit first computes the optimal (desired) control force for the MR damper using the control algorithms described in Section 4.2.2. According to the hysteresis status, the wireless control unit decides the appropriate command voltage that should be applied to the MR damper to attain a damping force closest to the desired control force. The wireless control unit decides the command voltage by iterating through seven trial voltages, ranging from 0.0V to 1.2V at a resolution of 0.2V. For each trial voltage, the coefficients $C(V)$ and $\Theta(V)$ can be decided using Equation (4.43). The $C(V)$ and $\Theta(V)$ coefficients for the three MR dampers used in the experiments are summarized in Table 4.3. To reduce the computing time of the wireless control units when the system is in operation, these $C(V)$ and $\Theta(V)$ coefficients are pre-computed and

embedded in the microcontrollers of the wireless units. With the coefficients $C(V)$ and $\Theta(V)$ readily available, the control unit then computes coefficients $\Phi[k\text{-}1]$ in Equation (4.42) using the hysteresis force and damper velocity at the previous time step, and predicts the achievable hysteresis force $z[k]$ and total damping force $u[k]$ using Equation (4.40). The predicted damping forces $u[k]$ for the seven trial voltages are compared with the desired control force for the damper. Then the command voltage is selected to be the trial voltage by which the damper achieves a damping force closest to the desired control force.

Table 4.3. Constant coefficients $C(V)$ and $\Theta(V)$ for the three MR dampers at the seven trial voltages [Courtesy: Prof. C.-H. Loh and Dr. P.-Y. Lin, National Taiwan University]

	V [Volt]	$C(V)$ [MN/(m/s)]	$\theta_1(V)$	$\theta_2(V)$	$\theta_3(V)$	$\theta_4(V)$	$\theta_5(V)$
Damper on Floor-0	0.0	5.00E-03	1.08E+00	-3.89E+02	-1.60E+02	-7.76E-01	-3.16E-01
	0.2	6.70E-03	2.09E+00	-4.13E+02	-1.94E+02	-2.41E+00	-1.66E+00
	0.4	8.30E-03	4.31E+00	-4.51E+02	-2.29E+02	-4.09E+00	-2.97E+00
	0.6	1.00E-02	7.09E+00	-5.01E+02	-2.64E+02	-5.82E+00	-4.26E+00
	0.8	1.16E-02	9.79E+00	-5.64E+02	-2.99E+02	-7.61E+00	-5.52E+00
	1.0	1.33E-02	1.18E+01	-6.40E+02	-3.35E+02	-9.45E+00	-6.75E+00
	1.2	1.50E-02	1.24E+01	-7.28E+02	-3.71E+02	-1.13E+01	-7.95E+00
Damper on Floor-1	0.0	2.00E-02	1.19E+00	-2.48E+02	-1.97E+02	-1.34E+00	-1.22E+00
	0.2	4.00E-02	2.12E+00	-2.34E+02	-1.46E+02	-3.07E+00	-2.30E+00
	0.4	5.00E-02	4.73E+00	-3.26E+02	-2.02E+02	-5.41E+00	-4.22E+00
	0.6	6.00E-02	6.84E+00	-3.67E+02	-2.44E+02	-6.65E+00	-5.71E+00
	0.8	6.00E-02	9.56E+00	-4.37E+02	-2.72E+02	-9.45E+00	-7.56E+00
	1.0	8.00E-02	6.22E+00	-2.44E+02	-1.60E+02	-5.25E+00	-4.51E+00
	1.2	1.00E-01	5.67E+00	-2.34E+02	-1.44E+02	-5.80E+00	-4.45E+00
Damper on Floor-2	0.0	2.00E-03	2.57E-02	-2.63E+01	-7.97E+00	-9.01E-02	-3.32E-02
	0.2	2.00E-03	7.23E-01	-1.34E+02	-5.18E+01	-1.09E+00	-5.45E-01
	0.4	2.00E-03	1.75E+00	-2.08E+02	-8.05E+01	-2.20E+00	-1.13E+00
	0.6	2.00E-03	3.20E+00	-2.84E+02	-1.10E+02	-3.71E+00	-1.93E+00
	0.8	4.00E-03	4.04E+00	-3.19E+02	-1.29E+02	-4.46E+00	-2.49E+00
	1.0	8.00E-03	6.41E+00	-4.71E+02	-1.98E+02	-5.21E+00	-3.80E+00
	1.2	9.00E-03	9.94E+00	-5.72E+02	-2.77E+02	-9.91E+00	-6.72E+00

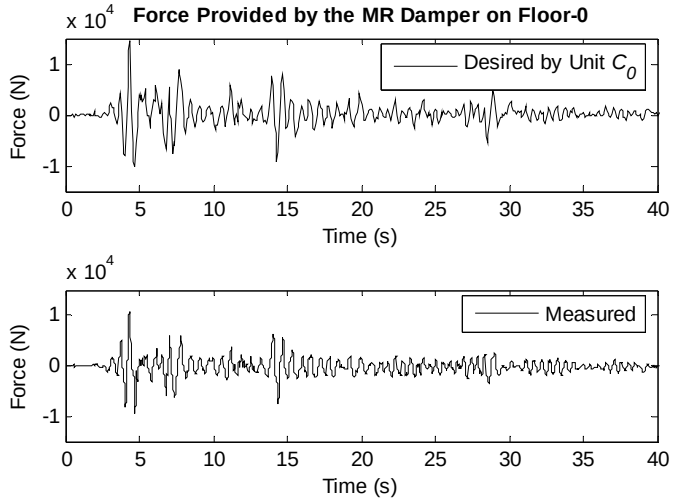

(a) Force provided by the MR damper on Floor-0

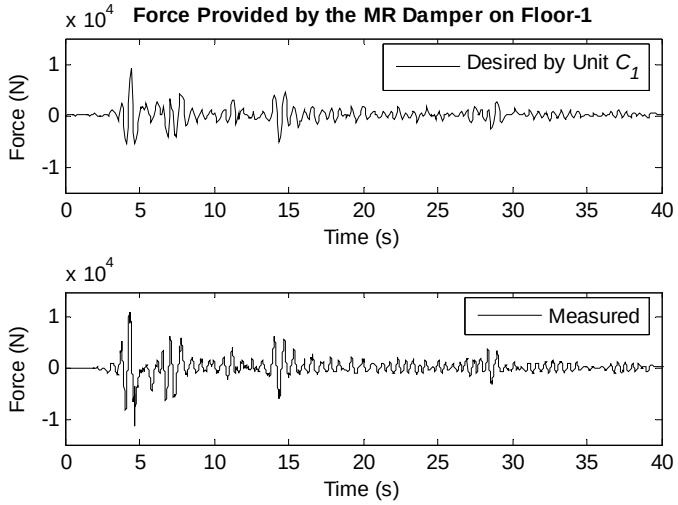

(b) Force provided by the MR damper on Floor-1

Figure 4.15. Damper forces desired by the control units and achieved by the MR dampers during an experimental test

In order to illustrate the performance of the MR damper model, Figure 4.15 shows the comparison between the control force desired by the wireless control units and the actual force (as measured by the load cells) achieved by the MR dampers on Floor-0 and Floor-1 during a wireless centralized control test. The ground excitation in this test is the 1940 El Centro NS earthquake record scaled to a peak ground acceleration of $1 m/s^2$. The

strong similarity between the desired and achieved control forces validates the damper hysteresis computation accomplished by the wireless control units, and the effectiveness of the modified Bouc-Wen MR damper model.

4.3.4 Experimental Results

In order to ensure that appropriate control decisions are computed by the wireless control units, one necessary condition is that the real-time velocity data used by the control units are reliable. Rarely experiencing data losses during the experiments, our prototype wireless sensor network proves to be robust (as reported by Lynch, *et al*. (2007), data losses less than 2% are experienced). Should data loss be encountered, the wireless control unit is currently designed to simply use a previous data sample. To illustrate the reliability of the velocity data collected and transmitted by the wireless units, Figure 4.16 presents the Floor-1 time history data during the same centralized wireless control test as presented in Figure 4.15. The data is collected separately by the wired DAQ system and recorded by the three wireless control units. During the test, unit C_1 measures the data from the associated velocity meter directly, stores the data in its own memory bank, and transfers the data wirelessly to unit C_0 and C_2. After the test run is completed, data from all the three control units are sequentially streamed to the experiment command server, where the results are plotted as shown in Figure 4.16. These plots illustrate strong agreement among data recorded by the three wireless control units and by the wired system using a separate set of velocity meters and data acquisition system. This result shows that the velocity data are not only reliably measured by unit C_0, but also properly transmitted to the other wireless control units in real-time.

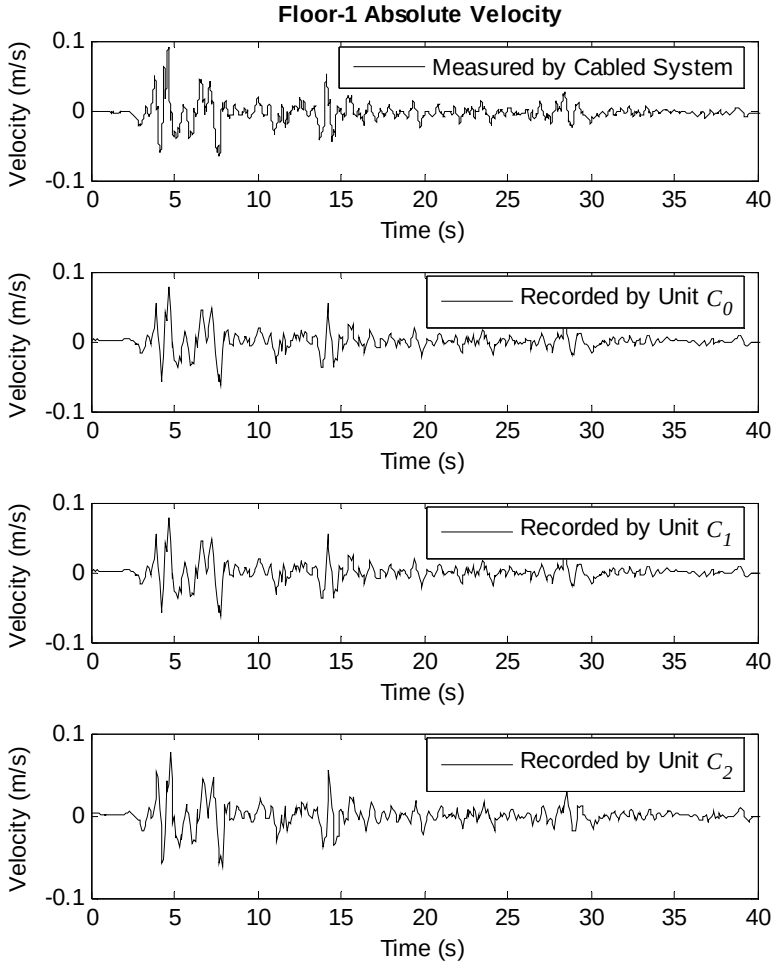

Figure 4.16. Floor-1 absolute velocity data recorded by the wired and wireless sensing systems

The time histories of the inter-story drifts from the same centralized wireless control test are plotted in Figure 4.17, together with the drifts of a centralized wired control test and a dynamic test when the structure is not instrumented with any control system (i.e. the MR dampers are not yet installed). The same ground excitations (e.g. the 1940 El Centro NS earthquake record scaled to a peak ground acceleration of 1m/s^2) are used for all the three cases shown in Figure 4.17. The results show that both the wireless and wired control

systems achieve considerable performance in limiting inter-story drifts. Running at a much shorter sampling time step, the wired centralized control system achieves slightly better control performance than the wireless centralized system in terms of mitigating inter-story drifts.

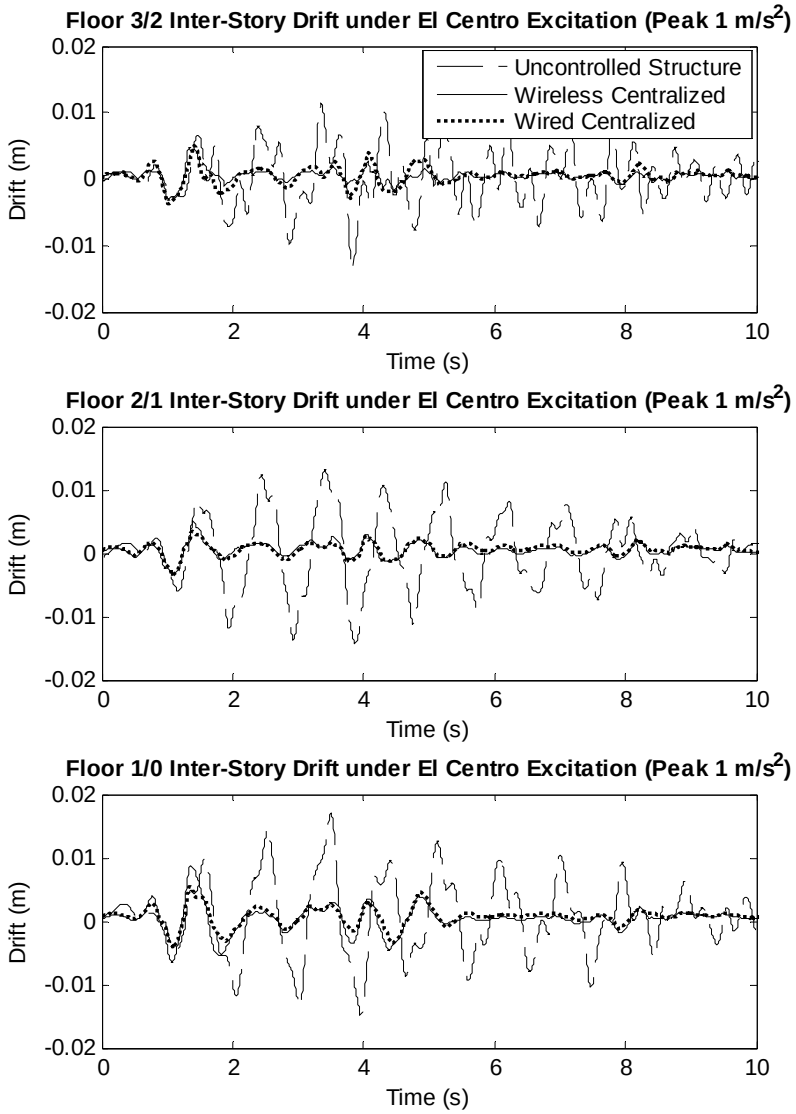

Figure 4.17. Inter-story drifts of the structure with and without control

In order to further study different decentralized schemes with different communication latencies, Figure 4.18 shows the peak inter-story drifts and floor accelerations for the original uncontrolled structure and the structure controlled by the four different wireless and wired control schemes, as defined in Table 4.2. Three earthquake records, the 1940 El Centro NS, 1999 Chi-Chi NS, and 1995 Kobe NS records, are employed for the experimental tests, with their peak ground accelerations all scaled to $1 m/s^2$. Compared with the uncontrolled structure, all wireless and wired control schemes achieve significant reduction with respect to maximum inter-story drifts and absolute accelerations. Among the four control cases, the wired centralized control scheme shows good performance in mitigating both peak drifts and peak accelerations. For example, when the 1940 El Centro NS earthquake is applied (Figure 4.18a), the wired centralized control scheme achieves the smallest peak drifts and the second smallest overall peak accelerations. This result is expected because the wired system has the advantages of lower communication latency and utilizes sensor data from all floors (complete state data). The wireless schemes, although running at longer sampling steps, achieve control performance comparable to the wired system. For all three earthquake records, the fully decentralized wireless control scheme (case #1) results in low peak inter-story drifts and the smallest peak floor accelerations at most of the floors. This result illustrates that in the decentralized wireless control cases, the higher sampling rate (achieved due to lower communication latency) potentially compensates for the lack of available data since sensor data from faraway floors is ignored.

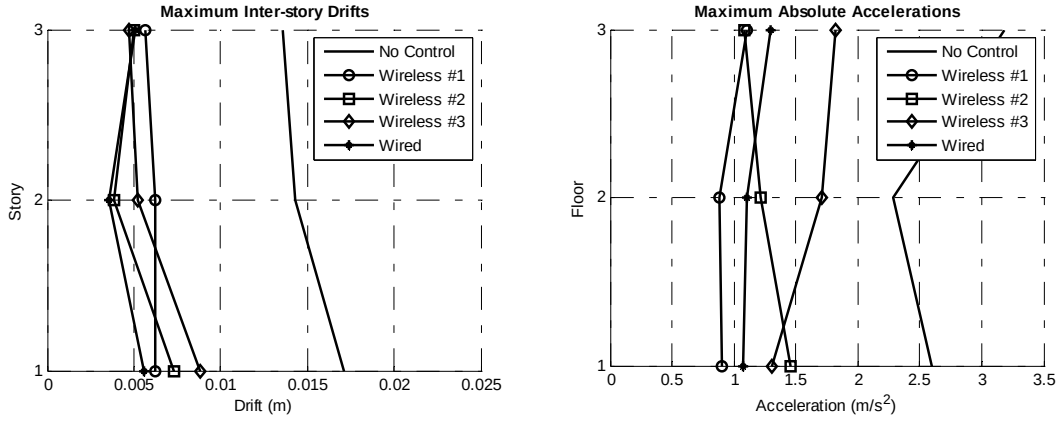

(a) 1940 El Centro NS with PGA scaled to 1m/s^2

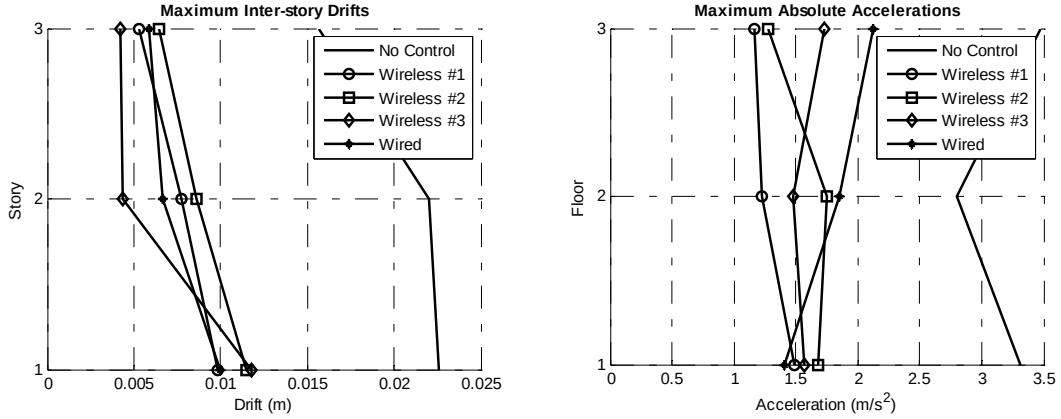

(b) 1999 Chi-Chi NS with PGA scaled to 1m/s^2

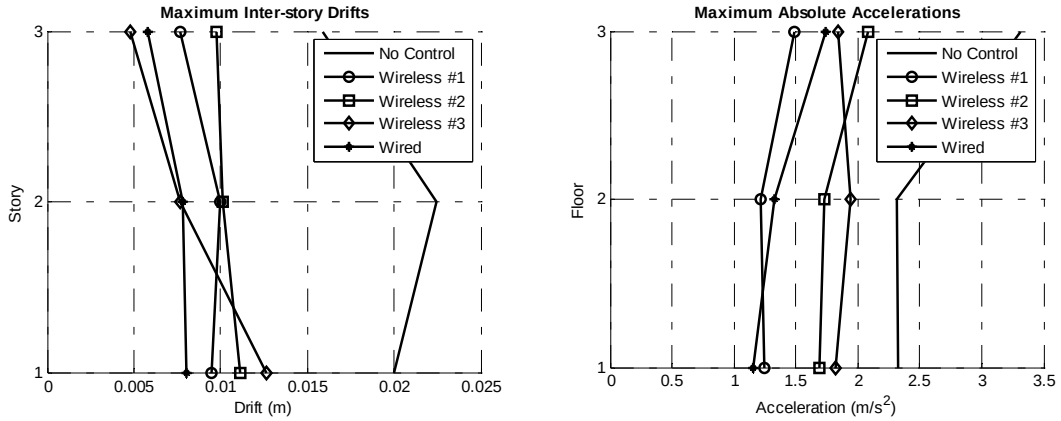

(c) 1995 Kobe NS with PGA scaled to 1m/s^2

Figure 4.18. Experimental results of different control schemes under three earthquake excitations with peak ground accelerations (PGA) scaled to 1m/s^2

4.3.5 Comparison between Experimental and Simulation Results

In order to further validate the numerical models of the structure and the MR dampers, numerical simulations to the experimental runs are conducted. The overall flow chart of the simulation program is schematically shown in Figure 4.19. The program starts with inputting the ground motion data and creating the structural model. Then the decentralized information feedback pattern is defined, and the optimal control gain matrix is computed using the algorithm in Figure 4.7. For the results presented herein, the average acceleration method (Chopra 2001) is employed for simulating the dynamic response of the structure controlled by MR dampers. A time step of 0.001s is used for the Newmark integration.

It is important to notice that the time step for Newmark integration is in general different from the control sampling time step, i.e. the T parameter in Equation (4.5). For the simulations presented herein, the control sampling time step is assumed to be an integer multiplying the time step for Newmark integration. As shown in Figure 4.19, the control decision is required only when the current Newmark integration time step coincides with a control sampling time step. To accurately simulate the scenario in the experiments, desired control forces are computed based on time-delayed information. Knowing the desired forces, the damper hysteresis model is used to compute an appropriate input voltage to the damper, so that the achieved damper force is as close as possible to the desired control force. When the Newmark integration step does not coincide with a control sampling time step, the input voltage to the MR damper is kept to be the same as the voltage at the last Newmark integration step.

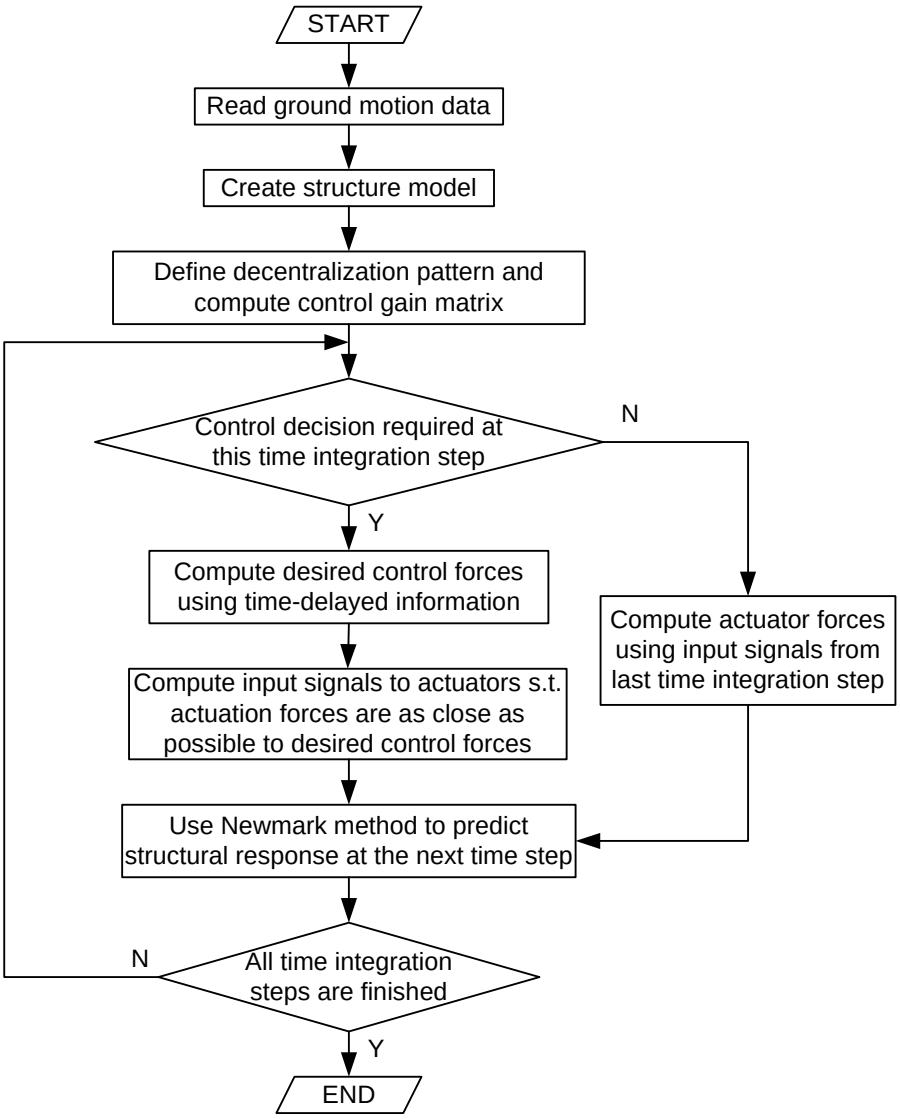

Figure 4.19. Program flow chart for the dynamic simulation of a structure controlled by actuators

Numerical simulations are conducted for experimental runs when the structure is under different earthquake excitations and when different control schemes (see Table 4.2) are adopted. Close similarity is generally observed between the simulated response and the response measured during the experiments. For illustration, Figure 4.20 to Figure 4.22

present the comparison between the simulated structural response and the experimental measurement: Figure 4.20 shows the comparison when the structure is excited with the scaled Chi-Chi earthquake record and when wireless control scheme #1 (fully decentralized, 20ms sampling period) is adopted. Figure 4.21 shows the comparison when the structure is excited with the scaled Kobe earthquake record and wireless control scheme #2 is adopted (partially decentralized, 60ms sampling period). Figure 4.22 shows the comparison when the structure is excited with the scaled El Centro earthquake record and wireless control scheme #3 is adopted (centralized, 80ms sampling period). For each simulation, the ground acceleration measured during the individual experiments is used as the input to the simulation program. Experimental and simulated displacements relative to the base at all three stories are plotted in these figures. The root-mean-square (RMS) errors between the simulated and the experimental results in these three figures are listed in Table 4.4. The close match between the simulated and experimental responses successfully validates the numerical models of the structure and the MR dampers. The validation also shows that as a reliable prediction to experimental results, numerical simulation can be employed to investigate large-scale structural control problems.

Table 4.4. RMS Errors between Simulated and Experimental Floor Displacements

	Figure 4.20	Figure 4.21	Figure 4.22
RMS Error at Floor-1	0.0005m	0.0004m	0.0004m
RMS Error at Floor-2	0.0008m	0.0008m	0.0008m
RMS Error at Floor-3	0.0013m	0.0010m	0.0011m

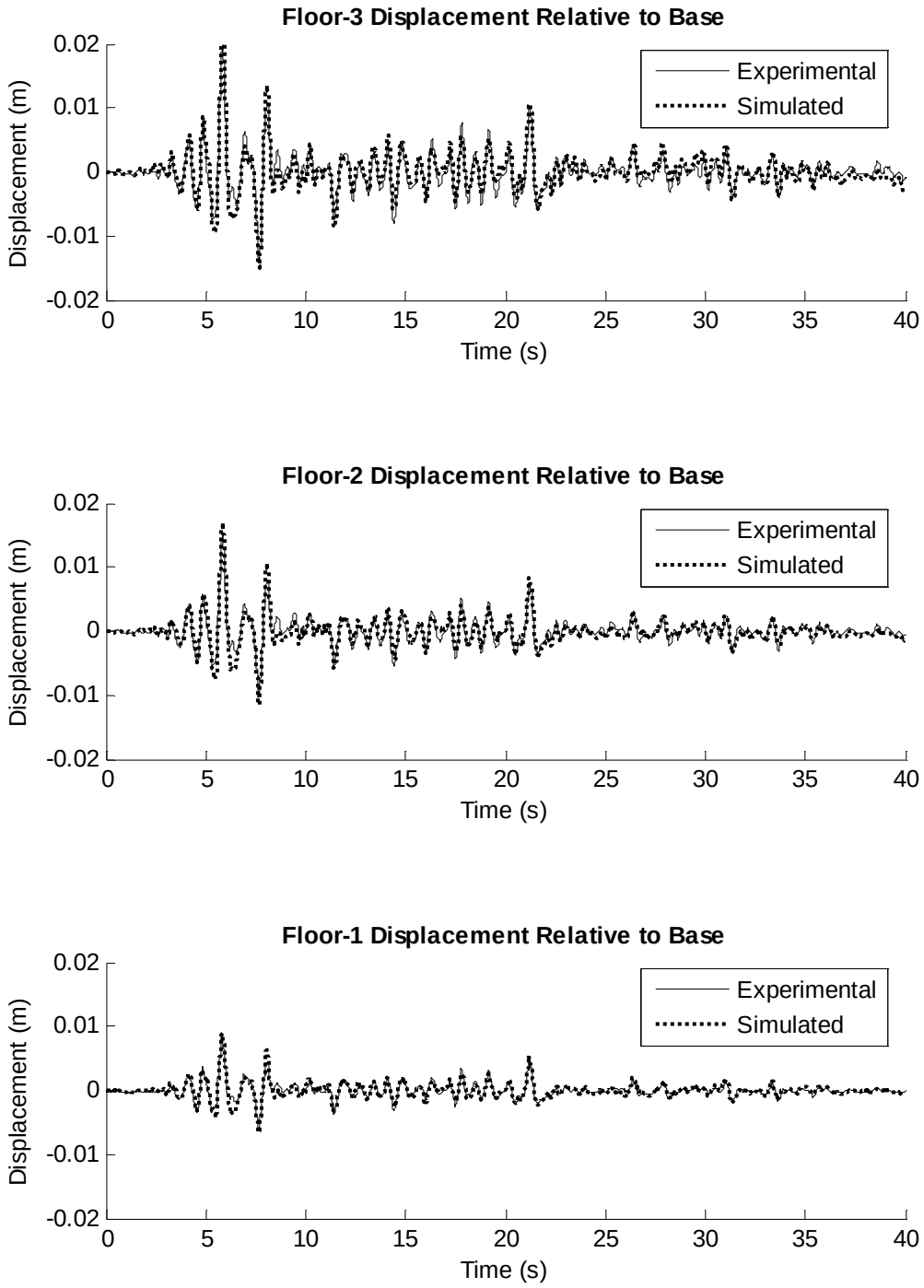

Figure 4.20. Comparison between simulated structural response and experimental measurement: ground motion is 1999 Chi-Chi NS with PGA scaled to 1m/s^2; control scheme is wireless #1 as shown in Table 4.2 (fully decentralized, with a sampling period of 20ms)

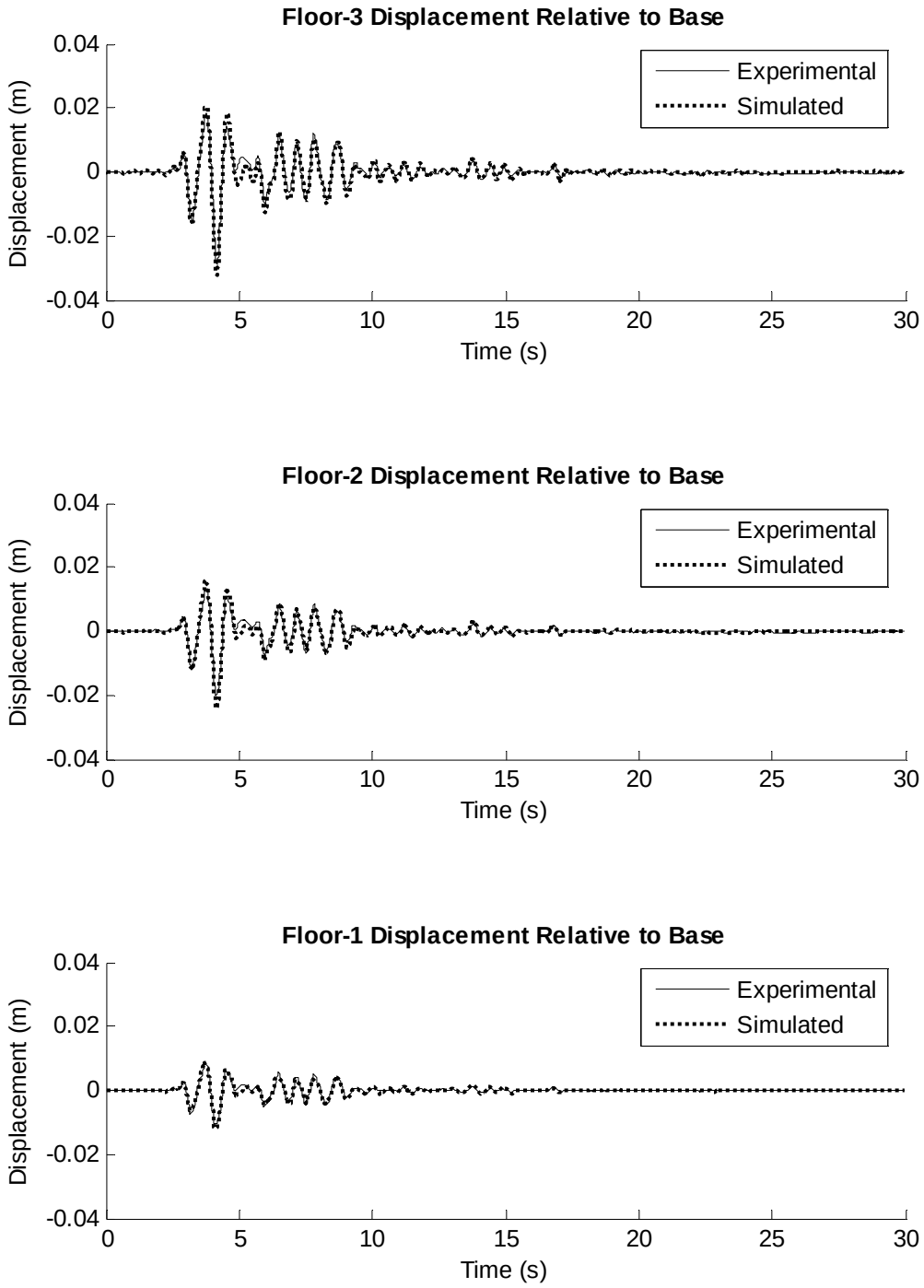

Figure 4.21. Comparison between simulated structural response and experimental measurement: ground motion is 1995 Kobe NS with PGA scaled to 1m/s^2; control scheme is wireless #2 as shown in Table 4.2 (partially decentralized, with a sampling period of 60ms)

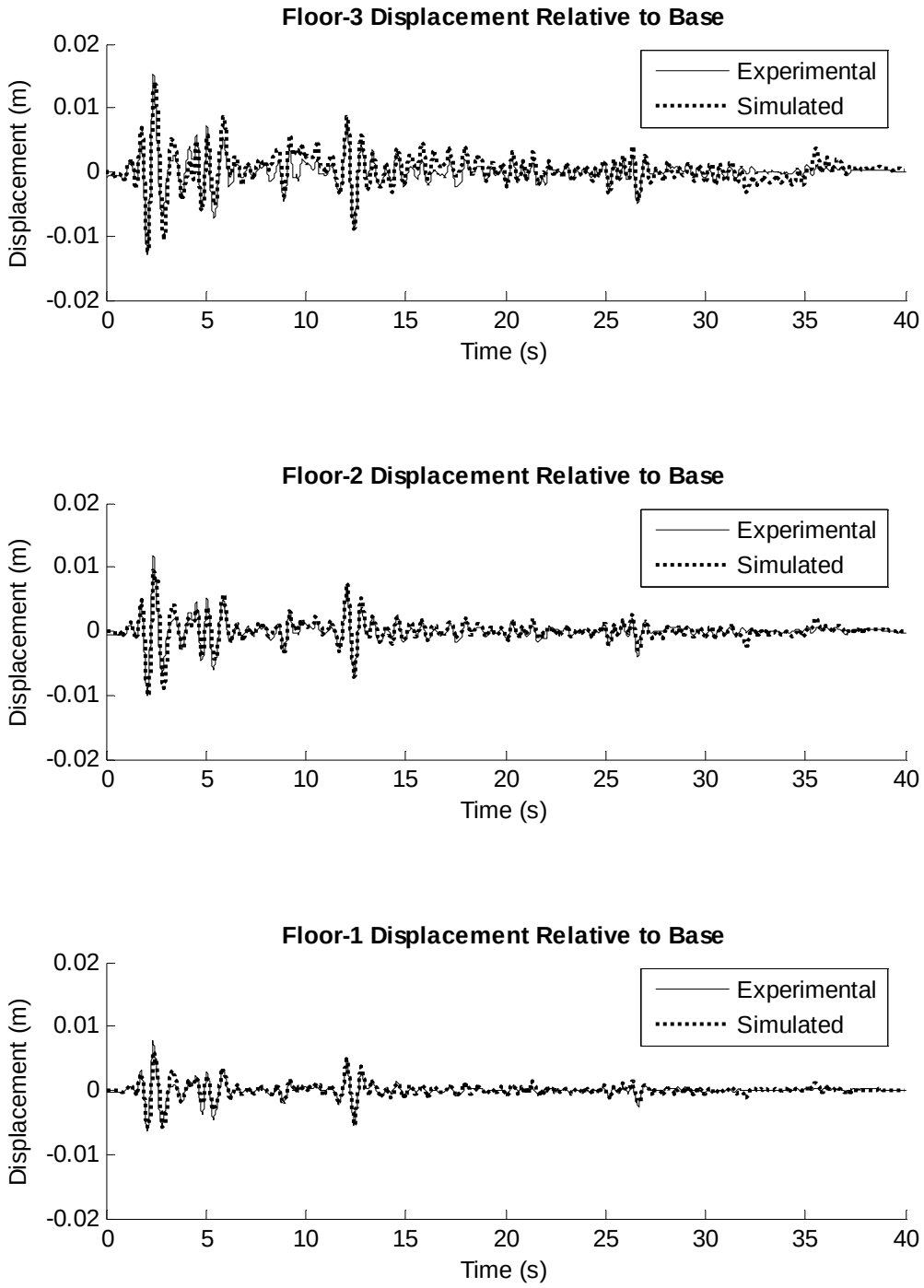

Figure 4.22. Comparison between simulated structural response and experimental measurement: ground motion is 1940 El Centro NS with PGA scaled to 1m/s^2; control scheme is wireless #3 as shown in Table 4.2 (centralized, with a sampling period of 80ms)

4.4 Effects of Decentralization and Time Delay on Large Structures

With encouraging results from the NCREE experimental tests, further investigations of the decentralized measurement feedback control strategies are performed with numerical simulations. Specifically, different decentralization patterns and sampling time delays are investigated for two structural models, namely a 5-story Kajima-Shizuoka building (Kurata, *et al.* 1999) and a 20-story benchmark structure designed for the Structural Engineers Association of California (SAC) project (Spencer, *et al.* 1998). Numerical simulations are performed for the cases when the structures are instrumented with ideal actuators that are capable of producing any desired forces and with semi-active hydraulic dampers (SHD). The actuators are installed with a V-brace on each floor of the structures (see Figure 4.23). For the SHD dampers, the Maxwell element proposed by Hatada, *et al.* (2000) is employed to model the damping force and is described by the following differential equation:

$$\dot{u}(t) + \frac{k_{eff}}{c_{SHD}(t)} u(t) = k_{eff} \Delta\dot{q}(t) \tag{4.44}$$

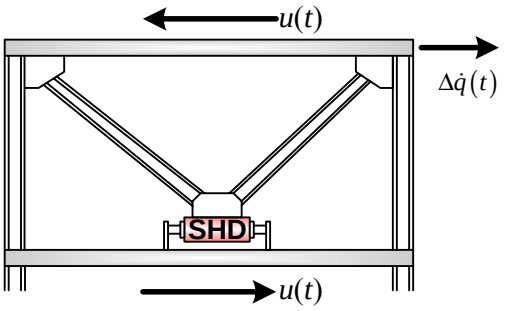

Maximum Control Force	1,000 kN
Maximum Displacement	+/- 6 cm
Stiffness of the SHD	400,000 kN/m
Maximum Damping Coefficient	200,000 kN-s/m
Minimum Damping Coefficient	1,000 kN-s/m
Maximum Shaft Velocity	25 cm/s
Power Consumption	70 Watts

Figure 4.23. Key parameters of the SHD damper employed

where $u(t)$ and $\Delta\dot{q}(t)$ denote the damping force and the inter-story velocity, respectively, k_{eff} represents the effective stiffness of the damper in series with the V-brace, and $c_{SHD}(t)$ is the adjustable damping coefficient of the SHD damper. If the desired damper force is in an opposite direction to the inter-story velocity, as shown in Figure 4.23, the damping coefficient is adjusted so that a damper force closest to the desired force is generated. If the desired force is in the same direction to the inter-story velocity, the damping coefficient is set to its minimum value.

4.4.1 Formulation for the Numerical Simulations

In this study, it is assumed that the inter-story drifts and velocities are measurable. For notational convenience in later derivation, Equation (4.3) is first rewritten by replacing the symbols **x**, **A**, **B**, and **E** with $\mathbf{x}_I$, $\mathbf{A}_I$, $\mathbf{B}_I$, and $\mathbf{E}_I$, respectively:

$$\dot{\mathbf{x}}_I(t) = \mathbf{A}_I\mathbf{x}_I(t) + \mathbf{B}_I\mathbf{u}(t) + \mathbf{E}_I\mathbf{w}(t) \tag{4.45}$$

where $\mathbf{x}_I = \left[\mathbf{q}(t); \dot{\mathbf{q}}(t)\right]$ contains the displacements and velocities relative to the ground. It is assumed that the external excitation is unidirectional ground motion, i.e. $\mathbf{w}(t)$ is a scalar ($m_1 = 1$) containing the ground acceleration history. The state-space matrices can be written as:

$$\mathbf{A}_I = \begin{bmatrix} \mathbf{0}_{n\times n} & \mathbf{I}_{n\times n} \\ -\mathbf{M}^{-1}\mathbf{K} & -\mathbf{M}^{-1}\mathbf{C} \end{bmatrix},\ \mathbf{B}_I = \begin{bmatrix} \mathbf{0}_{n\times m_2} \\ \mathbf{M}^{-1}\mathbf{T}_\mathbf{u} \end{bmatrix},\ \mathbf{E}_I = \begin{bmatrix} \mathbf{0}_{n\times 1} \\ -\mathbf{1}_{n\times 1} \end{bmatrix} \tag{4.46}$$

where an example of $\mathbf{T}_\mathbf{u}$ for a 3-story structure is provided in Equation (4.2). The displacement and velocity variables in the state vector $\mathbf{x}_I$, which are relative to the ground, are transformed into drifts and velocities between neighboring floors: $\mathbf{x} = \mathbf{\Gamma}_I\mathbf{x}_I$ = $[q_1;\ q_2 - q_1;\ \ldots;\ q_n - q_{n-1};\ \dot{q}_1;\ \dot{q}_2 - \dot{q}_1;\ \ldots;\ \dot{q}_n - \dot{q}_{n-1}]$. The $2n \times 2n$ transformation matrix $\mathbf{\Gamma}_I$ is defined as:

$$\mathbf{\Gamma}_I = \begin{bmatrix} \tilde{\mathbf{\Gamma}}_I & \\ & \tilde{\mathbf{\Gamma}}_I \end{bmatrix}, \text{ and } \tilde{\mathbf{\Gamma}}_I = \begin{bmatrix} 1 & & & \\ -1 & 1 & & \\ & \ddots & \ddots & \\ & & -1 & 1 \end{bmatrix}_{n \times n} \tag{4.47}$$

Substituting $\mathbf{x}_I = \mathbf{\Gamma}_I^{-1}\mathbf{x}$ into Equation (4.45) and left-multiplying the equation with $\mathbf{\Gamma}_I$, the state space variables are transformed into inter-story drifts and velocities that are grouped by the stories:

$$\dot{\mathbf{x}}(t) = \mathbf{A}\mathbf{x}(t) + \mathbf{B}\mathbf{u}(t) + \mathbf{E}\mathbf{w}(t),\ \mathbf{A} = \mathbf{\Gamma}_I \mathbf{A}_I \mathbf{\Gamma}_I^{-1},\ \mathbf{B} = \mathbf{\Gamma}_I \mathbf{B}_I, \text{ and } \mathbf{E} = \mathbf{\Gamma}_I \mathbf{E}_I \tag{4.48}$$

The continuous system represented by the above state-space equations is then discretized using the formulation shown in Section 4.2.1, and centralized or decentralized gain matrices can be computed using the algorithms presented in Section 4.2.2.

4.4.2 Decentralized Structural Control Simulations of a 5-Story Building

A five-story model similar to the Kajima-Shizuoka Building is employed (Kurata, *et al.* 1999). The steel-structure building has a total height of about 19m (Figure 4.24). For this study, two actuators are installed at each floor. In the numerical simulations, it is assumed that both the inter-story drifts and inter-story velocities between every two neighboring floors are measurable. The state-space system is formulated such that the state-space vector contains inter-story drifts and inter-story velocities, as shown in Section 4.4.1. For direct state feedback, the measurement matrix $\mathbf{C}_\mathbf{y}$ is defined to be a $2n \times 2n$ identity matrix. The weighting matrices for the quadratic index J in Equation (4.12) are defined as:

$$\mathbf{Q} = \begin{bmatrix} 10^{15}\mathbf{I}_{5\times5} & \mathbf{0}_{5\times5} \\ \mathbf{0}_{5\times5} & \mathbf{0}_{5\times5} \end{bmatrix} \text{ and } \mathbf{R} = 10^{-9}\mathbf{I}_{5\times5} \tag{4.49}$$

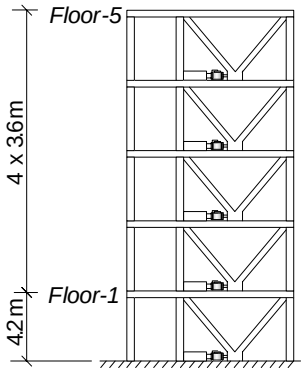

(a) Side elevation of the building

Seismic Mass		Inter-story Stiffness	
F1	215.2 x 10^3 kg	F1	147 x 10^3 kN/m
F2	209.2 x 10^3 kg	F2	113 x 10^3 kN/m
F3	207.0 x 10^3 kg	F3	99 x 10^3 kN/m
F4	204.8 x 10^3 kg	F4	89 x 10^3 kN/m
F5	266.1 x 10^3 kg	F5	84 x 10^3 kN/m

Damping 5% Natural Damping

(b) Model parameters of the lumped mass structure

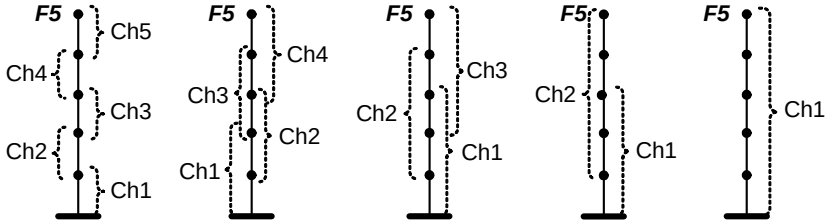

(c) Information group partitioning for different degrees of centralization (DC)

Figure 4.24. A five-story model similar to the Kajima-Shizuoka Building

The simulations are conducted for different degrees of centralization (DC), as illustrated in Figure 4.24(c); the case where DC equal to *i* represents that the neighboring *i* floors constitute a communication subnet and share their sensor data. For example, the case where DC = 1 implies each group consists of only one floor. For the case where DC = 3, each group consists of three floors, resulting in 3 wireless subnets for the 5 story building. For DC = 5, all 5 floors share their sensor data, resulting in a centralized information architecture. Based on the above definitions for measurement matrix $\mathbf{C}_y$ and degrees of centralization, the gain matrix consists of two square submatrices with the same symmetric shape constraints. In each square submatrix, the diagonal entries and the j^{th} (j = 1, .., i-1) entry above and below the diagonal entry are non-zero. For example, when DC = 2, the gain matrix has the following shape constraint:

$$\mathbf{G_d} = \left[\begin{array}{ccccc|ccccc} \blacksquare & \blacksquare & 0 & 0 & 0 & \blacksquare & \blacksquare & 0 & 0 & 0 \\ \blacksquare & \blacksquare & \blacksquare & 0 & 0 & \blacksquare & \blacksquare & \blacksquare & 0 & 0 \\ 0 & \blacksquare & \blacksquare & \blacksquare & 0 & 0 & \blacksquare & \blacksquare & \blacksquare & 0 \\ 0 & 0 & \blacksquare & \blacksquare & \blacksquare & 0 & 0 & \blacksquare & \blacksquare & \blacksquare \\ 0 & 0 & 0 & \blacksquare & \blacksquare & 0 & 0 & 0 & \blacksquare & \blacksquare \end{array}\right]_{5\times 10} \tag{4.50}$$

The left submatrix and the right submatrix correspond to the displacement part and the velocity part, respectively, of the measurement vector $\mathbf{y_d}$. The various combinations of centralization degrees (1 through 5) and sampling time steps ranging from 0.005s to 0.06s (at a resolution of 0.005s) are simulated. As one step of time delay is assumed, the amount of feedback delay is equal to the length of the control sampling time step in each simulation. Four ground motion records are used for each simulation: the 1940 El Centro NS record (Imperial Valley Irrigation District Station) scaled to a peak ground acceleration (PGA) of 1m/s^2, the same 1940 El Centro NS record scaled to a PGA of 2m/s^2, the 1999 Chi-Chi NS record (TCU-076 Station) scaled to a PGA of 1m/s^2, and the 1995 Kobe NS record (JMA Station) scaled to a PGA of 1m/s^2. Performance indexes proposed by Spencer *et al*. (1998) are adopted. In particular, the two representative performance indexes employed are the same as defined in Section 4.2.3.2:

$$PI_1 = \max_{\text{Earthquakes}} \left\{ \frac{\max_{t,i} d_i(t)}{\max_{t,i} \hat{d}_i(t)} \right\}, \text{ and } PI_2 = \max_{\text{Earthquakes}} \left\{ \frac{J_{LQR}}{\hat{J}_{LQR}} \right\} \tag{4.51}$$

where PI_1 and PI_2 are the performance indexes corresponding to inter-story drifts and LQR cost indexes, respectively. The performance indexes are defined by normalizing the controlled structural response with the response of the uncontrolled structure. Detailed explanation for the two indexes can be found in Section 4.2.3.2. When computing the LQR index over time, a uniform time step of 0.001s is used to collect the structural response data, regardless of the sampling time step of the control scheme.

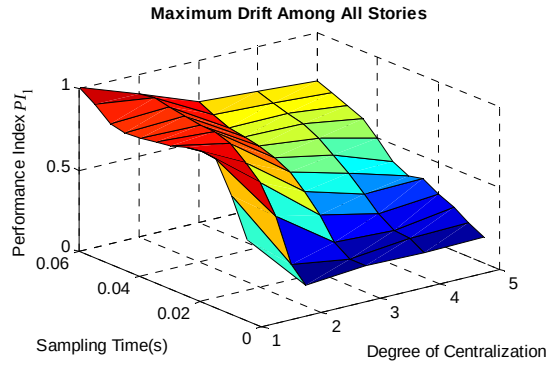

(a) 3D plot for performance index PI_1

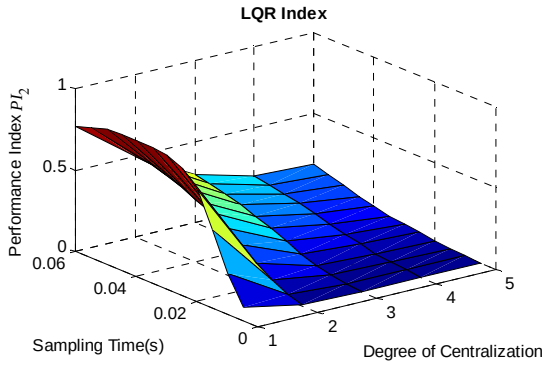

(b) 3D plot for performance index PI_2

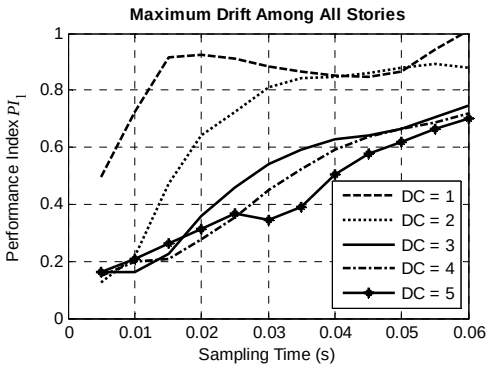

(c) Condensed 2D plot for PI_1

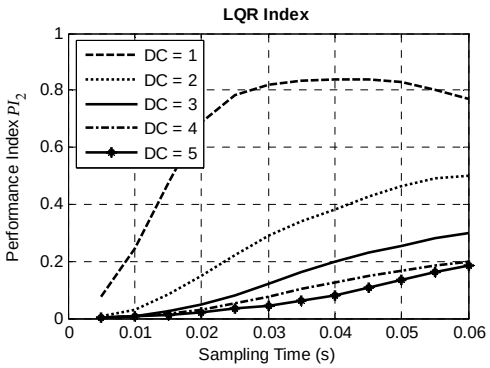

(d) Condensed 2D plot for PI_2

Figure 4.25. Simulation results for the five-story Kajima-Shizuoka Building instrumented with ideal actuators. The plots illustrate performance indexes for different sampling time steps and degrees of centralization (DC).

Figure 4.25 and Figure 4.26 show the values of the two control performance indexes for the 5-story structure instrumented with ideal actuators and SHD dampers, respectively. Different combinations of degrees of centralization and sampling time steps are employed for the simulations. The plots clearly illustrate that the degrees of centralization and sampling steps could have significant impact on the performance of the control system. Generally speaking, control performance is better for higher degrees of centralization and shorter sampling times. To better review the simulation results, the performance indexes for the five different control schemes are also plotted as a function of sampling time. For example, as shown in Figure 4.26(c), if a partially decentralized control system with DC equal to 2 can achieve 0.01s sampling time and a centralized

system can only achieve 0.03s due to additional communication latency, the partially decentralized system can result in much lower maximum inter-story drifts. Similar trends are observed in Figure 4.26(d) for the LQR performance indexes. These simulation results verify the performance of the decentralized control algorithms, and demonstrate the feasibility of decentralized control for the 5-story Kajima Shizuoka structure.

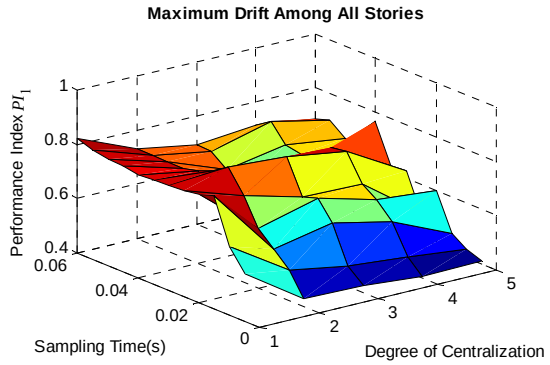

(a) 3D plot for performance index PI_1

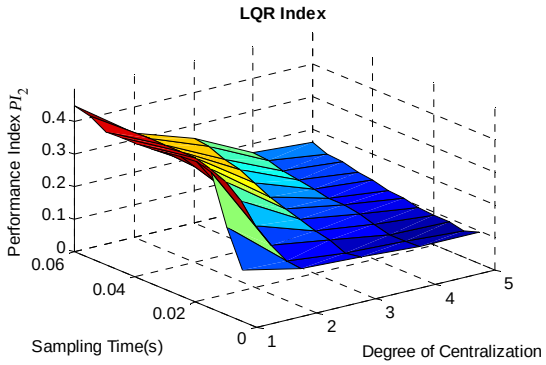

(b) 3D plot for performance index PI_2

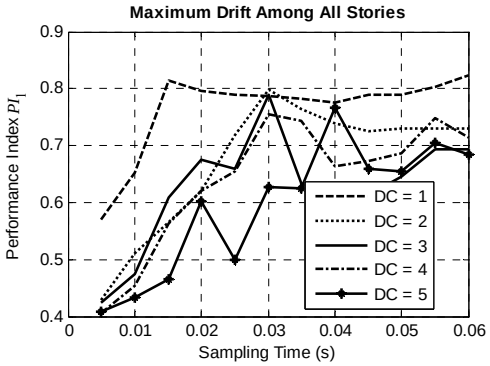

(c) Condensed 2D plot for PI_1

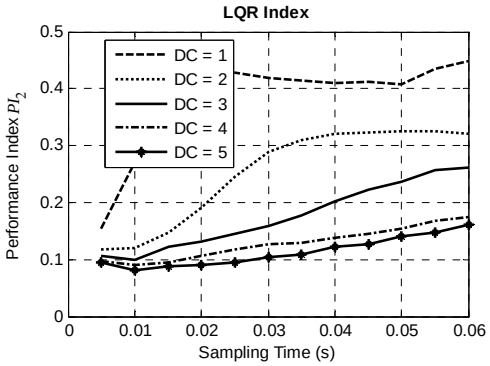

(d) Condensed 2D plot for PI_2

Figure 4.26. Simulation results for the five-story Kajima-Shizuoka Building instrumented with semi-active hydraulic dampers (SHD). The plots illustrate performance indexes for different sampling time steps and degrees of centralization (DC).

4.4.3 Decentralized Structural Control Simulations of a 20-Story Building

A 20-story benchmark structure designed for the Structural Engineers Association of California (SAC) project is also selected for numerical simulations (Spencer, *et al.* 1998). To simplify the analysis, the building is modeled as an in-plane lumped-mass structure (Figure 4.27). In the numerical simulations, it is assumed that both the inter-story drifts and inter-story velocities between every two neighboring floors are measurable. The system state-space equations are formulated such that the state-space vector again contains inter-story drifts and velocities, rather than the displacements and velocities relative to the ground. The measurement matrix $\mathbf{C}_y$ is defined as a $2n \times 2n$ identity matrix, as in the case of the 5-story structure, so that the state-space vector is used for control feedback directly. The weighting matrices for the quadratic index J in Equation (4.12) are defined as:

$$\mathbf{Q} = 10^{14}\begin{bmatrix} \mathbf{Q}_I & \mathbf{0}_{20\times 20} \\ \mathbf{0}_{20\times 20} & \mathbf{Q}_I \end{bmatrix} \text{ and } \mathbf{R} = 10^{-14}\mathbf{I}_{20\times 20} \tag{4.52}$$

where $\mathbf{Q}_I$ is a 20×20 diagonal matrix, whose diagonal entries are 20, 19, …, 2, 1. The simulations are conducted for different degrees of centralization (DC), as illustrated in Figure 4.27(c). The degrees of centralization reflect different communication network architectures, with each channel representing one communication subnet. The actuators covered within a subnet are allowed to access the wireless sensor data within that subnet. For example, the case where DC = 1 implies each wireless channel covers only five stories and a total of four wireless channels (subnets) are utilized. Of all the different degrees of centralization, the case where DC = 1 represents the lowest requirement to the wireless communication range and achieves lowest communication latency as a smaller number of wireless sensors need to broadcast their data in the subnet. Constrained by this decentralized information structure, the gain matrix for the case where DC = 1 has the following sparsity pattern:

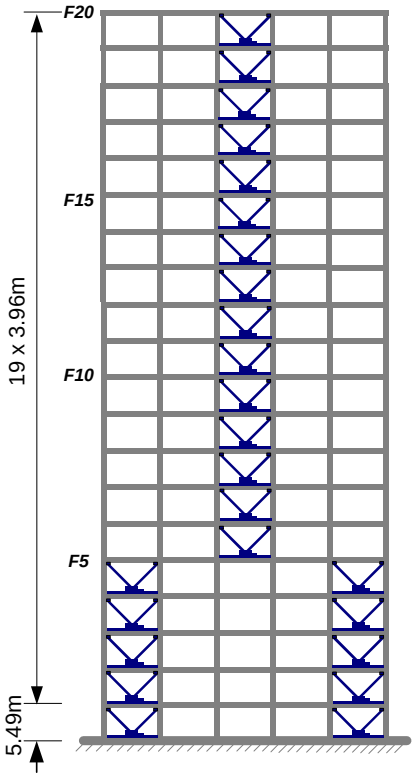

(a) Building elevation

Seismic Mass		Inter-story Stiffness	
F1	1.126 x 10^6 kg	F1-F5	862.07 x 10^3 kN/m
F2 – F19	1.100 x 10^6 kg	F6-F11	554.17 x 10^3 kN/m
F20	1.170 x 10^6 kg	F12-F14	453.51 x 10^3 kN/m
		F15-F17	291.23 x 10^3 kN/m
Damping		F18-F19	256.46 x 10^3 kN/m
5% Natural Damping		F20	171.70 x 10^3 kN/m

(b) Model parameters of the lumped mass structure

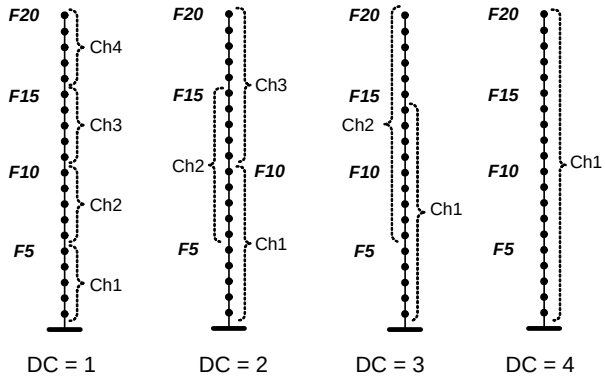

(c) Wireless subnet partitioning for different degrees of centralization (DC)

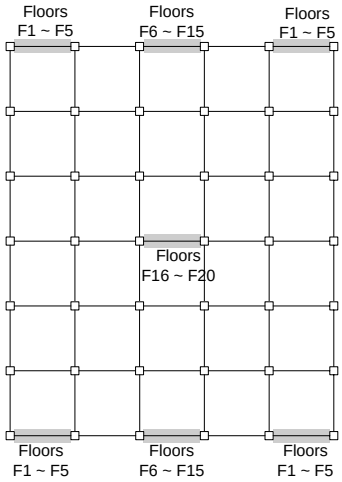

(d) Layout of semi-active hydraulic dampers (SHD) dampers on the floor plans

Figure 4.27. Twenty-story SAC Building for numerical simulations

$$\mathbf{G}_d = \left[\begin{array}{ccccc|ccccc} \blacksquare & & & & & \blacksquare & & & & \\ & \blacksquare & & & & & \blacksquare & & & \\ & & \blacksquare & & & & & \blacksquare & & \\ & & & \blacksquare & & & & & \blacksquare & \end{array}\right]_{20\times 40} \quad \text{when DC} = 1 \tag{4.53}$$

The left submatrix and the right submatrix correspond to the inter-story drift and the inter-story velocity components, respectively, of the measurement vector $\mathbf{y}_d$. The left and right submatrices are block-diagonal, with every block being a 5-by-5 square matrix. For

the case where DC = 2, each wireless channel covers ten stories and a total of three wireless channels are utilized. Constrained by the overlapping information structure, the gain matrix for DC = 2 has the following sparsity pattern:

$$\mathbf{G}_d = \left[\begin{array}{cc|cc} \blacksquare & \blacksquare & \blacksquare & \blacksquare \\ \blacksquare & \blacksquare\ \blacksquare & \blacksquare & \blacksquare\ \blacksquare \\ \blacksquare\ \blacksquare & \blacksquare & \blacksquare\ \blacksquare & \blacksquare \\ \blacksquare & & \blacksquare & \end{array}\right]_{20\times 40} \quad \text{when DC} = 2 \tag{4.54}$$

For the case when DC = 3, the number of stories covered by each of the two wireless subnets increases accordingly. That leads to fewer communication subnets and fewer zero blocks in the gain matrices. The case where DC = 4 specifies that one wireless channel covers all twenty floors, which results in a centralized information structure.

Figure 4.28 shows the numerical simulation results for the 20-story structure instrumented with ideal actuators. Various combinations of centralization degrees (DC = 1,…,4) and sampling time steps ranging from 0.01s to 0.06s (at a resolution of 0.01s) are simulated. Three ground motion records are used for each simulation: the 1940 El Centro NS record (Imperial Valley Irrigation District Station), the 1995 Kobe NS record (JMA Station), and the 1999 Chi-Chi NS record (TCU-076 Station), all scaled to a peak ground acceleration (PGA) of 1m/s^2. The two performance indices defined in Equation (4.51) are plotted in Figure 4.28 for different combinations of degrees of centralization and sampling time steps. Similar to the simulations for the 5-story structural model, when computing the LQR index over time, a uniform time step of 0.001s is used to collect the structural response, regardless of the sampling time step of the control scheme. Generally speaking, the results are similar to the previous results for the 5-story structure where the control performance is better for higher degrees of centralization and shorter sampling times. The plots show that except for the case where DC = 1, the control schemes with certain overlapping information structures achieve comparable performance. As shown in Figure 4.28(c), if a partially decentralized control system with DC equal to 2 can achieve a sampling step of 0.02s and a centralized system can only achieve 0.04s due to additional communication latency, the partially decentralized system

can result in lower maximum inter-story drifts. Similar trends are observed in Figure 4.28(d), except that the plots are smoother due to the summation process for computing the LQR indices.

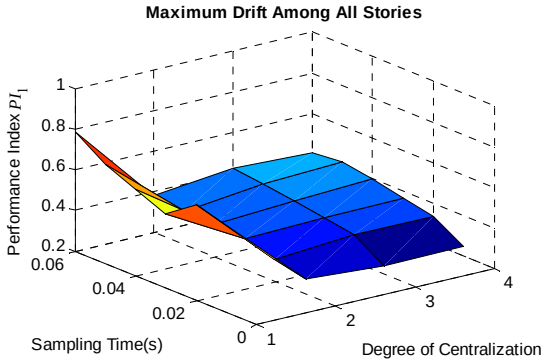

(a) 3D plot for performance index PI_1

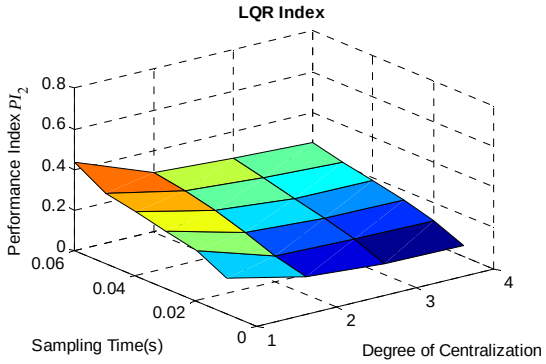

(b) 3D plot for performance index PI_2

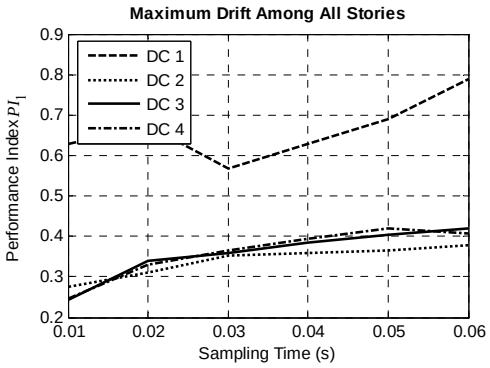

(c) Condensed 2D plot for PI_1

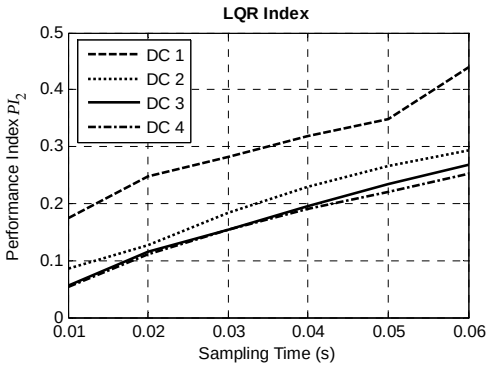

(d) Condensed 2D plot for PI_2

Figure 4.28. Simulation results for the 20-story SAC Building instrumented with ideal actuators. The plots illustrate performance indexes for different sampling time steps and degrees of centralization (DC).

Numerical simulations are also conducted for the four control strategies where semi-active hydraulic dampers (SHD) are employed on the structure. The arrangement of SHD dampers is shown in Figure 4.27(d); the number of instrumented SHD dampers decreases gradually from 4 to 1 in the higher floors. Figure 4.29 presents the simulated maximum inter-story drifts when the structure is excited using the same three ground motions, except that the PGAs are scaled up to $5m/s^2$, instead of $1m/s^2$. To compare the performance of decentralized versus centralized control, the case where DC = 2 (partially decentralized) and the case where DC = 4 (centralized) are plotted. As shown in Figure 4.27, each subnet covers ten floors when DC = 2, or twenty floors when DC = 4. That is, the induced time delay when DC = 2 is about half of the delay when DC = 4, and the time delays of 20ms and 40ms are assigned, respectively, for these two cases. As shown in Figure 4.29, both of the two control schemes significantly reduce the maximum inter-story drifts compared with the uncontrolled case. For the Kobe and Chi-Chi ground motions, the partially decentralized case where DC = 2 achieves almost equivalent performance compared with the centralized case where DC = 4, while for the El Centro earthquake record, the case with DC = 2 achieves slightly better performance than the case where DC = 4. These results again illustrate that although decentralized control has the disadvantage of computing control decisions without complete sensor data, the lower time delay in decentralized control could make the control scheme perform as well as centralized control, given that the centralized case, using wireless communication, requires longer latencies.

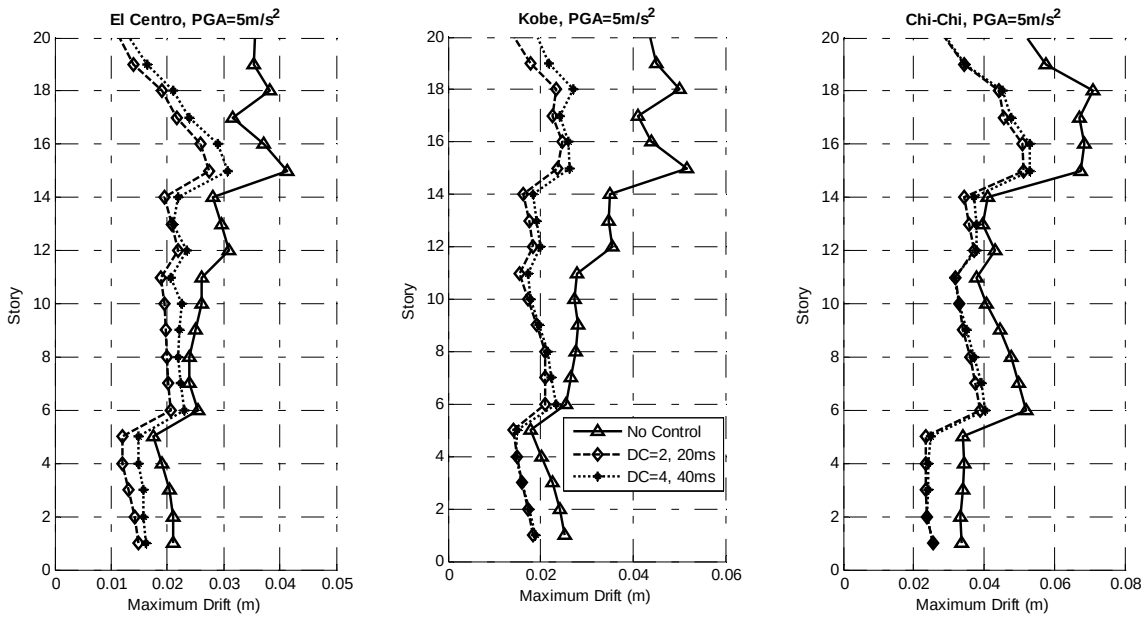

Figure 4.29. Maximum inter-story drifts for cases where DC = 2 with 20ms time delay and DC = 4 with 40ms time delay

4.5 Summary

In this chapter, the prototype wireless feedback control system for civil structures has been described. Unlike traditional wire-based control systems, wireless communication is employed as the information link between the sensors and the actuators. The traditional centralized controller is decomposed into individual controllers embedded in the wireless control units. To effectively overcome the range and latency constraints of wireless communication, decentralized information structure is proposed for the wireless structural control system. In a decentralized control system, only neighborhood sensor data is required to make control decisions for an actuator, so that communication latency can be greatly reduced, and the requirement on communication range is much lower.

State machine concept is used to design and implement the program flow of the wireless sensing and control units.

This study adopts the formulation to the structural control problem proposed by Chung, *et al.* (1995), which is developed based on the classical Linear Quadratic Regulator (LQR) control design. Time delay of the measurement feedback is considered in this formulation. The derivation results in a set of nonlinearly coupled matrix equations with the control gain matrix as one of the variables. To compute centralized or decentralized control gain matrices, the iterative algorithm described by Lunze (1992) is modified. Numerical simulations using a 3-story structural model illustrate the importance of considering time delay in the problem formulation, and the importance of the iterative scheme for shape-constrained gradient search while computing decentralized control gain matrices. The simulations for different sampling time steps and centralization degrees also demonstrate the efficacy and reliability of the heuristic algorithm for centralized and decentralized gain matrices.

In order to properly design the wireless control system, a detailed analysis of the communication time delay of the wireless sensing and control units is performed. With the centralized/decentralized control schemes embedded in the distributed wireless sensing and control units, a half-scale 3-story laboratory structure is employed to validate the performance of the wireless structural control system. Three magnetorheological (MR) dampers are deployed on three floors of the structure, each damper being commanded by one wireless sensing and control unit. Real-time wireless sensor data collected from velocity meters are used to make optimal control decisions. With different sparsity patterns in the control gain matrices, three centralized/decentralized wireless control schemes are adopted. The three wireless control schemes achieve reasonable performance compared with a baseline wired control system. Among the three wireless control schemes, the experimental results show that decentralized wireless control strategies may provide equivalent or even superior control performance, given that their centralized counterparts suffer longer sampling periods due to wireless communication

latencies. Furthermore, the experimental results are compared with numerical simulation results. The close similarity between the two sets of results demonstrates the accuracy of the numerical models for the structure and the MR dampers.

In order to further investigate the performance of the decentralized wireless structural control in large-scale structures, numerical simulations using the LQR-based decentralized control algorithm are conducted for a 5-story and a 20-story building structure instrumented with ideal actuators and SHD dampers, by varying the degrees of centralization and feedback time delays of the control system. Wireless communication subnets in the structure are allocated to form different decentralized information feedback patterns. The simulation results demonstrate the reliability of the optimal control algorithms, and illustrate that decentralized wireless sensing and control is viable for future structural control systems. It is also observed that decentralized control strategies may provide equivalent or even superior control performance, if the centralized control schemes suffer longer feedback time delay due to communication latencies.

Future research will continue to improve both the theory and implementation of wireless decentralized structural control. On the theory side, other decentralized control algorithms may be investigated for application in civil structures. For implementation, system performance can be improved by adopting wireless technologies that have lower communication latency, and employing more powerful embedded computing devices.

Chapter 5

Summary, Conclusions and Future Directions

The adoption of wireless communication technology in a structural sensing and control network may significantly reduce installation costs while greatly increasing the flexibility of system architectures. This thesis has described the development and validation of a wireless structural sensing and control system, together with a decentralized optimal structural control solution that is integrated within the system. This chapter first provides a summary and conclusion of the thesis, and then discusses future research directions.

5.1 Summary

In order to construct a wireless sensing and control network for civil structures, wireless sensing and control units need be designed. Chapter 2 describes the integrated hardware and software design approach pursued to develop a state-of-the-art prototype wireless sensing and actuation unit. A basic wireless sensing unit consists of three functional modules: sensor signal digitization, computational core, and wireless communication. To

assist in amplifying, filtering, and offsetting analog sensor signals prior to digitization, an auxiliary sensor signal conditioning module is designed. Another auxiliary module, the actuation signal generation module, is designed to offer an interface through which the wireless unit sends analog control commands to structural actuators. A number of design features have been achieved by properly selecting the hardware components for the wireless unit: high-fidelity sensing, reliable wireless communication, and the capability of on-board computing. Besides the hardware design, embedded software for the microcontroller is developed in tandem. The embedded software design follows a three-layer architecture, which consists of microcontroller peripherals, system management modules, and application software routines. With one layer built upon another, this hierarchical design allows the embedment of high-level application software routines while fully utilizing the rich functionalities provided by the low-level unit hardware.

Chapter 3 describes the design, implementation, and validation of a wireless structural sensing system. The prototype wireless sensing system includes a single data server and multiple wireless sensing units that can be distributively deployed in a large-scale civil structure. Efficient communication protocols between the server and the wireless units are designed for precise time-synchronization and robust wireless sensor data collection. Using a dual-stack memory management scheme, the system also supports continuous data streaming from a network of wireless sensors. State machine concepts prove to be effective in representing and designing robust communication program flows concurrently executed on the data server and the wireless sensing units. Chapter 3 also presents three validation tests for the prototype wireless structural sensing system: the half-scale 3-story structural test at NCREE, Taiwan, the Geumdang Bridge test in Icheon, South Korea, and the Voigt Bridge test in San Diego, CA. These tests validate the following system features: (1) operational robustness (i.e. no data loss) and excellent data fidelity of the wireless sensors, (2) the embedded computing capability of the wireless units, (3) the enhancement of sensor signal quality using the specially-designed signal conditioning module, and (4) easy re-configurability of the wireless sensor network topology in field settings. Operating deflection shape analysis has been successfully

conducted for the two bridge structures where the bridge decks are instrumented with tens of wireless accelerometers.

Chapter 4 describes the prototype wireless feedback control system for civil structures. The traditional centralized controller is decomposed so that wireless control units can act as individual controllers. Thus, the risk of single-point failure as is typical in centralized control systems is eliminated. To effectively overcome the range and latency constraints of wireless communication, a decentralized feedback architecture is proposed for the wireless structural control system. In a decentralized control system, only neighborhood sensor data is required to make control decisions for an actuator; hence, communication latency is greatly reduced and communication range requirements can also be reduced. With time delay effect considered in the formulation, a heuristic algorithm for solving optimal centralized and decentralized control gain matrices is developed based on linear quadratic regulator (LQR) control theory. Numerical simulations using a 3-story structural model illustrate the efficacy and reliability of the heuristic algorithm.

With centralized and decentralized control schemes embedded in the distributed wireless sensing and control system, validation tests are conducted. A half-scale 3-story laboratory structure is employed for the validation experiments. Three magnetorheological (MR) dampers are deployed on three floors of the structure, with each damper commanded by one wireless sensing and control unit. Using different sparsity patterns imposed on the control gain matrices, three centralized/decentralized wireless control schemes are adopted. The three wireless control schemes achieve reasonable performance compared with a baseline wired control system. To further investigate the performance of decentralized wireless structural control for large-scale structures, numerical simulations using the LQR-based decentralized control algorithm are conducted for 5-story and 20-story building structures instrumented with ideal actuators and SHD dampers. Various degrees-of-centralization and communication time delay are employed for the wireless control system. The simulation results demonstrate

the reliability of the optimal control algorithm and illustrate that decentralized wireless sensing and control is viable for future structural control systems.

5.2 Conclusions

This research on decentralized wireless structural sensing and control leads to following main conclusions:

- Wireless structural sensing and feedback control is proved to be feasible and reliable through field and laboratory validation tests. The system may include multiple wireless sensing and actuation nodes that are capable of peer-to-peer communication and making intelligent decisions for structural monitoring and control purposes. This distributed wireless sensing and actuation architecture represents a new paradigm in structural sensing and control.

- To make the wireless structural sensing and control system scalable for large-scale civil structures, decentralized wireless sensing and control schemes can be employed. Experiments and simulations demonstrate that decentralized wireless control strategies may provide equivalent or even superior control performance, given that their centralized counterparts suffer longer sampling periods due to wireless communication latencies.

- A heuristic decentralized optimal structural control algorithm that explicitly accounts for time delay has been developed. Both experimental tests and numerical simulations have been conducted to validate the reliability and efficacy of this output feedback control algorithm.

5.3 Future Research

A great amount of research is to be accomplished before fully autonomous wireless structural monitoring and control systems can be reliably adopted in actual civil structures. In the near future, developments in many other engineering fields, such as electrical engineering, mechanical engineering, material science, and computer science, will continue to offer many exciting new opportunities for structural monitoring and control applications. For example, to capitalize on the rapidly-evolving electronics market, new hardware components that consume less power while achieving similar or superior performance should be explored for developing future generations of the wireless sensing and actuation unit. Particularly, the market will continue to provide alternatives for the wireless transceiver and the microcontroller. Furthermore, as power harvesting technologies mature, battery-dependency can be reduced. The current wireless sensing and actuation units are employed for both structural monitoring and control applications. However, depending on the specific requirements for structural monitoring and control, separate hardware designs for the wireless units may be explored in the near future.

5.3.1 Wireless Structural Monitoring

Future improvement of the wireless structural monitoring system may include multi-hopping multi-layer wireless sensor networks densely deployed in civil structures. Emerging wireless technologies, such as WiMAX (Worldwide Interoperability for Microwave Access) and UWB (ultra-wideband), can be explored for implementation of multi-layer wireless sensor networks. WiMAX technology is oriented for high-speed transmissions over long distances, which may support a data rate up to tens of Mbps (megabit per second) at a distance of 10km while consuming about 1W of power (Andrews, *et al.* 2007). On the other hand, UWB technology is oriented for high-speed

transmission at short distances, which may support up to tens of Mbps at a distance of 10m and consuming only tens of mW (Di Benedetto, *et al.* 2006). Therefore, wireless technologies such as UWB may be utilized by low-power wireless units that constitute multi-hopping local subnets, while WiMAX can be dedicated to communication hubs that wirelessly transfer information over long distances.

Distributed intelligence in the wireless sensing nodes is yet to be better harnessed so that the wireless sensing nodes can collaboratively monitor structural conditions and detect the onset of possible damage. First, the ATmega128 microcontroller that is currently employed in the wireless sensing unit is suitable for low-power operation, but its computing capability may not be sufficient for heavy-duty data processing. One solution is to employ a dual-processor architecture as introduced by Lynch, *et al.* (2004a). In this dual-processor design, a low-power microcontroller is adopted for normal operations, and another high-performance microcontroller is only powered when heavy-duty computing is required. Secondly, with structural health monitoring algorithms embedded in the wireless units, it is envisioned that future structural health monitoring systems will be fully autonomous. Towards this end, reliable damage diagnosis algorithms need to be developed and verified by researchers. Common approaches for damage diagnosis include vibration-based damage detection algorithms (Doebling, *et al.* 1998) and statistical pattern classification methods (Sohn and Farrar 2001, Nair, *et al.* 2006). These advanced damage diagnosis algorithms can be embedded in the wireless sensing units and tested through laboratory and field validation experiments.

5.3.2 Decentralized Wireless Structural Control

Future research in decentralized wireless structural control will continue to advance in both theory and implementation. Besides the decentralized control algorithm based on linear quadratic regulator (LQR) control theory, other decentralized control algorithms that achieve better control performance are worth exploring. One possibility is to design

decentralized $\mathcal{H}_\infty$ controllers that minimize the $\mathcal{H}_\infty$ norm of the closed-loop system transfer function matrix (Zhou, *et al.* 1996). The $\mathcal{H}_\infty$ controller can offer excellent control performance when "worst-case" external disturbances are encountered (Skogestad and Postlethwaite 2005). $\mathcal{H}_\infty$ controller design is also convenient when model uncertainties exist (as is typical in most civil structures). Furthermore, Rotkowitz and Lall (2006) recently discovered a necessary and sufficient condition, viz. the quadratic invariance, that decides the convexity of an optimal feedback control problem. The quadratic invariance condition can be used to determine whether a decentralized controller achieves global optimality.

Centralized $\mathcal{H}_\infty$ controller design implemented in the continuous-time domain for civil structural control has been studied by other researchers (Chase and Smith 1996, Chase, *et al.* 1996, Yang, *et al.* 2004, Balandin and Kogan 2005). One important feature of $\mathcal{H}_\infty$ control is that the controller design can be formulated using linear matrix inequalities (LMI) (Boyd, *et al.* 1994). For an optimization problem with LMI constraints, sparsity patterns can be easily applied to the matrix variables. This property can be utilized to design decentralized controllers where the gain matrices with sparsity patterns corresponding to decentralized feedback architectures can be determined. Initial progress has been achieved in developing discrete-time decentralized $\mathcal{H}_\infty$ control algorithms (Wang, *et al.* 2007c). However, the current controller design cannot yet consider the effect of time delay in the formulation; therefore, the design is not yet ready for practical implementation in wireless structural control systems that may suffer time delays on the order of tens of milli-seconds.

On the implementation side, the performance of a wireless structural control system can be greatly improved by further reducing feedback delay thereby increasing the sampling rate of the control system. As described in Section 4.3.1, the feedback time delay mostly results from the wireless communication latency. Therefore, new wireless technologies

that have lower communication latency (such as the IEEE 802.11 and 802.15.4 standards) can be adopted to significantly reduce time delay. Both of the two technologies may achieve a single-transmission latency of a few milli-seconds, which is much smaller than the 15ms latency that is achieved by the 24XStream transceiver. Other parts of the feedback time delay mostly results from the computation time. The computation delay may become significant when dynamic measurement feedback (e.g. the Kalman estimator) is used, when data from larger neighborhoods are used for making control decisions, or when the hysteresis model updating for the actuator involves a large amount of computing. In these situations, more powerful embedded computing platforms can be adopted for reducing computation time. Besides reducing the feedback time delay, a wireless control system with multiple communication subnets operating simultaneously could be implemented to achieve various decentralized feedback information structures. With new decentralized control algorithms available and more advanced wireless control systems being implemented, further experiments using large-scale laboratory structures can be conducted to better quantify the merits and limitations of future decentralized wireless structural sensing and control systems.

Bibliography

Akyildiz, I.F., Weilian, S., Sankarasubramaniam, Y. and Cayirci, E. (2002). "A survey on sensor networks," *Communications Magazine, IEEE*, **40**(8): 102-114.

Andrews, J.G., Ghosh, A. and Muhamed, R. (2007). *Fundamentals of WiMAX: Understanding Broadband Wireless Networking*, Prentice hall, Upper Saddle River, NJ.

Arms, S.W., Townsend, C.P., Galbreath, J.H. and Newhard, A.T. (2004). "Wireless strain sensing networks," *Proceedings of the 2nd European Workshop on Structural Health Monitoring*, Munich, Germany, July 7 - 9, 2004.

Balandin, D.V. and Kogan, M.M. (2005). "LMI-based optimal attenuation of multi-storey building oscillations under seismic excitations," *Structural Control and Health Monitoring*, **12**(2): 213-224.

Boyd, S.P., El Ghaoui, L., Feron, E. and Balakrishnan, V. (1994). *Linear Matrix Inequalities in System and Control Theory*, SIAM, Philadelphia, PA.

Cao, D.Q., Ko, J.M., Ni, Y.Q. and Liu, H.J. (2000). "Decentralized active tendon control and stability of cable-stayed bridges," *Advances in Structural Dynamics*, **2**: 1257-1264.

Casciati, F. and Rossi, R. (2003). "Fuzzy chip controllers and wireless links in smart structures," *Proceedings of the AMAS/ECCOMAS/STC Workshop on Smart Materials and Structures (SMART'03)*, 1-24, Warsaw, Poland, September 2 - 5, 2003.

Çelebi, M. (2002). *Seismic Instrumentation of Buildings (with Emphasis on Federal Buildings)*. Report No. 0-7460-68170, United States Geological Survey, Menlo Park, CA.

Chang, P.C., Flatau, A. and Liu, S.C. (2003). "Review paper: health monitoring of civil infrastructure," *Structural Health Monitoring*, **2**(3): 257-267.

Chase, J.G. and Smith, H.A. (1996). "Robust H_∞ control considering actuator saturation. I: theory," *Journal of Engineering Mechanics*, **122**(10): 976-983.

Chase, J.G., Smith, H.A. and Suzuki, T. (1996). "Robust H_∞ control considering actuator saturation. II: applications," *Journal of Engineering Mechanics*, **122**(10): 984-993.

Chase, S. (2001). "The role of smart structures in managing an aging highway," *SPIE 8th Annual International Symposium on Smart Structures and Materials*, Keynote Presentation, Newport Beach, CA, March 4 - 8, 2001.

Chopra, A.K. (2001). *Dynamics of Structures: Theory and Applications to Earthquake Engineering*, Prentice Hall, Upper Saddle River, NJ.

Chu, S.Y., Soong, T.T. and Reinhorn, A.M. (2005). *Active, Hybrid, and Semi-active Structural Control: a Design and Implementation Handbook*, Wiley, Hoboken, NJ.

Chung, L.L., Lin, C.C. and Lu, K.H. (1995). "Time-delay control of structures," *Earthquake Engineering & Structural Dynamics*, **24**(5): 687-701.

Churchill, D.L., Hamel, M.J., Townsend, C.P. and Arms, S.W. (2003). "Strain energy harvesting for wireless sensor networks," *Proceedings of SPIE 10th Annual International Symposium on Smart Structures and Materials*, **5055**: 319-327, San Diego, CA, March 2 - 6, 2003.

Cooklev, T. (2004). *Wireless Communication Standards : a Study of IEEE 802.11, 802.15, and 802.16*, Standards Information Network IEEE Press, New York.

Di Benedetto, M.-G., Kaiser, T., Molish, A.F., Oppermann, I., Politano, C. and Porcino, D. (2006). *UWB Communication Systems: A Comprehensive Overview*, Hindawi Publishing Corporation, New York, NY.

Doebling, S.W., Farrar, C.R. and Cornwell, P.J. (1997). "DIAMOND: A graphical interface toolbox for comparative modal analysis and damage identification," *Proceedings of the 6th International Conference on Recent Advances in Structural Dynamics*, 399-412, Southampton, UK, July 14 - 17, 1997.

Doebling, S.W., Farrar, C.R. and Prime, M.B. (1998). "A summary review of vibration-based damage identification methods," *The Shock and Vibration Digest*, **30**(2): 91-105.

Doyle, J.C. (1983). "Synthesis of robust controllers and filters," *Proceedings of the 22nd IEEE Conference on Decision and Control*, **22**: 109-114, San Antonio, TX, December 14 - 16, 1983.

Dyke, S.J., Spencer, B.F., Jr., Quast, P., Kaspari, D.C., Jr. and Sain, M.K. (1996). "Implementation of an active mass driver using acceleration feedback control," *Microcomputers in Civil Engineering*, **11**: 305-323.

Eker, J., Cervin, A. and Hörjel, A. (2001). "Distributed wireless control using Bluetooth," *Proceedings of IFAC Conference on New Technologies for Computer Control*, Hong Kong, P. R. China, November 19 - 22, 2001.

Ewins, D.J. (2000). *Modal Testing: Theory, Practice, and Application*, Research Studies Press, Baldock, Hertfordshire, England.

Farrar, C.R., Sohn, H., Hemez, F.M., Anderson, M.C., Bement, M.T., Cornwell, P.J., Doebling, S.W., Schultze, J.F., Lieven, N. and Robertson, A.N. (2003). *Damage Prognosis: Current Status and Future Needs*. Report No. LA-14051-MS, Los Alamos National Laboratory, Los Alamos, NM.

Franklin, G.F., Powell, J.D. and Workman, M.L. (1998). *Digital Control of Dynamic Systems*, Addison-Wesley, Menlo Park, CA.

Fraser, M., Elgamal, A. and Conte, J.P. (2006). *UCSD Powell Laboratory Smart Bridge Testbed*. Report No. SSRP 06/06, Department of Structural Engineering, University of California, San Diego, La Jolla, CA.

Glaser, S.D. (2004). "Some real-world applications of wireless sensor nodes," *Proceedings of SPIE 11th Annual International Symposium on Smart Structures and Materials*, **5391**: 344-355, San Diego, CA, March 14 - 18, 2004.

Grisso, B.L., Martin, L.A. and Inman, D.J. (2005). "A wireless active sensing system for impedance-based structural health monitoring," *Proceedings of the 23rd International Modal Analysis Conference (IMAC XXIII)*, Orlando, FL, January 31 - February 3, 2005.

Hatada, T., Kobori, T., Ishida, M. and Niwa, N. (2000). "Dynamic analysis of structures with Maxwell model," *Earthquake Engineering & Structural Dynamics*, **29**(2): 159-176.

Hill, J.L. (2003). *System Architecture for Wireless Sensor Networks*. PhD Thesis, Department of Electrical Engineering and Computer Science, The University of California, Berkeley, Berkeley, CA.

Horowitz, P. and Hill, W. (1989). *The Art of Electronics*, Cambridge University Press, Cambridge, England.

Hou, T.-C. and Lynch, J.P. (2006). "Rapid-to-deploy wireless monitoring systems for static and dynamic load testing of bridges: validation on the Grove Street Bridge," *Proceedings of SPIE 13th Annual International Symposium on Smart Structures and Materials*, **6178**: 61780D, San Diego, CA, February 26 - March 2, 2006.

Housner, G.W., Bergman, L.A., Caughey, T.K., Chassiakos, A.G., Claus, R.O., Masri, S.F., Skelton, R.E., Soong, T.T., Spencer, B.F., Jr. and Yao, J.T.P. (1997). "Structural control: past, present, and future," *Journal of Engineering Mechanics*, **123**(9): 897-971.

Embedded Results Ltd. (2006). *Datasheet for STK300 ATmega128 AVR Starter Kit*. Aberystwyth, Wales, U.K.

Kay, S.M. (1988). *Modern Spectral Estimation: Theory and Application*, Prentice Hall, Englewood Cliffs, NJ.

Kim, S., Pakzad, S., Culler, D., Demmel, J., Fenves, G., Glaser, S. and Turon, M. (2007). "Health monitoring of civil infrastructures using wireless sensor networks," *Proceedings of the 6th International Conference on Information Processing in Sensor Networks (IPSN '07)*, 254-263, Cambridge, MA, April 25 - 27, 2007.

Kling, R., Adler, R., Huang, J., Hummel, V. and Nachman, L. (2005). "Intel Mote-based sensor networks," *Structural Control and Health Monitoring*, **12**(3-4): 469-479.

Ko, J.M., Ni, Y.Q., Chen, Z.Q. and Spencer, B.F., Jr., (2002). "Implementation of MR dampers to Dongting Lake Bridge for cable vibration mitigation," *Proceedings of the 3rd World Conference on Structural Control*, **3**: 777-786, Como, Italy, April 7 - 12, 2002.

Kottapalli, V.A., Kiremidjian, A.S., Lynch, J.P., Carryer, E., Kenny, T.W., Law, K.H. and Lei, Y. (2003). "Two-tiered wireless sensor network architecture for structural health monitoring," *Proceedings of SPIE 10th Annual International Symposium on Smart Structures and Materials*, **5057**: 8-19, San Diego, CA, March 2 - 6, 2003.

Kurata, N., Kobori, T., Takahashi, M., Niwa, N. and Midorikawa, H. (1999). "Actual seismic response controlled building with semi-active damper system," *Earthquake Engineering & Structural Dynamics*, **28**(11): 1427-1447.

Lee, C.-G., Lee, W.-T., Yun, C.-B. and Choi, J.-S. (2004). *Summary Report - Development of Integrated System for Smart Evaluation of Load Carrying Capacity of Bridges*. Korea Highway Corporation, Seoul, South Korea.

Lei, Y., Kiremidjian, A.S., Nair, K.K., Lynch, J.P. and Law, K.H. (2005). "Algorithms for time synchronization of wireless structural monitoring sensors," *Earthquake Engineering & Structural Dynamics*, **34**(6): 555-573.

Lian, F.-L., Moyne, J. and Tilbury, D. (2002). "Network design consideration for distributed control systems," *Control Systems Technology, IEEE Transactions on*, **10**(2): 297-307.

Lin, P.-Y., Roschke, P.N. and Loh, C.-H. (2005). "System identification and real application of the smart magneto-rheological damper," *Proceedings of the 2005 International Symposium on Intelligent Control*, 989-994, Limassol, Cyprus, June 27 - 29, 2005.

Liu, L., Yuan, F.G. and Zhang, F. (2005). "Development of wireless smart sensor for structural health monitoring," *Proceedings of SPIE Smart Structures and Materials 2005: Sensors and Smart Structures Technologies for Civil, Mechanical, and Aerospace Systems*, **5765**: 176-186, San Diego, CA, March 7, 2005.

Liu, S.-C., Tomizuka, M. and Ulsoy, G. (2006). "Strategic issues in sensors and smart structures," *Structural Control and Health Monitoring*, **13**(6): 946-957.

Ljung, L. (1999). *System Identification: Theory for the User*, Prentice Hall PTR, Upper Saddle River, NJ.

Lu, K.-C., Wang, Y., Lynch, J.P., Loh, C.-H., Chen, Y.-J., Lin, P.-Y. and Lee, Z.-K. (2006). "Ambient vibration study of Gi-Lu cable-stay bridge: application of wireless sensing units," *Proceedings of SPIE 13th Annual Symposium on Smart Structures and Materials*, **6174**: 61741D, San Diego, CA, February 26 - March 2, 2006.

Lunze, J. (1992). *Feedback Control of Large Scale Systems*, Prentice-Hall, Englewood Cliffs, NJ.

Luo, N., Rodellar, J., de la Sen, M. and Vehí, J. (2002). "Decentralized active control of a class of uncertain cable-stayed flexible structures," *International Journal of Control*, **75**(4): 285-296.

Lynch, J.P., Sundararajan, A., Law, K.H., Kiremidjian, A.S. and Carryer, E. (2004a). "Embedding damage detection algorithms in a wireless sensing unit for operational power efficiency," *Smart Materials & Structures*, **13**(4): 800-810.

Lynch, J.P., Sundararajan, A., Sohn, H., Park, G., Farrar, C. and Law, K.H. (2004b). "Embedding actuation functionalities in a wireless structural health monitoring system," *Proceedings of the 1st International Workshop on Advanced Smart Materials and Smart Structure Technology*, Honolulu, HI, January 12 - 14, 2004b.

Lynch, J.P. and Tilbury, D.M. (2005). "Implementation of a decentralized control algorithm embedded within a wireless active sensor," *Proceedings of the 2nd Annual ANCRiSST Workshop*, Gyeongju, Korea, July 21 - 24, 2005.

Lynch, J.P., Wang, Y., Loh, K.J., Yi, J.-H. and Yun, C.-B. (2006a). "Performance monitoring of the Geumdang Bridge using a dense network of high-resolution wireless sensors," *Smart Materials and Structures*, **15**(6): 1561-1575.

Lynch, J.P. and Loh, K.J. (2006). "A summary review of wireless sensors and sensor networks for structural health monitoring," *The Shock and Vibration Digest*, **38**(2): 91-128.

Lynch, J.P., Wang, Y., Lu, K.-C., Hou, T.-C. and Loh, C.-H. (2006b). "Post-seismic damage assessment of steel structures instrumented with self-interrogating wireless sensors," *Proceedings of the 8th National Conference on Earthquake Engineering*, San Francisco, CA, April 18 - 21, 2006b.

Lynch, J.P., Wang, Y., Swartz, R.A., Lu, K.-C. and Loh, C.-H. (2007). "Implementation of a closed-loop structural control system using wireless sensor networks," *Structural Control and Health Monitoring*: in press.

Mastroleon, L., Kiremidjian, A.S., Carryer, E. and Law, K.H. (2004). "Design of a new power-efficient wireless sensor system for structural health monitoring," *Proceedings of SPIE 9th Annual International Symposium on NDE for Health Monitoring and Diagnostics*, **5395**: 51-60, San Diego, CA, March 14 - 18, 2004.

MathWorks Inc. (2005). *Control System Toolbox : for Uses with MATLAB® : Getting Started*, MathWorks Inc., Natick, MA.

Moore, M., Phares, B., Graybeal, B., Rolander, D. and Washer, G. (2001). *Reliability of Visual Inspection for Highway Bridges*. Report No. FHWA-RD-01-020, Federal Highway Administration, McLean, VA.

Mutambara, A.G.O. (1998). *Decentralized Estimation and Control for Multisensor Systems*, CRC Press, Boca Raton, FL.

Nair, K.K., Kiremidjian, A.S. and Law, K.H. (2006). "Time series-based damage detection and localization algorithm with application to the ASCE benchmark structure," *Journal of Sound and Vibration*, **291**(1-2): 349-368.

Ou, J.P., Li, H. and Yu, Y. (2004). "Development and performance of wireless sensor network for structural health monitoring," *Proceedings of SPIE 11th Annual International Symposium on Smart Structures and Materials*, **5391**: 765-773, San Diego, CA, March 14 - 18, 2004.

Ploplys, N.J., Kawka, P.A. and Alleyne, A.G. (2004). "Closed-loop control over wireless networks," *Control Systems Magazine, IEEE*, **24**(3): 58-71.

Press, W.H. (1995). *Numerical Recipes in C*, Cambridge University Press, Cambridge, England.

Richardson, M.H. (1997). "Is it a mode shape, or an operating deflection shape?," *Sound and Vibration Magazine*, **31**: 54-61.

Rotkowitz, M. and Lall, S. (2006). "A characterization of convex problems in decentralized control," *Automatic Control, IEEE Transactions on*, **51**(2): 274 - 286.

Roundy, S.J. (2003). *Energy Scavenging for Wireless Sensor Nodes with a Focus on Vibration to Electricity Conversion*. PhD Thesis, Department of Mechanical Engineering, The University of California, Berkeley, Berkeley, CA.

Sandell, N., Jr., Varaiya, P., Athans, M. and Safonov, M. (1978). "Survey of decentralized control methods for large scale systems," *Automatic Control, IEEE Transactions on*, **23**(2): 108-128.

Seth, S., Lynch, J.P. and Tilbury, D.M. (2005). "Wirelessly networked distributed controllers for real-time control of civil structures," *Proceedings of the 2005 American Controls Conference*, **4**: 2946-2952, Portland, OR, June 8 - 10, 2005.

Shinozuka, M., Feng, M.Q., Chou, P., Chen, Y. and Park, C. (2004). "MEMS-based wireless real-time health monitoring of bridges," *Proceedings of the 3rd International Conference on Earthquake Engineering*, Nanjing, China, October 19 - 21, 2004.

Siljak, D.D. (1991). *Decentralized Control of Complex Systems*, Academic Press, Boston.

Skogestad, S. and Postlethwaite, I. (2005). *Multivariable Feedback Control: Analysis and Design*, John Wiley, Chichester, West Sussex, England.

Sodano, H.A., Inman, D.J. and Park, G. (2004). "A review of power harvesting from vibration using piezoelectric materials," *The Shock and Vibration Digest*, **36**(3): 197-205.

Sohn, H. and Farrar, C.R. (2001). "Damage diagnosis using time series analysis of vibration signals," *Smart Materials & Structures*, **10**(3): 446-451.

Sohn, H., Farrar, C.R., Hemez, F.M., Shunk, D.D., Stinemates, D.W. and Nadler, B.R. (2003). *A Review of Structural Health Monitoring Literature: 1996-2001*. Report No. LA-13976-MS, Los Alamos National Laboratory, Los Alamos, NM.

Solomon, I., Cunnane, J. and Stevenson, P. (2000). "Large-scale structural monitoring systems," *Proceedings of SPIE Non-destructive Evaluation of Highways, Utilities, and Pipelines IV*, **3995**: 276-287, Newport Beach, CA, March 7 - 9, 2000.

Soong, T.T. (1990). *Active Structural Control: Theory and Practice*, Wiley, Harlow, Essex, England.

Soong, T.T. and Spencer, B.F., Jr. (2002). "Supplemental energy dissipation: state-of-the-art and state-of-the-practice," *Engineering Structures*, **24**(3): 243-259.

Spencer, B.F., Jr., Christenson, R.E. and Dyke, S.J. (1998). "Next generation benchmark control problem for seismically excited buildings," *Proceedings of the 2nd World Conference on Structural Control*, Kyoto, Japan, June 29 - July 2, 1998.

Spencer, B.F., Jr. and Nagarajaiah, S. (2003). "State of the art of structural control," *Journal of Structural Engineering*, **129**(7): 845-856.

Spencer, B.F., Jr., Ruiz-Sandoval, M.E. and Kurata, N. (2004). "Smart sensing technology: opportunities and challenges," *Structural Control and Health Monitoring*, **11**(4): 349-368.

Stallings, J.M., Tedesco, J.W., El-Mihilmy, M. and McCauley, M. (2000). "Field performance of FRP bridge repairs," *Journal of Bridge Engineering*, **5**(2): 107-113.

Stevens, W.R. (1994). *TCP/IP Illustrated*, Addison-Wesley Pub. Co., Reading, MA.

Straser, E.G. and Kiremidjian, A.S. (1998). *A Modular, Wireless Damage Monitoring System for Structures*. Report No. 128, John A. Blume Earthquake Eng. Ctr., Stanford University, Stanford, CA.

Syrmos, V.L., Abdallah, C., Dorato, P. and Grigoriadis, K. (1997). "Static output feedback: a survey," *Automatica*, **33**(2): 125-137.

Tweed, D. (1994). "Designing real-time embedded software using state-machine concepts," *Circuit Cellar Ink*, (53): 12-19.

Volz, P., Magana, M.E., Henried, A.G. and Miller, T.H. (1994). "A decentralized active controller for cable-stayed bridges," *Proceedings of the 1st World Conference on Structural Control*, Los Angeles, CA, August 3 - 5 1994.

Wang, Y., Lynch, J.P. and Law, K.H. (2005). "Wireless structural sensors using reliable communication protocols for data acquisition and interrogation," *Proceedings of the 23rd International Modal Analysis Conference (IMAC XXIII)*, Orlando, FL, January 31 - February 3, 2005.

Wang, Y., Swartz, R.A., Lynch, J.P., Law, K.H., Lu, K.-C. and Loh, C.-H. (2006a). "Wireless feedback structural control with embedded computing," *Proceedings of SPIE 11th International Symposium on Nondestructive Evaluation for Health Monitoring and Diagnostics*, **6177**: 61770C, San Diego, CA, February 26 - March 2, 2006a.

Wang, Y., Loh, K.J., Lynch, J.P., Fraser, M., Law, K.H. and Elgamal, A. (2006b). "Vibration monitoring of the voigt bridge using wired and wireless monitoring systems," *Proceedings of the 4th China-Japan-US Symposium on Structural Control and Monitoring*, Hangzhou, China, October 16 - 17, 2006b.

Wang, Y., Swartz, R.A., Lynch, J.P., Law, K.H., Lu, K.-C. and Loh, C.-H. (2007a). "Decentralized civil structural control using real-time wireless sensing and embedded computing," *Smart Structures and Systems*, **3**(3): 321-340.

Wang, Y., Lynch, J.P. and Law, K.H. (2007b). "A wireless structural health monitoring system with multithreaded sensing devices: design and validation," *Structure and Infrastructure Engineering*, **3**(2): 103-120.

Wang, Y., Lynch, J.P. and Law, K.H. (2007c). "Decentralized H_∞ controller design for large-scale wireless structural sensing and control systems," *Proceedings of the 6th International Workshop on Structural Health Monitoring*, Stanford, CA, Sept 11 - 13, 2007c.

Warneke, B.A. and Pister, K.S.J. (2002). "MEMS for distributed wireless sensor networks," *Proceedings of 9th International Conference on Electronics, Circuits and Systems*, **1**: 291-294, Dubrovnik, Croatia, September 15 - 18, 2002.

Yang, J.N., Lin, S. and Jabbari, F. (2004). "H_∞-based control strategies for civil engineering structures," *Structural Control and Health Monitoring*, **11**(3): 223-237.

Yao, J.T.P. (1972). "Concept of structural control," *Journal of Structural Division, ASCE*, **98**(7): 1567-1574.

Yook, J.K., Tilbury, D.M. and Soparkar, N.R. (2002). "Trading computation for bandwidth: reducing communication in distributed control systems using state estimators," *Control Systems Technology, IEEE Transactions on*, **10**(4): 503-518.

Zhang, Y. and Iwan, W.D. (2002a). "Active interaction control of civil structures. Part 1: SDOF systems," *Earthquake Engineering & Structural Dynamics*, **31**(1): 161-178.

Zhang, Y. and Iwan, W.D. (2002b). "Active interaction control of civil structures. Part 2: MDOF systems," *Earthquake Engineering & Structural Dynamics*, **31**(1): 179-194.

Zhou, K., Doyle, J.C. and Glover, K. (1996). *Robust and Optimal Control*, Prentice Hall, Englewood Cliffs, NJ.

Zimmerman, A., Swartz, R.A., Saftner, D., Lynch, J.P., Shiraishi, M. and Setareh, M. (2007). "Parallel data processing architectures for identification of structural modal properties using a dense wireless sensor network," *Proceedings of the World Forum on Smart Materials and Smart Structures Technology (SMSST07)*, Chongqing & Nanjing, China, May 22 - 27, 2007.